

AUTOMATED MODEL COMPLEXITY MONITORING AND
ADJUSTMENT USING BOND GRAPHS

KAZI TAYUBUL HAQ



Automated Model Complexity Monitoring and Adjustment Using Bond Graphs

By

© Kazi Tayubul Haq

**A Thesis Submitted to the School Of Graduate Studies in Partial
Fulfillment for the Degree of Masters of Engineering**

**Faculty of Engineering and Applied Science
Memorial University of Newfoundland**

November, 2008

St. John's, Newfoundland, Canada

Abstract

Using models of appropriate complexity is important for effective simulation-based design. Throughout a simulated event, systems can have varying inputs, or may have varying system parameters. A single model may not have the most appropriate level of complexity throughout all phases of the maneuver. Therefore using a variable-complexity model could predict the system response accurately while achieving computational savings. can be achieved

This thesis presents an approach for switching system model elements “on” and “off” as their importance changes, using bond graphs. Three element importance calculating methods are used to determine an element’s contribution to overall system dynamics. Once the power falls below a user-defined threshold, a modified transformer element sets the output from the element to the rest of the system equal to zero. Importance of an element can still be computed as soon the element is “off” by passing the input to the element through the transformer. Again, the element can be switched back “on” if necessary.

Three case studies are done using a half car, a quarter car and a vehicle frame model. The switching is performed according to the element importance metrics. The computational overhead of power calculations offsets any increase in processing speed due to model reduction even though the appropriate model complexity is used at all stages. Still the

method is useful to determine the required model complexity at any instant without prior knowledge of input or parameter changes, and it is able to show how a sequence of systematically reduced models would perform.

Acknowledgements

First I offer my sincerest gratitude to my supervisor, Dr Geoff Rideout, who has supported me throughout my thesis with his patience and knowledge whilst allowing me to work in my own way. I attribute the level of my Masters degree to his encouragement and effort and without him this thesis, too, would not have been completed or written. One simply could not wish for a better or friendlier supervisor.

I am as ever, especially indebted to my parents, Mr. K. Mamun Haq and Mrs. K. Jahanara Haq for their love and support throughout my life. I also wish to thank my sisters, Ms. Tona and Mrs. Nipu for their support and understanding during my study. I am also thankful to Mr. Refaul Ferdous, who guided me about the direction of my thesis from the beginning. Moreover, my sincere thanks go to my friends, who shared their love and experiences with me. Finally, I wish to express my appreciation to Shibly Rahman, Wasimul Bari and Mst. Kamrunnahar who helped me overcome my doubts in doing this thesis.

Table of Contents

Abstract.....	ii
Acknowledgements.....	iv
Table of contents.....	v
List of Figures.....	ix
List of Tables.....	xiii
List of Symbols.....	xiv
Chapter 1 Introduction.....	1
1.1 Proper modeling and model complexity	
1.2 Discontinuous system modeling.....	3
1.3 Bond Graphs.....	4
1.4 Scope of current research.....	6
Chapter 2 Literature Review.....	10
2.1 Proper model generation algorithms.....	10
2.2 Application of MORA for variable complexity modeling.....	13
2.3 Switching techniques.....	14
Chapter 3 Evaluation of Metrics for Element Importance.....	19
3.1 Metrics.....	19
3.1.1 Activity index.....	19

3.1.2 Relative activity	21
3.1.3 Moving average of power index	22
3.2 U signal	24
Chapter 4 Bond Graph Switches.....	29
4.1 Review of causality.....	29
4.2 Switches for causally weak bonds	31
4.3 Switch for causally strong bonds	33
4.3.1 Strong <i>I</i> element switch	33
4.3.1.1 Parasitic <i>R</i> element.....	34
4.3.1.2 Parasitic <i>I</i> element	36
4.3.2 Other causally strong bond switches.....	39
4.4 Internal bond switch.....	40
Chapter 5 Half and Quarter Car Case Studies.....	42
5.1 Half car case study.....	42
5.1.1 Results of prior research into variable complexity half-car	43
modeling.....	43
5.2 Continuous element importance monitoring methods	51
5.2.1 Activity based metric	51
5.2.2 Global MAP based metric.....	54
5.2.3 Local MAP based metric.....	58

5.3 Global MAP based strong and weak causality bond switch.....	60
5.5 Quarter car model case study.....	72
5.5.1 Simple quarter car model.....	72
5.5.2 Continuous monitoring of importance of the quarter car model elements	75
5.5.2.2 Relative activity	78
5.5.2.3 MAP Index.....	80
5.5.3 Switching for quarter car model.....	81
5.5.3.1 Quarter car model with switch for casually weak bonds	81
5.5.3.2 Switching causally strong bond for unsprung mass and weakly causal sprung mass.....	86
5.5.3.3 Switching causally strong bond for sprung and unsprung mass	89
Chapter 6 Vehicle Frame Model Case Study	96
6.1 Brief description of Bernoulli-Euler beam	97
6.2 Vehicle frame model.....	100
6.3 Partitioning of vehicle frame model.....	104
6.4 Partitioning by using switches	106
6.4.1 Assessment of partitioning possibility using MAP sensors.....	106
6.4.2 Switched vehicle frame model.....	109
6.5 Result of switching the vehicle frame model.....	111
Chapter 7 Conclusions and Recommendations	115

7.1 Conclusions	115
7.2 Recommendations	117
References.....	119

List of Figures

Figure 1.1: Quarter car modeled	4
Figure 2.1: Switching device and bond graph	14
Figure 2.2: Ideal switch with 0 flow or effort source	15
Figure 2.3: Switching device bond graph	15
Figure 2.4: Controlled 0-junction	16
Figure 2.5: Switched 0- and 1-junction (0s and 1s)	18
Figure 3.1: Activity index calculation using bond graph	20
Figure 3.2: Relative activity calculation using bond graph	22
Figure 3.3: MAP index calculation using MAP sensors	23
Figure 3.4: Schematic diagram and bond graph of a simple spring-mass-damper system	Error! Bookmark not defined.
Figure 3.5: (a) 'U' values using relative activity (b) 'U' values using activity index	26
Figure 4.1: Causality assignment of bond graph elements	30
Figure 4.2: Switch arrangement for causally strong I element	33
Figure 4.3: Adding 0-junction and parasitic R element to a strongly casual I element	34
Figure 4.4: Causally strong R element attached to a 1-junction	36
Figure 4.5: Adding parasitic I element	37

Figure 5.1: Schematic diagram of the half car model	44
Figure 5.2: The half car full model with activity sensors	46
Figure 5.3: System response of four individual-stage MORA-reduced models executed Sequentially.....	49
Figure 5.4: Response of full model running together (all stages) and separately (for each stage), and reduced model (for each stage).....	50
Figure 5.5: ‘U’ values of the half car model using activity metric	52
Figure 5.6: Comparing ‘U’s from Kypuros and Longoria [9] and continuous activity	53
Figure 5.7: Comparing ‘U’s from Kypuros and Longoria [9] and MAP based metric	56
Figure 5.8: Local MAP metric for half car model	58
Figure 5.9: Comparing ‘U’s from Kypuros and Longoria [9] and local MAP based metric	59
Figure 5.10: Global MAP based switches for half car model.....	61
Figure 5.11 shows plots of switched and full model system responses. Front and rear unsprung mass movement demonstrate a good similarity between the switched and full	62
Figure 5.12: U values from global MAP switch for the half car model	63
Figure 5.13: (a) MAPs of adjacent bonds at $0_{F_{fs}}$ -junction (b) MAPs of adjacent at at $0_{F_{rs}}$	64
Figure 5.14: Half car model with internal bond switch.....	66
Figure 5.15: (a) U values from the bonds attached to the 1_w (1 junction at rotational	

inertia) (b) U values from the bonds attached to the 1_{v_ms} (1 junction at sprung mass).....	69
Figure 5.16: Flow from MTF2 of Figure 5.14.....	70
Figure 5.17: U values from different elements from the internal bond switched half car	70
Figure 5.19: Free body diagram of a quarter car.....	73
Figure 5.20: Bond graph model of the quarter car.....	74
Figure 5.21: Calculating activity indices for the quarter car.....	76
Figure 5.22: U values of the elements of the quarter car model.....	77
Figure 5.23: Plot of the U values using relative activity.....	79
Figure 5.24: U values of the quarter car model using MAP sensors.....	80
Figure 5.26: Full model of quarter car with constant signal to MTF.....	83
Figure 5.27: (a) Sprung mass momentum of full model (b) Sprung mass momentum	84
Figure 5.28: Plot of U values from a switched model compared with full model.....	86
Figure 5.29: A casually weak sprung mass switched model for quarter car.....	88
Figure 5.30: Plot of mass momentum for casually weak sprung mass switched model of the quarter car.....	89
Figure 5.31: Quarter car model with switched sprung mass for eigenvalue analysis.....	89
Figure 5.32: Quarter car model with strongly causal sprung mass switch.....	92
Figure 5.33: Comparison of switched and full model output.....	93

List of Tables

Table 1.1: List of bond graphs elements	7
Table 4.1: Causality assignment for graph elements	
Table 4.2: Switches for causally weak bonds	32
Table 4.3: Causally strong bond switches	40
Table 4.4: Switch for internal bond	41
Table 5.1: Parameter values for the elements of the half car model.....	45
Table 5.2: Activity, activity index and cumulative activity index at the end of stage 2 sequentially	48
Table 5.3: Simulation time and steps for full and reduced model for each stage	50
Table 5.4: Simulation time and steps for a switched and full half car model.....	72
Table 5.5: Parameter values of different elements used in bond graph model of the	75
Table 5.6: Simulation time and step for full and switched model.....	84
Table 5.7: Eigenvalues for switched sprung mass	91
Table 6.1: Parameter values of the vehicle frame model.....	101
Table 6.2: Modal parameters used in the model.....	103
Table 6.3: Simulation time and step for switched and full model	111

List of Symbols

- A : Activity (pg.10)
- A : Beam cross-sectional area (pg.96)
- AI : Activity Index (pg.11)
- A_i : Activity of i^{th} element (pg.20)
- $bMTF$: Boolean modulated transformers (pg.18)
- b_{fs} : Front suspension damping (pg.45)
- b_{rs} : Rear suspension damping (pg.45)
- b_{ft} : Front tire damping (pg.45)
- b_{rt} : Rear tire damping (pg.45)
- C : Capacitive Element (pg. 5)
- E : Young's modulus (pg.96)
- e : Effort (pg.29)
- f :flow (pg.29)
- Ffz : Front displacement (pg.112)
- $Fmid$: Middle displacement (pg.112)
- Frz :Rear displacement (pg.112)
- $F_1(t)$: Point force (pg.96)
- $F_2(t)$: Point force (pg.96)
- GY-: Gyrator (pg.5)
- I : Area moment of inertia (pg.96)

I : Inductive Element (pg. 5)

I_c : Rotational Inertia (pg.45)

I_{par} : Parasitic inertial element (pg.61)

J_g : Centroidal moment of inertia (pg.98)

K : Number of elements in the model (pg.11)

k : Parameter of capacitive element (pg.36)

k_{fs} : Front suspension stiffness (pg.45)

k_{rs} : Rear suspension stiffness (pg.45)

k_{ft} : Front tire stiffness (pg.45)

k_{rt} : Rear tire stiffness (pg.45)

k_n : n^{th} modal stiffness (pg.97)

L : Length (pg.96)

L : Distance between the tires (pg.45)

L_r : Longitudinal distance between sprung and rear unsprung mass (pg.45)

L_f : Longitudinal distance between sprung and front unsprung mass (pg.45)

MAP: Moving average of power (pg.22)

MORA: Model Order Reduction Algorithm (pg.7)

MTF: Modulated Transformer (pg.6)

MAPI: Moving average of power index (pg.27)

m : Parameter of inductive element (pg.37)

m_s : Sprung mass (pg.45)

m_{fus} :Front unsprung inertia (pg.45)

m_{us} : Rear unsprung inertia (pg.45)

NGY: Modulated Gyrator (pg.6)

$n00$: First rigid mode (pg.101)

$n0$: Second rigid mode (pg.101)

$n1$: First flexible mode (pg.101)

$n2$: Second flexible mode (pg.101)

$n3$: Third flexible mode (pg.101)

P: Power (pg.11)

P : Generalized momentum (pg.38)

$para_R$: Parasitic resistive element (pg.61)

\dot{p} : Effort (pg.38)

q: Displacement (pg.37)

\dot{q} : Flow (pg.37)

R: Resistive Element (pg. 5)

R_par : Parasitic resistive element (pg.67)

r: Modulus of modulated the transformer (pg.32)

SMPC: Switched mode power converters (pg.17)

SPJ: Switched power junction (pg.17)

SPST: Single pole single throw (pg.17)

S_e : Effort Source (pg.5)

S_f : Flow source (pg.5)

T_0 : Time window for averaging (pg.23)

$-TF-$: Transformer (pg.5)

t: Time (pg.11)

U: Signal which is generated from a element importance calculating sensor (pg.24)

$u(t)$: Road input (pg.72)

V: Translational Velocity (pg.45)

$Y_n(x)$: n^{th} mode shape (pg.97)

y_c : Displacement of the sprung mass (pg.47)

y_{rus} : Rear unsprung mass displacement (pg.47)

y_{fus} : Front unsprung mass displacement (pg.47)

ρ : mass density (pg.96)

ω : Road input angular frequency (pg.75)

ω_n : n^{th} modal frequency (pg.97)

$\ddot{\eta}_{(0)}$: First rigid mode acceleration (pg.98)

$\ddot{\eta}_0$: Second rigid mode acceleration (pg.98)

Chapter 1

Introduction

1.1 Proper modeling and model complexity

A dynamic model is said to be proper if it maintains desired accuracy with minimal complexity. Efficient and accurate models help to understand, optimize and control the system dynamics. Tractability in system identification and optimization can only be ensured by simplicity of a model [4]. A proper model must satisfy modeling objectives and maintain physically meaningful design parameters and variables [5]. The simulation community prefers a simple model to a complex one. According to Salt [1993] “simplification is the essence of simulation [1].” Though a proper model is desired, it requires efficient modelers to generate such models. Designers who do not have such skill face three problems:

- Making models oversimplified and therefore inaccurate.
- Making them too complicated, obscuring the relationship between design parameters and system performance.
- Not making formal use of models.

Thus, automated modeling tools are desired which can generate proper models with appropriate complexity [3]. Balancing accuracy and simplicity through proper modeling facilitates optimization, real-time simulation and control design

Although complexity is in some sense an intuitive concept, there is no general definition or single accepted definition of complexity when applied to a model. Still complexity can be described into two categories:

- Complexity due to complication in understanding the system.
- Complexity due to number of system components [1].

Models are reduced to generate a proper model. The following are some potential reasons for obtaining a reduced order model [6, 7]

- To simplify the understanding of a system.
- To increase computational efficiency.
- To generate simpler controller laws.

A larger and complex model can increase computation time despite using a high speed computer [8]. On the other hand simpler models often but not always can simulate at a faster speed that can be valuable for applications like hardware-in-the loop simulation or embedded model-reference control [4]. Moreover, companies want to gain competitive advantage by reducing time to simulate a model [5]. Achieving both simplicity and accuracy is difficult as often increasing accuracy increases model complexity. Thus, a trade off results. With larger and more complex systems, such competition grows more.

Hence an optimum is needed in which the essential dynamics have been captured using a proper model generation technique [4].

1.2 Discontinuous system modeling

Modeling theory typically addresses problems with systems having continuously changing properties, represented by a set of algebraic and/or differential equations that are continuously differentiable functions of time. Sometimes abrupt changes are also found, such as during transitions between modes of operation. Examples of systems exhibiting such switching phenomena include electrical diodes, hydraulic check valves, and mechanical free wheeling devices. Switching appears within a very short time for ideal switches and no power loss is considered [12].

A quarter car represents one corner of a full car model and includes only a single tire and suspension system as shown in Figure 1.1. A jumping quarter car that goes off the ground and comes back again exhibits system discontinuity which can be shown as a switching phenomenon between sub-systems. As the tire loses contact with the ground the tire damper-spring pair is disconnected from the rest of the system. The normal force becomes zero, and the tire is reconnected as soon as it reaches the ground [13].

A collision phenomenon is observed as a discontinuous system example by Stromberg and Soderman [12]. Switching occurs during a collision of a wagon and a wall modeled as spring-damper submodel. Once the wagon collides with the wall the two submodels

get connected and the switch is 'on'. Before and after the collision the wagon and wall models are disconnected and switching 'off' occurs.

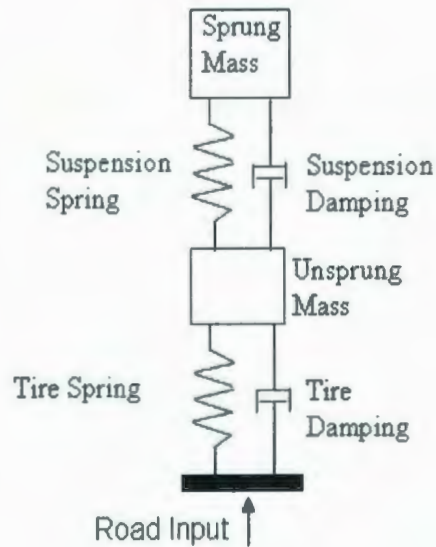


Figure 1.1: Quarter car model

1.3 Bond Graphs

Prof. H. M. Paynter (1959) developed the idea of expressing systems in terms of power bonds, connecting the elements of the physical system to so-called junction structures. This energy based graphical technique for representing the mathematical model of the physical system is called a Bond Graph, which can be both power and information oriented. Later on, many researchers like Karnopp [16], Rosenberg [22], Margolis [23], and Breedveld [24] worked on extending this modeling technique to power hydraulics, mechatronics, and general thermodynamic systems and recently to electronics and non-energetic systems like economics and queuing theory.

The main idea of bond graph theory is that power is transmitted through and into elements of a model as the product of 'flow' and 'effort'. The power flow paths through the system components are explicitly identified and state equations are generated in terms of only two variables, generalized momentum and displacement. The main components of the bond graph formalism are inductive (I), capacitive (C) and resistive (R) elements. The first two are energy storing element and the third one is the energy dissipative element. Constitutive laws for these elements relate effort and flow through a parameter and the derivative or integral of momentum or displacement. The resistive element has an algebraic constitutive law to relate the flow and effort.

There are two types of junctions present in bond graphs, 1-junctions and 0-junctions. At 0-junctions, the flow of all bonded elements sums to zero and the efforts are equal. This corresponds to a node in an electrical circuit (where Kirchhoff's current law applies). In a 1-junction, the efforts sum to zero while all bonded elements have common flow. This corresponds to force balance at a mass in a mechanical system.

The effort (S_e) and flow (S_f) source are the elements by which the system interacts with the environment. Sources are also called active ports.

There are two types of two-port elements, "Transformer" and "Gyrator". The bond graph symbols for these elements are $-TF-$ and $-GY-$, respectively. They conserve power and multiply effort and flow with proper scaling as defined by the modulus. The elements of effort and flow vectors are algebraically related by the transformers. Whereas the transformer relates flow-to-flow and effort-to-effort, a gyrator relates flow to effort and

effort to flow, again keeping the power on the input and output ports equal. A modulated transformer (*MTF*) and modulated gyrator (*MGY*) is also used in bond graphs presentation [11]. Table 1.1 summarizes a list of useful bond graphs elements [22].

The advantages of using bond graphs are

- Power flow paths through the system can be identified
- Power flow through the elements and their connections can be easily calculated.
- It is unlikely to accidentally introduce extra energy into a system as it works on the principle of conservation of energy.
- Virtually any type of physical system (mechanical, electrical, electro-mechanical, etc.) can be modeled.
- Needs very few basic variables to express even a very complex multi-domain system [11].

1.4 Scope of current research

Many proper modeling algorithms exist to generate proper models, such as the Model Order Reduction Algorithm (MORA) [2], and Relative Activity-Based Partitioning [21]. Such algorithms attempt to generate a proper model, but that model has a fixed structure,

Table 1.1: List of bond graphs elements

	SYMBOL	CONSTITUTIVE LAW (LINEAR)	CAUSALITY CONSTRAINTS
SOURCES			
Flow	Sf \rightarrow	$f = f(t)$	fixed flow out
Effort	Se \rightarrow	$e = e(t)$	fixed effort out
ENERGETIC ELEMENTS			
Inertia	\rightarrow I	$f = \frac{1}{I} \int e dt$	preferred integral
	\rightarrow I	$e = I \frac{df}{dt}$	
Capacitor	\rightarrow C	$e = \frac{1}{C} \int f dt$	preferred integral
	\rightarrow C	$f = C \frac{de}{dt}$	
Resistor	\rightarrow R	$e = Rf$	none
	\rightarrow R	$f = \frac{1}{R} e$	
2-PORT ELEMENTS			
Transformer	$\xrightarrow{1} \text{TF} \xrightarrow{2}$ n	$e_2 = n e_1$ $f_1 = n f_2$	effort in-effort out or flow in- flow out
Modulated Transformer	$\downarrow ?$ \rightarrow MTF \rightarrow n(?)	$e_2 = n(?) e_1$ $f_1 = n(?) f_2$	
Gyrator	$\xrightarrow{1} \text{GY} \xrightarrow{2}$ n	$e_2 = n f_1$ $e_1 = n f_2$	flow in-effort out or effort in- flow out
Modulated Gyrator	$\downarrow ?$ \rightarrow MGY \rightarrow n(?)	$e_2 = n(?) f_1$ $e_1 = n(?) f_2$	
CONSTRAINT NODES			
1-junction	$\xrightarrow{1} \text{1} \xrightarrow{2}$ \swarrow 3	$e_2 = e_1 - e_3$ $f_1 = f_2$ $f_3 = f_2$	one flow input
0-junction	$\xrightarrow{1} \text{0} \xrightarrow{2}$ \swarrow 3	$f_2 = f_1 - f_3$ $e_1 = e_2$ $e_3 = e_2$	one effort input

is only valid in the neighborhood of the original parameters and inputs, and doesn't change automatically if there are parameter or input changes.

Another limitation of existing proper modelling methods is that they compute the reduced model using aggregate power flow over a pre-set time interval. If that time window is broad, then the instantaneous model complexity that is required may change frequently. A single reduced model may perform well at certain times but poorly at others. This research proposes a switching technique that continuously monitors the required level of model complexity using MORA or Partitioning, and switches between different reduced models as necessary.

Switching techniques found in the literature mostly deal with modeling a system with physical switches. Switches are used in power electronics applications such as converter circuits, phase-inverters, in the hydraulic domain for pump systems or in modeling clutched transmissions. While algorithms have been developed to generate a proper model, a fully automated technique to continuously monitor and switch complexity has not been developed.

This research attempts to generate reduced order models automatically. A switching method is used to switch off any inactive elements from a bond graph model of the system when they are unimportant and to switch them back on if they are required again later.

Chapter 2 surveys some proper modeling methods, switch modeling with bond graphs and variable complexity models. In Chapter 3, power-based measures of element importance are studied and compared. Such metrics are used as a tool to determine which elements of a model are important to the system dynamics and which are not. Activity Index, Relative Junction Activity and Moving Average of Absolute Power are studied with application to a simple mass-spring-damper system.

Chapter 4 describes a bond graph switch library that has been designed and applied in the current research. Chapter 5 is a case study of half car and quarter car models using the switching technique and a study of the computational savings resulting from model switching.

In Chapter 6, power-based metrics and switches are used to predict when models can be partitioned into “driving” and “driven” dynamics. A free-free beam case is studied (in which flexible modes are eliminated if appropriate). Chapter 7 includes concluding points about this research and makes some recommendations for future works.

If the current research goal were achieved i.e., model reduction could be done automatically this would certainly save computational steps for variable complexity models. Such automated modelling would result in faster simulation speeds which would be very useful to industries in competitive environments.

Chapter 2

Literature Review

In this chapter some model reduction algorithms are discussed such as MORA [2] and System Partitioning [10]. Issues regarding different switching methods are also reviewed. Approaches to discontinuous system modelling which are relevant to the current research are discussed.

2.1 Proper model generation algorithms

Louca *et al.* [2] proposed a model reduction algorithm (MORA) to generate minimum complexity models. They developed a metric called element activity that measures relative importance of an element in a model. Activity is defined as the time integral of absolute power of a bond where power is the product of generalized effort and flow (for example, force and velocity in a mechanical system or voltage and current in an electrical system).

$$A = \int_0^t |P| dt \quad (2.1)$$

Where,

A= Activity

P=Power

t =Time

Activity index for each element is found by dividing the activity of an element by the sum of all element activities from the model.

$$AI_i = \frac{A_i}{\sum_{i=1}^k A_i} \quad (2.2)$$

where k = number of model elements .

Elements are ranked from highest to lowest activity. A threshold limit is set and an element is removed as soon as addition of its activity index takes the cumulative activity indices above the threshold limit. A case study with a quarter car model is done to generate a proper model using MORA by Louca *et al.* [2]. Despite its usefulness as a metric to identify non-contributing elements, activity is not a “fast-responding” metric if the time window is too wide. It cannot track an element if it becomes unimportant for an instant during the whole simulation period.

Ye and YoucefToumi [18] showed a use of energy exchange patterns as a metric to determine the contribution of an element to the dynamic system behavior. Unlike Louca *et al.* [2] it measures energy associated with adjacent bonds at junctions containing energy storage elements. Bonds having lower energy level at an instant compared to other bonds are eliminated. A case study is done with an electronic circuit and system response of the reduced model shows a close resemblance with the full model. Though an element might be contributing significantly at a junction, it can be insignificant when compared to

all the elements globally. Such an element should not necessarily be retained in the reduced model. Moreover, while the responsiveness of their method is good for monitoring required model complexity, sensitivity functions used can become singular at points where the energy storage element's state is zero.

Rideout *et al.* [10] presented a partitioning algorithm to find the decoupling among the elements of the model and thus partition the model. It compares the relative activities of the bonds attached to each 1- or 0- junction, and converts the low activity bonds into a modulated source. This 'conditioned' bond graph can be divided into "driving" and "driven" parts if all the modulating sources are directed from one subgraph to another. The driving part excites the driven part. On the other hand the driven sub-system response has negligible impact on the driving portion. Once such partitioning is found, the driving portion can be simulated first and using the output the driven portion can be simulated. If the driving portion only is of interest, then the driven part can be removed completely. Such decoupling or partitioning can facilitate model reduction and can allow parallel simulation of the driving and driven parts. Algorithms such as MORA can then be applied to the partitioned system. As both MORA and the partitioning method create models with a subset of the parameters of the full model, it is possible to gain a physical interpretation of the result. Case studies have shown the computational savings resulting from partitioning system models, which can lead to a faster simulation. As with MORA, no means of automatically switching between partitioned and non-partitioned models is proposed in [10].

2.2 Application of MORA for variable complexity modeling

Kypuros and Longoria [9] used the MORA algorithm developed by Louca *et al.* [2] to find the separate reduced order models for a model with four sequential sinusoidal input stages. A half car model was used to simulate a vehicle ride maneuver. Four different frequency inputs were used that resulted in four different proper models to predict ride quality – one proper model for each input frequency. Activity of all the energy storing elements was calculated and elements were ranked from highest to lowest value according to their activity index. For each stage some elements were found to be non-contributing. Therefore for each stage a different reduced model was generated. The appropriate model for the first stage was executed, and the final state variable values were used as initial values for the second stage. The second stage was simulated, and the same pattern was repeated through the fourth stage. System response from the reduced and full model for each stage was compared and showed significant similarity. Simulation steps taken for each stage with reduced and full models were compared. Using an appropriate reduced model for each stage gave significant step savings compared to a full model. Simulation was done with MATLAB software using the state equations derived from the reduced bond graph model. Despite the method's ability to identify appropriate model complexity for each time period, it needs *a priori* knowledge of the time span at which the model complexity should change. Therefore, an automated model complexity change mechanism is still required.

2.3 Switching techniques

Asher [14] described a bond graph of an electronic switching circuit. It used a combination voltage or current generator with a resistor that acted as a causality generator for the switching device as shown in Figure 2.1. A causality switching algorithm was developed that changes the switching state and the circuit equations automatically considering a switching 'off' or 'on' condition.

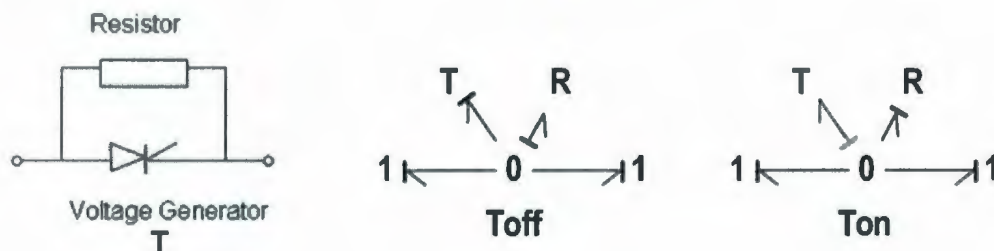


Figure 2.1: Switching device and bond graph [14]

A composite switch element was introduced with a combination of voltage generator element, 'causality' resistor and a 1-junction [Section 1.3] that overcomes the limitation of being forced into a restrictive causality assignment. Stromberg *et al.* [12] presented a new bond graph element 'ideal switch' that consists of a zero effort or zero flow source and switches between different sub-systems. The arrangement is shown in Figure 2.2. This method accepted variability in causality. Two case studies with discontinuous

systems were discussed where such switching was implemented with an electrical diode

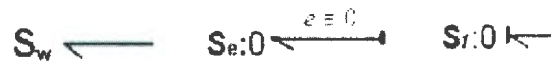


Figure 2.2: Ideal switch with 0 flow or effort source [12]

and a colliding rigid body. Causality reassignment could be done automatically; however this required symbolic derivation of new system equations with each switching event and precluded the use of commercial bond graph software available at the present time.

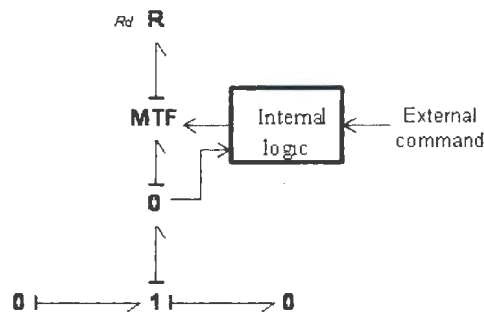


Figure 2.3: Switching device bond graph [15]

Ducreux *et al.* [15] presented a switch for power electronic circuits that showed a way to model such circuits with all their discontinuities. Such switches contain a combination of *MTF* and *R* elements as shown in Figure 2.3. The *MTF* connects the linear *R* with the rest of the system. It gets an external command that dictates switching states. A zero flow results for the rest of the system when an element goes ‘off’. A case study was demonstrated with a three phase voltage inverter. Mosterman [17] developed a theory for hybrid physical systems. Hybrid physical systems combined continuous and discrete

system behavior. An algorithm was developed that transfers a continuous state vector between the modes in a hybrid model. Once a discontinuity occurs, mode switching is obtained by using a controlled junction. The switching element controls the junction to get an 'on' or 'off' mode. During 'on' mode the junction acts like a usual 1- or 0-junction. Figure 2.4 shows that as soon as the mode is 'off', the controlled junction is loaded with a source having 0 value to meet the boundary condition of the disconnected model part. For a 0- junction an effort source with a 0 value (and for a 1-junction a flow source having 0 value) was used as a load to deactivate the junction. As 0 effort or flow is forced, transfer of energy through the junction becomes 0; therefore it acts like an ideal switch. The local switching logic is developed by a combinational automaton which is known as control specification (CSPEC). Therefore such switching is not strictly done within the bond graphs elements.



Figure 2.4: Controlled 0-junction [17]

Demir and Poyraz [19] developed software for switching a model based on switch models with an ideal flow or effort source. The sources are set to 0 to switch "off". While the bond graph model is prepared, a program is developed which forms the state and output equations of a model. The program is named as "BONDSO". Application of the software is illustrated with several examples. This method facilitates analysis of non-

linear systems. This method gets cumbersome as the number of switches is increased since 2^n different bond graphs are required for n switches.

Umarikar and Umanand [20] presented a switching method applied for modeling switched mode power converters (SMPC) using bond graphs. They used a switched power junction (SPJ) for switching in a SMPC. They proposed using switched 1- or 0-junctions which are represented as $1s$ and $0s$ respectively. They are capable of handling multiple efforts for a 0-junction and multiple flows to a 1-junction. There is a control signal for the junctions that decides which effort or flow is to be used. Using this modified junction a single pole single throw (SPST) switch is modeled. Also, boost and buck, two basic types of converters, are modeled. The bond graph models are used for large AC signals while a graphical method was proposed to find the model for average, steady state or small AC signals.

Junco et al. [13] used the concept of SPJ and presented SPJ with a combination of bond graph junction and Boolean modulated transformers (*bMTF*). A switched 0-junction, $0s$, is connected with a 1-junction that takes all the effort inputs while each input effort is followed by a *MTF*. In case of switched 1-junction, $1s$, the 1-junction is connected with a 0-junction that admits all the flow inputs followed by *MTFs*. Therefore $1s$ acts like a 1-junction that admits more than one flow causality and $0s$ acts like a 0-junction with multiple effort causality. Figure 2.5 shows the switched 0- and 1-junction. These SPJ are

applied in case studies with a three phase inverter, a series DC motor whose field

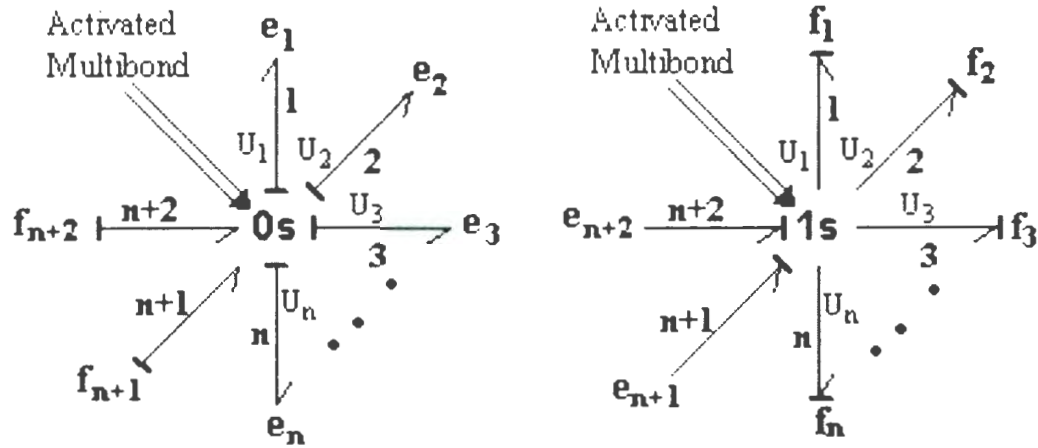


Figure 2.5: Switched 0- and 1-junction ($0s$ and $1s$) [13]

inductance has varying causality and a quarter car model with a dissipator and spring that changes causality as the car jumps and leaves the ground. However, power through the element that goes “off” cannot be monitored using such switched junctions.

Concepts from the switching techniques described in this chapter, along with MORA and system partitioning, are used in this thesis. Details are discussed in the following chapters.

Chapter 3

Evaluation of Metrics for Element Importance

Throughout this study some metrics are used to identify the extent of the contribution of a system element to the system dynamic behavior. By removing the less significant elements from a system model as indicated by the metric, a proper model [see Section 1.1] can be obtained. Three metrics are considered:

1. Activity Index
2. Relative Activity
3. Moving Average of Power Index

All the three types of metrics are discussed in the following sections.

3.1 Metrics

3.1.1 Activity index

This metric is introduced by Louca *et al.* [2] as described in Chapter 2. ‘Activity’ is defined as a time integral of absolute power that flows in and out of an element which is given by Eq.2.1. Total activity is given by

$$A_{total} = \sum_{i=1}^k A_i \quad (3.1)$$

Where:

A_i = Activity of i^{th} element

k = total number of energy elements in the model

Activity measured by Eq.2.1 and total activity from Eq.3.1 are used to calculate the activity index for each element as shown by Eq.2.2. This activity index indicates the portion of the total system energy that flows through an element over a time interval. With lower activity index an element is expected to have a negligible contribution to system dynamics whereas higher activity index elements exhibit greater importance.

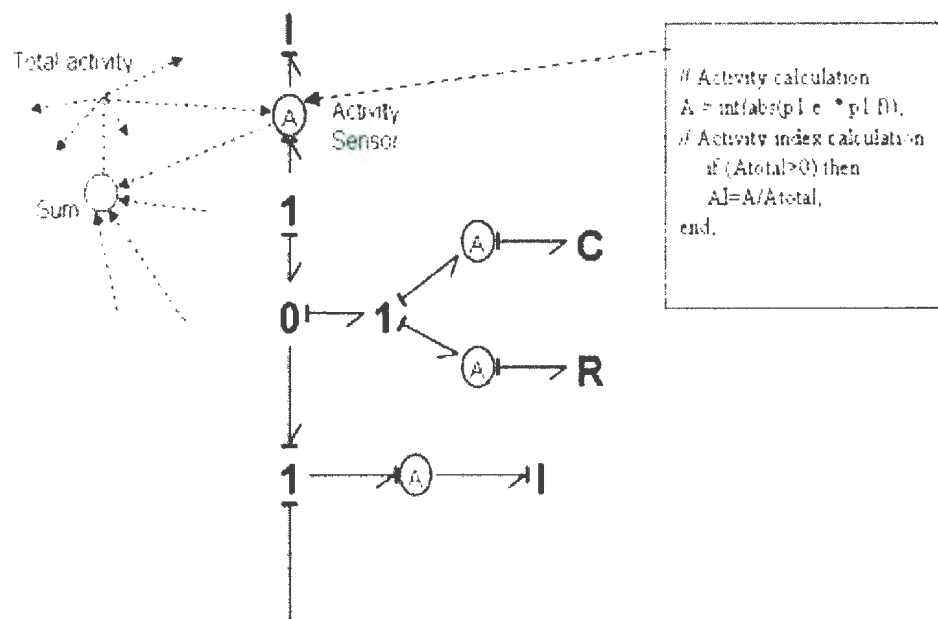


Figure 3.1: Activity index calculation using bond graph

Figure 3.1 shows a method for activity calculation in a bond graph model. Activity sensors ('A' blocks) having a code as shown in the figure calculate activity of the

corresponding bond. Activity sensors send an 'activity' signal to the 'Sum' block that sums all the element activities in the model to find the total activity. Again, 'Total Activity' signals go to the activity sensors for calculating the activity index.

3.1.2 Relative activity

Rideout *et al.* [21] developed a system partitioning method to generate proper [see Section 2.1] models using the concept of relative activity. In contrast to 'activity index', relative activity is a measure of relative importance of any adjacent bond attached to a 1- or 0-junction. Activity of each bond attached to a junction is calculated according to Eq.2.1. The maximum activity among the activities from all the bonds attached to the junction is determined. Activity of each adjacent bond is divided by the maximum activity to give the relative activity of the corresponding bond. This can be expressed as

$$RA_i = \frac{A_i}{\max(A_i)} \quad (3.2)$$

Where,

RA_i = Relative Activity

A_i = Activity of the ith bond

As shown in Figure 3.2, activity sensors are attached to all the adjacent bonds, 1, 2 and 3 of 1- junction 'One'. The sensors have the same code shown in Figure 3.1. Each sends activity to the 'Max' block which determines the maximum of the activities among the bonds 1, 2 and 3. It then sends the maximum activity value to the activity sensors and

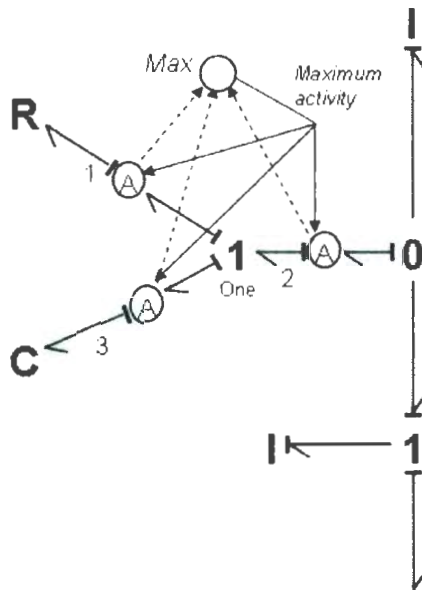


Figure 3.2: Relative activity calculation using bond graph

calculates the relative activity of the corresponding bond. 20SIM (2007) software has a built in 1-or 0-junction which can directly find the relative activities of the adjacent bonds attached to the junction.

3.1.3 Moving average of power index

Instead of defining activity according to Eq.2.1, moving average of power (MAP) can be used. MAP calculates a moving average of absolute power flow through a bond over a narrow time window as opposed to 'activity' which integrates absolute power over the

entire time span of the simulation. Since the absolute power flow is averaged within a moving time window it is called 'moving average'.

The equation is given by

$$MAP = \frac{\int_{t-T_0}^t |P(t)| dt}{T_0} \quad (3.3)$$

Where, t = Any instant of time

T_0 = Time window for averaging

$P(t)$ = Power flow through the bond

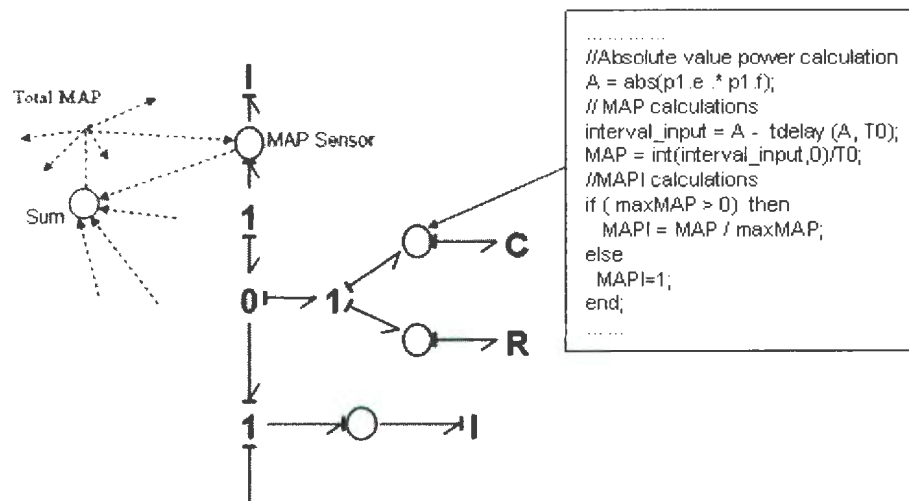


Figure 3.3: MAP index calculation using MAP sensors

Once the MAP is determined it is divided by total MAP of all the elements for any instant of time to find the MAP index of a bond. Figure 3.3 shows a bond graph model having

MAP sensors. The 'Sum' block sums the MAP signals from all the elements and sends back the total value to all the sensors. Dividing the MAP by the total, the moving average of absolute power index (MAPI) for each element is calculated. Sample code inside a MAP sensor is shown in Figure 3.3.

3.2 U signal

In this study 'U' is defined as a signal which is generated from a sensor that dictates when to remove an element from the model to obtain reduced complexity. A 'threshold' limit on the model reduction metric is established to obtain a reduced model. Activity index or MAP indices are summed from highest to lowest index order. Once its cumulative activity or MAP index exceeds the threshold, an element can be eliminated from the model. This elimination is indicated by the 'U' value. Code is written inside the sensors so that U=0 when an element is to be eliminated. Sample code inside an activity sensor that generates a 'U' signal is given below which uses the 20sim syntax.

```
.....  
// Activity  
A = int(abs(p1.e .* p1.f));  
//Activity index  
if (Atotal>0) then  
    AI=A/Atotal;  
else  
    AI=1;  
end;
```

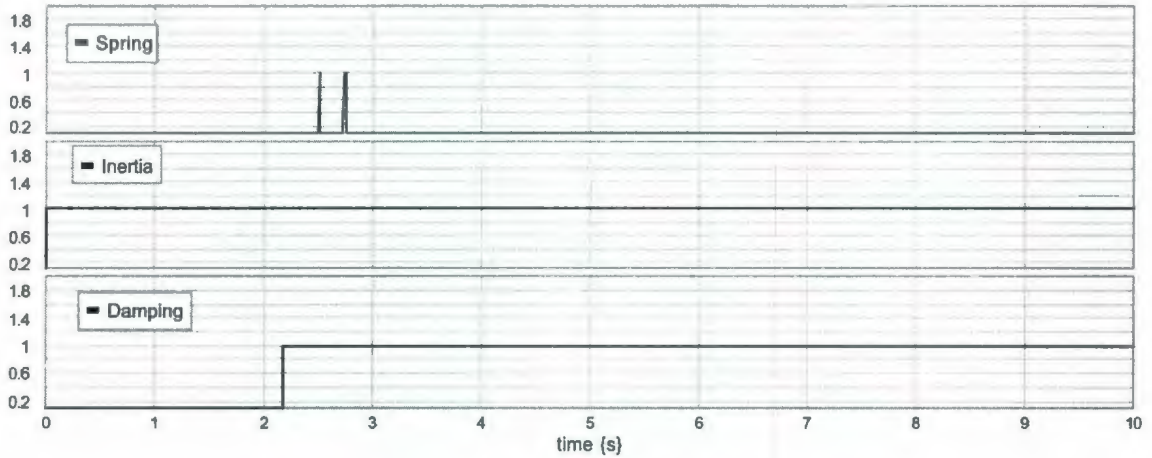
```
//U value
if (AI<threshold) then
u=0;
else
u=1;
end;
.....
```

An illustrative example is given here to show how activity index, relative activity and MAP can generate a ‘U’ signal. A simple mass-spring-damper system is analyzed as shown in Figure 3.4. The system is excited by an external force which is sinusoidal in

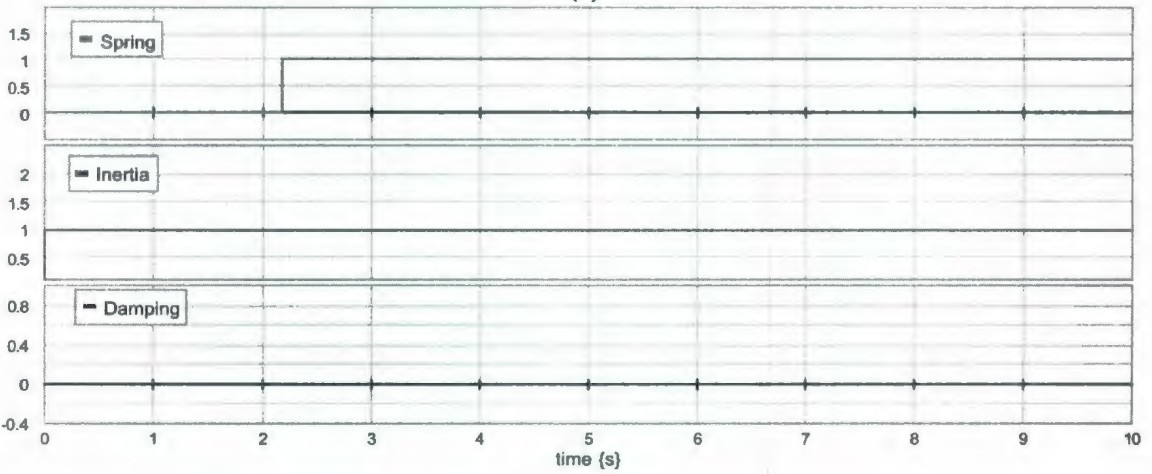


Figure 3.4: Schematic diagram and bond graph of a simple spring-mass-damper system

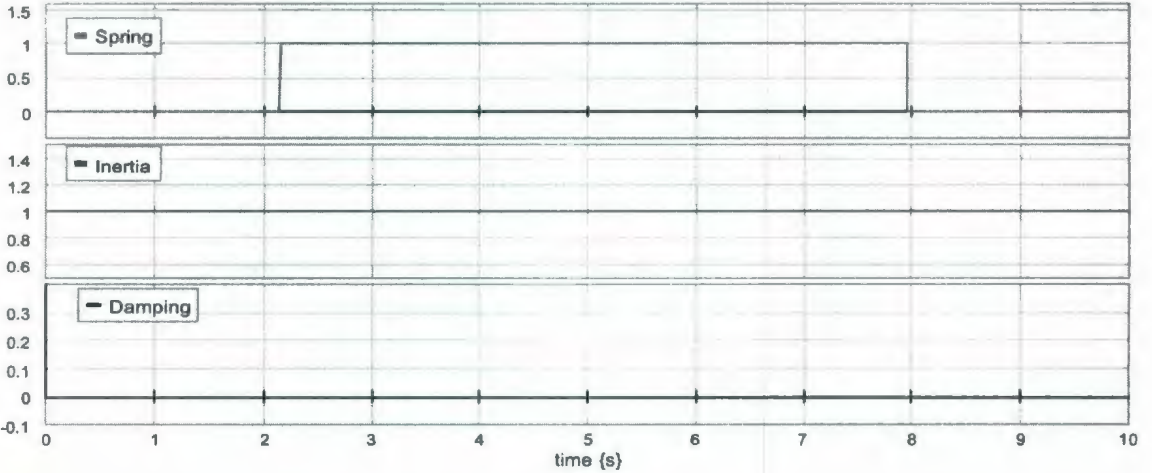
nature and is given by $F = 5 \sin(\omega t)$. The figure also shows the bond graph. The external force is varied with a frequency of 100 rad/s for the first 2 seconds, 10 rad/s for the next 2 seconds and again 100 rad/s thereafter. Therefore the system experiences a higher frequency input, then a lower frequency one, and again a higher frequency stage. All the three activity measuring methods described in this chapter are employed to find the ‘U’ value for all the elements in the system, i.e., spring, mass and damper. The resulting plot for all the metrics are shown in Figure 3.5. A threshold limit of 90% is set for all the cases.



(a)



(b)



(c)

Figure 3.5: (a) 'U' values using relative activity (b) 'U' values using activity index (c) 'U' values using MAPI

Activity index shows that the spring is insignificant in the higher frequency first stage, comes back on in the low frequency second stage and never goes off again. The MAPI shows the spring going off again in the higher frequency third stage, as it should. On the other hand, the spring remains unimportant for all the stages using relative activity, which seems incorrect. Inertia stays significant for all the three stages in every method. Damping goes off and stays off for all the stages using activity index and MAPI but it comes back on during second and third stage while the relative activity is used. Since MAPI can capture the fact that the spring becomes insignificant in the higher frequency third stage, which is not shown in the other methods, MAPI seems more responsive.

A step change in 'U' from 0 to 1 or vice versa, causes significant transient effects on the system response and can cause numerical instability. To overcome this problem 'smoothing' is done to linearly change 'U' from 1 to 0 or 0 to 1 with a finite slope. Sample code from the sensors is given below.

```

.....

AP = abs(eIb*fIb);           % absolute value of power at time t
MAP = integrate(AP(t)-AP(t-To))/To; % moving average over
                                   % user-defined time span To

MAPI = MAP/MAPtotal;         % MAPtotal from summation block
if MAPI > e then              % e is user-specified threshold, element active
if U < 1 then                  % MAPI greater than threshold but
                                   % U transitioning from 0 to 1
tevent = t - t01;             % t01 is time at beginning of
                                   % transition of U from 0 to 1
U = (tevent/tspan)*1;        % tevent describes how long U

```

```

% has been transitioning
% tspan is time interval over
% which U transitions

else
U = 1; % U = 1 if MAPI is greater than threshold and
% transition of U from 0 to 1 is completed
t10 = t; % t01 marks beginning of transition interval
% of U from 1 to 0 if MAPI falls below c on
% next time step

end;
else % routine falls to here if MAPI less than threshold
if U > 0 then % transition of U from 1 to 0 ongoing
tevent = t - t10;
U = 1 - (tevent/tspan)*1;
else
U = 0;
end;
.....

```

In the following chapters it will be shown how these metrics are used to generate reduced models automatically as system inputs are changed. Case studies will show how MAPI is more accurate than the other metrics to find the minimum number of elements in the model required to predict system response.

Chapter 4

Bond Graph Switches

Switches are employed as to allow or prevent an effort or flow through a bond. Thereby a zero effort or flow is output from a non-contributing element or bond to the rest of the system. Therefore a proper model [Section 1.2] can be generated that includes only the significantly contributing elements or sub-systems for the system dynamics. Switches for three types of bonds according to nature of causality are discussed. The switches are,

- Switches for causally weak bonds
- Switches for casually strong bonds
- Switches for internal bonds.

4.1 Review of causality

This section describes causality issues in bond graphs. Causality determines if effort (e) or flow (f) is the output from a bond graph element. It basically gives the cause-effect relation between the effort and flow. The casual stroke (short perpendicular line), a single mark on the bond, indicates the causality. As shown in Figure 4.1 causal stroke presents on the side of A element which means B element is determining the effort

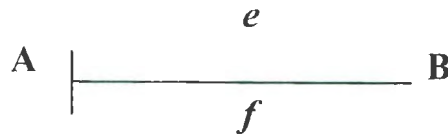


Figure 4.1: Causality assignment of bond graph elements

e and it results in a flow f response from the A element . There are two types of causality for the storage elements (C and I), integral causality and derivative causality. Integral causality relation integrates the cause to generate the effect. For example if flow is integrated over the specified time period to generate displacement and then effort in the case of a capacitive C element is found and the constitutive law has an integral form. On the other hand if the time derivative of the effort is taken to generate the flow, the casual relation is in differential form which results in derivative causality. Derivative causality gives the constitutive equations in implicit form, making them numerically difficult to solve. Therefore integral causality is preferred over derivative causality.

The resistive element R doesn't have an integral or differential form of constitutive relation. Therefore they can have either type of causality, conductive or resistive. Causal strokes for the source elements (S_e or S_f) are fixed . Table 4.1 gives a list of bond graph elements and their casual relationships [11].

Table 4.1: Causality assignment for graph elements

Elements	Acausal form	Causal form	Causal Relation
Effort source	$S_e \longrightarrow$	$S_e \longrightarrow \dashv$	$e(t) = F(t)$
Flow source	$S_f \longrightarrow$	$S_f \dashv \longrightarrow$	$f(t) = F(t)$
Resistor	$R \longleftarrow$	$R \longleftarrow \dashv$ $R \dashv \longleftarrow$	$e = \Phi_R(f)$ $f = \Phi_R^{-1}(e)$
Capacitor	$C \longleftarrow$	$C \longleftarrow \dashv$ $C \dashv \longleftarrow$	$e = \Phi_C^{-1} \left(\int f dt \right)$ $f = \frac{d}{dt} \Phi_C(e)$
Inertia	$I \longleftarrow$	$I \longleftarrow \dashv$ $I \dashv \longleftarrow$	$e = \frac{d}{dt} \Phi_I(f)$ $f = \Phi_I^{-1} \left(\int e dt \right)$

4.2 Switches for causally weak bonds

Flow to a 0-junction and effort to a 1-junction are considered as weakly causal inputs. Switching such bonds is done with a modified modulated transformer, *MTF* [Section 1.3]. The modulus of the *MTF* dictates mode of the bond as 'on' or 'off'. Once it gets a 1 value then the mode is 'on' and the flow or effort can pass. If the modulus gets a 0 value which is an 'off' mode, zero flow or effort comes from the *MTF*. This is how all the switching for causally weak bonds is done. Table 4.2 provides a list of causally weak switches.

For example the first switch of Table 4.2 is shown for a capacitive element C from which effort is a causally weak input to a 1-junction. Switching is done with a MTF as described above. The third column of the table gives the equation for the MTF that lets the flow go from the 1-junction to the C element. Since there is no 'r' in the flow equation, the flow

Table 4.2: Switches for causally weak bonds

Causally weak bonds	Switched bond	Equations
$1 \vdash \rightarrow C$	$1 \vdash \xrightarrow{1} MTF \vdash \xrightarrow{2} C$	$P_2.f = P_1.f$ $P_1.e = r P_2.e$ $r = 0$ for OFF $r = 1$ for ON
$0 \rightarrow \dashv I$	$0 \xrightarrow{1} \dashv MTF \dashv \xrightarrow{2} I$	$P_2.e = P_1.e$ $P_1.f = r P_2.f$ $r = 0$ for OFF $r = 1$ for ON
$1 \vdash \rightarrow R$	$1 \vdash \xrightarrow{1} MTF \vdash \xrightarrow{2} R$	$P_2.e = P_1.e$ $P_1.f = r P_2.f$ $r = 0$ for OFF $r = 1$ for ON
$0 \rightarrow \dashv C$	$0 \xrightarrow{1} \dashv MTF \dashv \xrightarrow{2} C$	$P_2.e = P_1.e$ $P_1.f = r P_2.f$ $r = 0$ for OFF $r = 1$ for ON
$0 \rightarrow \dashv R$	$0 \xrightarrow{1} \dashv MTF \dashv \xrightarrow{2} R$	$P_2.e = P_1.e$ $P_1.f = r P_2.f$ $r = 0$ for OFF $r = 1$ for ON
$\vdash \rightarrow I$	$1 \vdash \xrightarrow{1} MTF \vdash \xrightarrow{2} I$	$P_2.f = P_1.f$ $P_1.e = r P_2.e$ $r = 0$ for OFF $r = 1$ for ON

is unaffected. Later it will be shown how this facilitates ‘activity’ calculation. On the other hand ‘r’ is present in the effort equation which gives effort at port 1 ($P_1.e$) as the port 2 effort ($P_2.e$) multiplied by ‘r’. As soon the modulus ‘r’ becomes 0 the effort to the 1-junction becomes 0 and the ‘off’ mode is achieved.

4.3 Switch for causally strong bonds

4.3.1 Strong *I* element switch

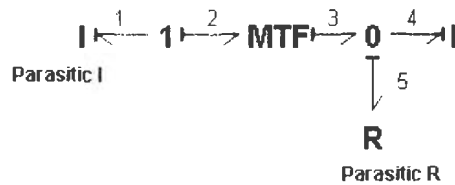


Figure 4.2: Switch arrangement for causally strong *I* element

An *I* element is causally strong at a 1-junction if it is in preferred integral causality. As shown in Figure 4.2 parasitic *R* and *I* elements [11] are introduced for switching such a bond. The *MTF* has the following equations.

$$P_3.f = P_2.f \quad (4.1)$$

$$P_1.e = r P_2.e \quad (4.2)$$

As soon the modulus r becomes 0 it is 'off' and for a value of 1 it is 'on'. The modulus value comes from any kind of metric sensor [see Chapter 3]. The following sections describe how these parasitic elements work to facilitate switching.

4.3.1.1 Parasitic R element

Since flow to a 1-junction is always causally strong, the flow cannot be switched off using a MTF only as in the case of causally weak bond. Setting 0 flow to a 1-junction makes all the other bond flows equal to 0, whereas the goal is to remove the effect of only one element. Using a 0-junction with a parasitic R [11] element changes the flow out to the 1-junction into an effort output which is causally weak. This arrangement also allows element importance [see Chapter 3] calculation when the bond is switched 'off'.

Now it will be shown that using a parasitic R does not significantly affect system dynamics. As shown in Figure 4.3, first, a 0-junction is added and then the parasitic R is attached. This result in effort-out causality to the 1-junction attached to bond 3.

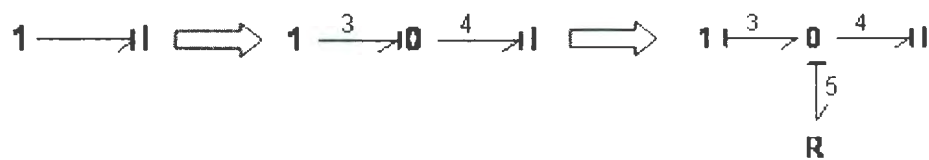


Figure 4.3: Adding 0-junction and parasitic R element to a strongly casual I element

Adding a 0-junction to a bond has no effect on it .As soon the 0-junction is added the flow equation becomes

$$f_3 = f_4 \quad (4.3)$$

When the parasitic R is added the flow equation is

$$f_3 = f_4 + f_5 \quad (4.4)$$

Again,

$$\begin{aligned} e_5 &= Rf_5 \\ f_5 &= \frac{e_5}{R} \end{aligned} \quad (4.5)$$

Substituting the value of f_5 in (4.4) from (4.5),

$$f_3 = f_4 + \frac{e_5}{R} \quad (4.6)$$

If R gets a very large value,

$$\frac{e_5}{R} \approx 0 \quad (4.7)$$

Therefore, Eq.4.6 approximates Eq.4.3. Hence, using a large parasitic R with a 0-junction gives the same output to 1-junction as it would be without the parasitic R .

4.3.1.2 Parasitic I element

The parasitic I element [11] in the switch is used as a causality generator which retains the flow causality to the 1-junction. It will be illustrated that parasitic I element with appropriate value doesn't significantly affect the system dynamics.

In this example C and R elements attached to a 1-junction are used. The R element generates a flow causality to the 1-junction. It will be shown that the system response remains the same once a parasitic I element is introduced that acts as a causality generator that gives flow causality to the 1-junction and thus changes the causality of the R element into an effort-out causality at the 1-junction.

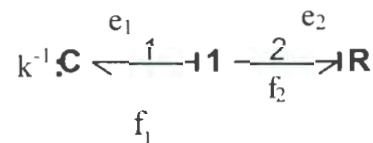


Figure 4.4: Causally strong R element attached to a 1-junction

From the bond graph shown in Figure 4.4 the following flow and effort equations can be written.

$$\begin{aligned}
 f_1 &= \dot{q} = f_2 \\
 e_1 + e_2 &= 0 \\
 \Rightarrow kq + Rf_2 &= 0 \\
 \Rightarrow kq + R\dot{q} &= 0 \\
 \Rightarrow \dot{q} &= -\frac{kq}{R}
 \end{aligned} \tag{4.8}$$

Using a Laplace Transformation,

$$sQ - q(0) = -\frac{k}{R}Q$$

$$\Rightarrow \left(s + \frac{k}{R}\right)Q = q(0)$$

Setting an initial condition $q(0) = q_0$, we get,

$$\Rightarrow \left(s + \frac{k}{R}\right)Q = q_0$$

$$\Rightarrow Q = \frac{q_0}{\left(s + \frac{k}{R}\right)} \quad (4.9)$$

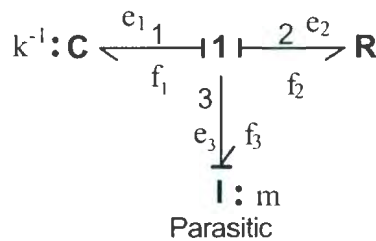


Figure 4.5: Adding parasitic I element

A parasitic I element is added in the bond graph of Figure 4.4 and is shown in Figure 4.5.

The following flow and effort equations are obtained.

$$f_1 = f_2 = f_3 = \dot{q} \quad (4.10)$$

$$e_1 + e_2 + e_3 = 0 \quad (4.11)$$

Now,

$$e_1 = kq$$

$$e_2 = Rf_2 = Rf_3 = R\frac{P}{m}, \text{ since } f_3 = \frac{P}{m}$$

$$\text{and } e_3 = \dot{p}$$

Putting these into Eq.4.11 the following equation is found,

$$\dot{p} = -kq - R\frac{P}{m}$$

Using a Laplace transformation,

$$sP - p(0) = -kQ - R\frac{P}{m}$$

Setting initial condition $p(0) = 0$, we get

$$\begin{aligned} sP &= -kQ - R\frac{P}{m} \\ \Rightarrow \left(s + \frac{R}{m}\right)P + kQ &= 0 \\ \Rightarrow P &= \left(-\frac{k}{s + \frac{R}{m}}\right)Q \end{aligned} \tag{4.12}$$

Again,

$$\dot{q} = f_3 = \frac{P}{m}$$

Using a Laplace transformation,

$$sQ - q(0) = \frac{P}{m}$$

(4.13)

$$\Rightarrow sQ - q_0 = \frac{P}{m}$$

Putting the value of P from Eq.4.12 into Eq.4.13 we get,

$$\begin{aligned} \Rightarrow sQ - \frac{1}{m} \left(-\frac{k}{s + \frac{R}{m}} \right) &= q_0 \\ \Rightarrow Q &= \frac{q_0}{s + \frac{k/m}{s + R/m}} \\ \Rightarrow Q &= \frac{q_0}{s + \frac{k}{sm + R}} \end{aligned}$$

If $m \approx 0$ then,

$$Q = \frac{q_0}{\left(s + \frac{k}{R} \right)} \quad (4.14)$$

This is the same equation as Eq.4.9 where no parasitic element was used. Thus using a very low value for parasitic I , the system response remains approximately the same.

4.3.2 Other causally strong bond switches

The following table summarizes some more strong bond switches, namely for strong C at 1-junction, strong R at 1-junction and 0-junction. Equations for these switches can be derived in the same way as described in Section 4.2.1.

Table 4.3: Causally strong bond switches

$1 \longrightarrow R$	$ \begin{array}{c} I_{per_low} \\ I \longleftarrow 1 \longrightarrow MTF \longrightarrow 0 \longrightarrow R \\ \downarrow \\ R \\ R_{per_hi} \end{array} $
$0 \longrightarrow C$	$ \begin{array}{c} C_{per_hi} \\ C \longleftarrow 0 \longrightarrow MTF \longrightarrow 1 \longrightarrow C \\ \downarrow \\ R \\ R_{per_low} \end{array} $
$0 \longrightarrow R$	$ \begin{array}{c} C_{per_hi} \\ C \longleftarrow 0 \longrightarrow MTF \longrightarrow 1 \longrightarrow R \\ \downarrow \\ R \\ R_{per_low} \end{array} $

4.4 Internal bond switch

Internal bonds are the bonds between two consecutive junctions. When such bonds are causally weak, a switch can be implemented using a simple modified *MTF* similar to those used in case of weak bonds. Table 4.4 summarizes such a switch and corresponding equations. This research excludes the issue of causally strong internal bond.

Table 4.4: Switch for internal bond

Internal Bond	Switched bond	Equations
$1 \longrightarrow 0$	$1 \xrightarrow{1} \text{MTF} \xrightarrow{2} 0$	$P_2.f = P_1.f$ $P_1.e = r P_2.e$ $r=0$ for OFF $r=1$ for ON

Switches described in this chapter will be used with element importance metrics that determines when to switch 'on' or 'off' an element. Details are discussed in the following chapters.

Chapter 5

Half and Quarter Car Case Studies

This chapter studies the application of the switches [Chapter 4] with a combination of metrics for element importance [Chapter 3]. Case studies with half car and quarter car models are done. The half car model studies, Section 5.1 to Section 5.4, reproduces the results of Kypuros and Longoria [9] with the half car model but instead of generating separate reduced models [Section 2.2] it can continuously switch between reduced models and therefore automation for generating variable-complexity model is obtained. Section 5.5 uses a quarter car model from Louca and Stein [8] to demonstrate another case study with switching.

5.1 Half car case study

Section 5.1.1 describes the previous research findings with variable complexity models where a maneuver of a half car model was studied. Section 5.1.2 reproduces the responses as in [9] but it uses activity sensors that continuously monitor activity of the elements in the model whereas [9] only takes activity during pre-defined intervals.

Section 5.1.3 generates the reduced models and it confirms the proof of concept as stated in [9] i.e., reduced models provide computational savings.

5.1.1 Results of prior research into variable complexity half-car modeling

Kypuros and Longoria [9] described an approach to increase the simulation efficiency of a vehicle mission. It uses a variable complexity method to build the reduced models. Element activity is measured to derive the reduced model using the power based method of Louca et al. [2] that quantifies the contribution of each element to the system dynamics. To find the activity, integral of absolute power flow in and out of an element over a specified time span is calculated. Normalizing each element activity by the total activity, activity index is determined which is a measure of relative importance of an element to the overall activity [Section 3.1]. Activity index is used to rank the contribution of elements to system dynamics. A threshold (percentage of total activity) is specified to represent the minimum level below which an element's contribution to overall system dynamics is considered negligible. The reduced model is obtained by augmenting elements from highest to lowest rank until the cumulative index exceeds the specified threshold. This approach is applied to a half car model. Four different frequencies of road input are used for four different stages. The reduced model for each stage is derived from the bond graph of the original model by removing the least active elements. The original model and the reduced model for each stage are simulated. The

results show that the reduced model can reasonably predict the system dynamics and it can reduce the simulation steps significantly, thus making the simulation more efficient. Model reductions, and changing from one reduced model to another, are done with a *priori* knowledge of input changes but not automatically.

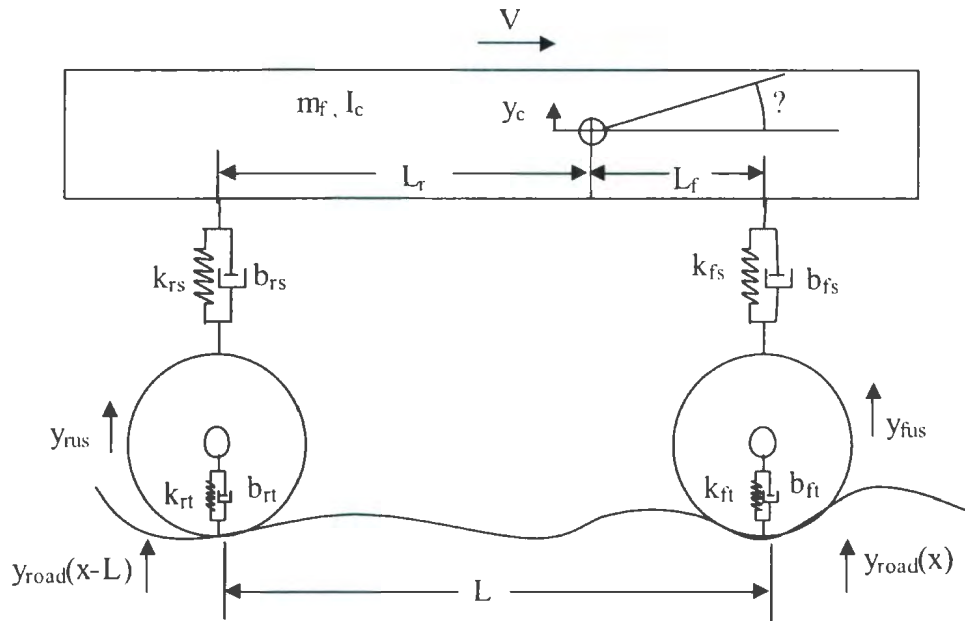


Figure 5.1: Schematic diagram of the half car model

Figure 5.1 shows the schematic diagram of the half car model taken from [9] and Table 5.1 gives the parameter values for different elements of the half car model. The four stages include four different road input frequencies: 10 rad/sec for 3.14 second (1st stage), 20 rad/sec for 3.14 seconds (2nd stage), 100 rad/sec for 1.26 seconds (3rd stage) and 10 rad/sec (4th stage) for another 3.28 seconds. Road input is given as $1.5\cos(\omega t)$ where ω is the frequency in radians/second and t is time in seconds.

Table 5.1: Parameter values for the elements of the half car model

Elements	Symbol	Parameter value
Translational velocity	V	72 kph
Distance between the tires	L	2.7 m
Longitudinal distance between centre of gravity and rear unsprung mass	L_r	1.6m
Longitudinal distance between centre of gravity and front unsprung mass	L_f	1.1m
Sprung mass	m_s	1700 kg
Rotational inertia	I_c	2704 kg-m ²
Front unsprung mass	m_{fus}	100 kg
Rear unsprung mass	m_{rus}	80 kg
Front suspension stiffness	k_{fs}	30 kN/m
Rear suspension stiffness	k_{rs}	30 kN/m
Front tire stiffness	k_{ft}	200 kN/m
Rear tire stiffness	k_{rt}	200 kN/m
Front suspension damping	b_{fs}	750 N-s/m
Rear suspension damping	b_{rs}	750 N-s/m
Front tire damping	b_{ft}	125 N-s/m
Rear tire damping	b_{rt}	125 N-s/m

The full bond graph model is shown in Figure 5.2. 20sim 4.0 [2007] is employed. Here the activity sensors are used to measure the activity of each element. The wave generator generates the four different frequencies for the previously specified time intervals. There is a time delay between the road input frequencies of the front and rear wheel which is generated by the delay signal. Activity of each element is measured for the four time

Table 5.2: Activity, activity index and cumulative activity index at the end of stage 2

Element	Activity	Activity Index	Cumulative Activity
<i>kfs</i>	1844	0.238300	0.238300
<i>krs</i>	1308	0.169178	0.407478
<i>brs</i>	848	0.116713	0.524191
<i>bfs</i>	902	0.109702	0.633893
<i>m_fus</i>	719	0.101173	0.735066
<i>ms</i>	783	0.092915	0.827981
<i>m_rus</i>	719	0.082059	0.910040
<i>lc</i>	634	0.043476	0.953516
<i>kft</i>	336	0.027836	0.981352
<i>krt</i>	215	0.017900	0.999252
<i>bft</i>	3.25	0.000421	0.999673
<i>brt</i>	2.5	0.000328	1.000001

Figure 5.3 demonstrates the plots of displacement of the sprung mass (y_c), the pitch angle (θ), the rear unsprung mass displacement (y_{rus}) and the front unsprung mass displacement (y_{fus}) for the four stages together from the full model bond graph. The plots show the similar system response as in [9].

The wave generator cannot be used to run the reduced models sequentially as after running each stage for the specified time span, the end results must be stored as initial conditions for the next stage. 20sim 4.0 can store the end states of the elements but not the end state of the signals of the wave generator. To overcome this difficulty the full

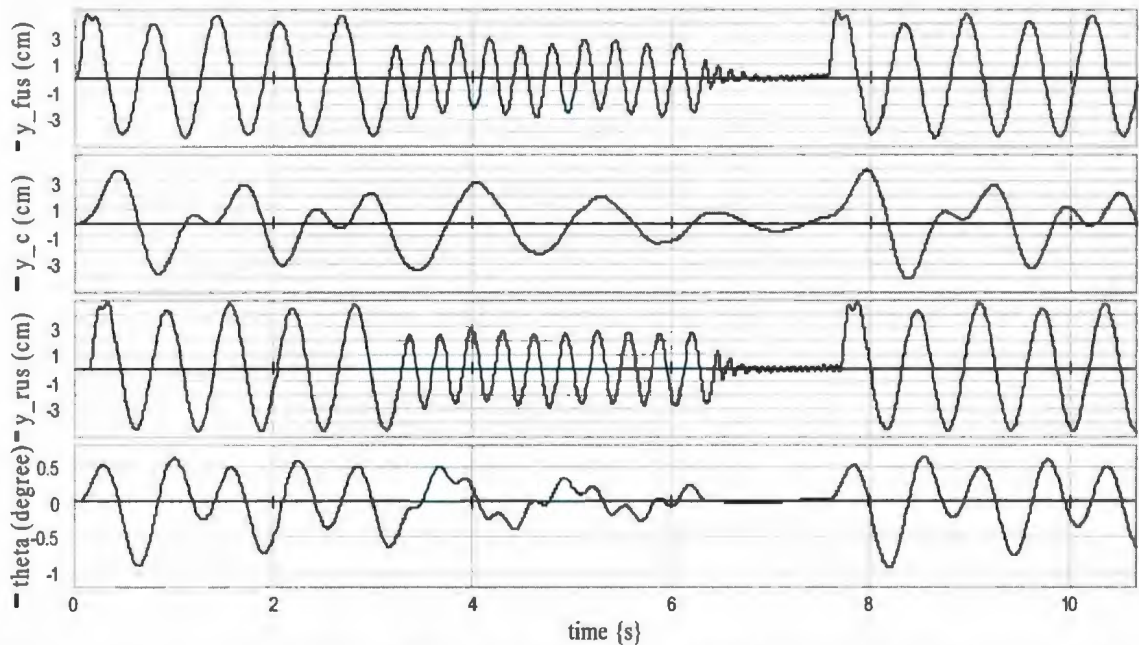


Figure 5.3: System response of four individual-stage MORA-reduced models executed sequentially

model is run at first and the generated road input signal data is stored in a data file .The full model is run for the four stages together, then for each stage separately and finally with the reduced model for each stage separately. The plot results are shown in Figure 5.4. Backward Euler integrator with step size: 0.01 and relative tolerance of $1e^{-005}$ was used. The plots are reasonably similar for the three cases. Still discrepancies are there, especially with the third stage since in the reduced model the rotational inertial element is completely removed .In the full model it remains in the model and contributes a displacement, though not significantly. Simulation time and steps are recorded for the full model for each stage separately and for the reduced model for each stage. The results are given in Table 5.3 which shows that reduced model can save simulation time and steps.

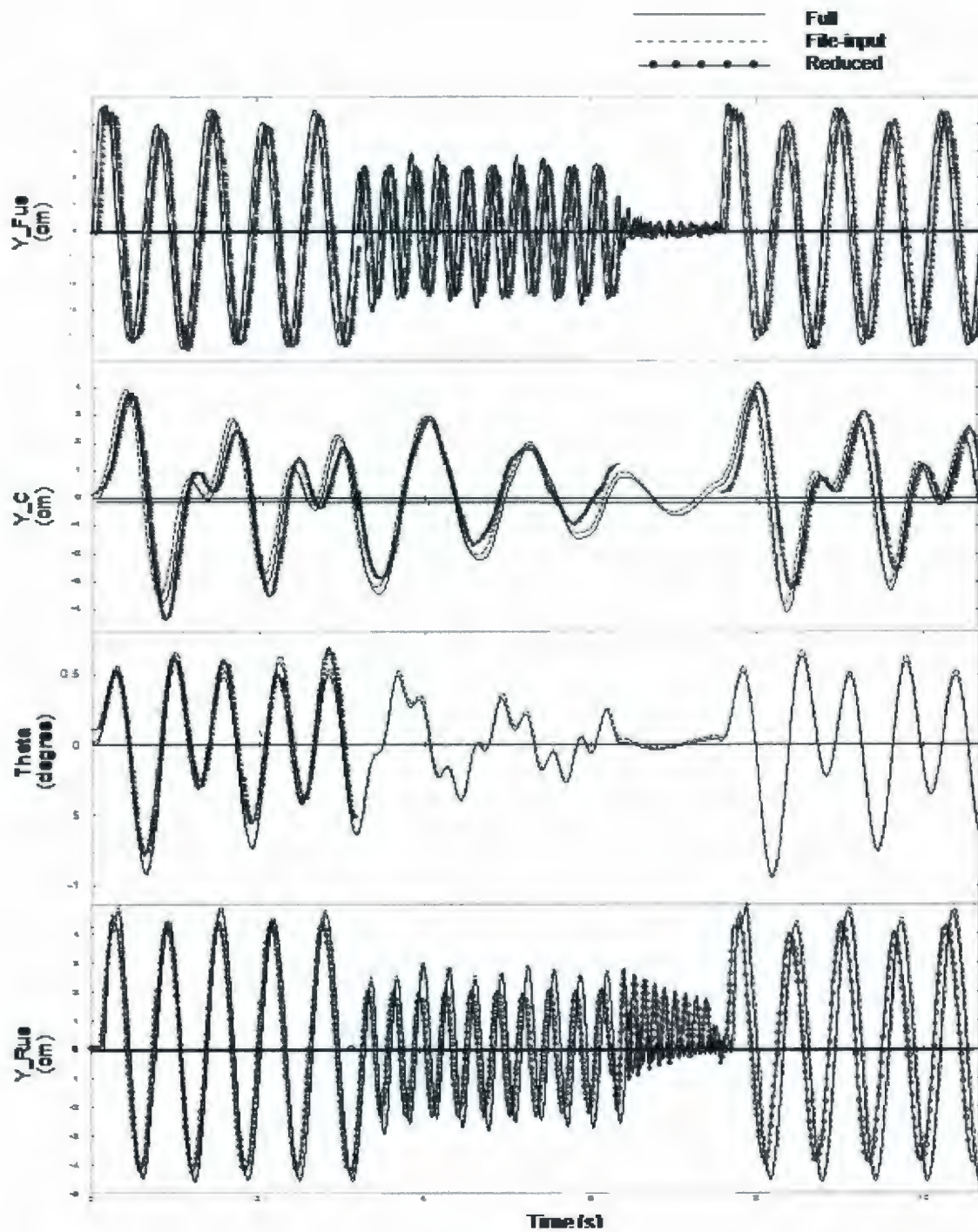


Figure 5.4: Response of full model running together (all stages) and separately (for each stage), and reduced model (for each stage)

The result shows that the step and time reduction of the half car model according to Kypuros and Longoria [9] is valid since step and time savings are observed. Limitations of this approach to variable-complexity modeling, which this thesis attempts to address, are

- the user requires prior knowledge of when the model complexity must be assessed
- the user must manually switch from one model to another.

Table 5.3: Simulation time and steps for full and reduced model for each stage

	Equations, Variables, Independent States for Full Model	Equations, Variables, Independent States for Reduced Model		Full Model	Reduced Model
Stage 1	38,25,13	33,22,11	Steps	5356	4729
			Time	0.11	0.109
Stage 2		25,18,7	Steps	5356	3466
			Time	0.133	0.091
Stage 3		19,12,7	Steps	2144	1387
			Time	0.096	0.075
Stage 4		26,15,11	Steps	5356	4726
			Time	0.128	0.107

5.2 Continuous element importance monitoring methods

Three continuous element importance monitoring methods are described in this section. These metrics can find when model switching should occur. ‘U’ values [Section 3.2] are determined to continuously monitor importance of an element in the model. These methods are

- Activity
- Global MAP
- Local MAP

5.2.1 Activity based metric

The activity sensors calculate the activity of the bond connected to a certain element. It uses the ‘activity’ equations of Louca *et al.* [2] described in Section 3.1.1. The calculated activity signals are sent to the ‘Sum_activity’ block that adds up the activities from the activity sensors of all the elements and the sum of all the activities is sent back to each element to calculate the activity index for each element according to Eq. 2.2.A “Threshold” block sends threshold signals to all the activity sensor blocks. The activity sensor block contains code as shown in Figure 5.2 which returns a 0 value for ‘U’ as the activity index for a certain element goes below the threshold value. If the activity index value remains above the threshold the ‘U’ value becomes 1. A 95% threshold limit is taken. The resultant ‘U’ values plot is shown in Figure 5.5.

According to this plot front and rear suspension damping (brs) never goes off. On the other hand, front and rear tire damping (bft and brt) stays off and never comes on. Front and rear suspension stiffness (kfs and krs) never goes off. Front and rear tire stiffness (kft and krt) goes off at the middle of the first stage, comes back on at third stage and stays on for rest of the time. Front unsprung inertia (m_{fus}) never goes off. Sprung mass (m_s)

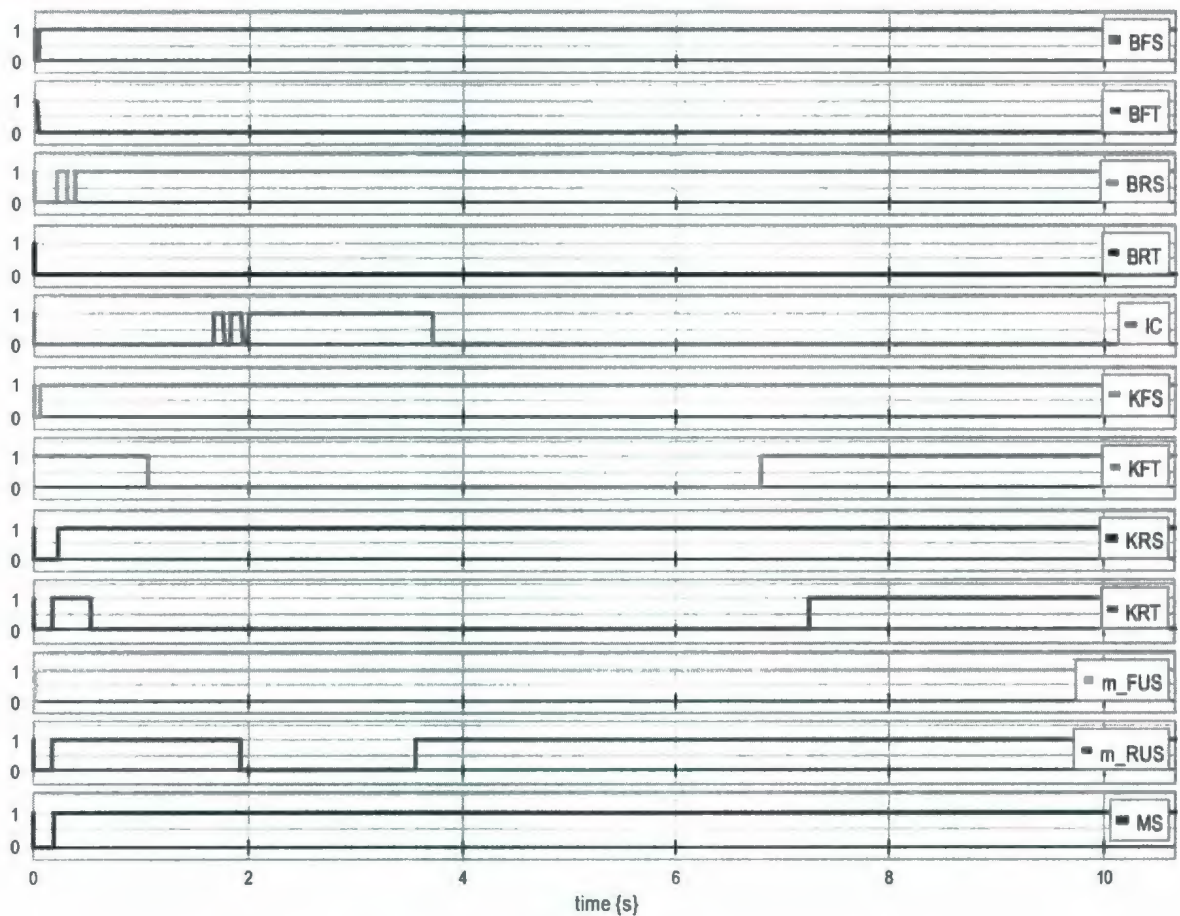


Figure 5.5: 'U' values of the half car model using activity metric

goes off for a very short duration at the first stage and then comes back on for rest of the time. Rear unsprung inertia (m_{rus}) goes off for at middle of the first stage and stays on

for rest of the stages. Rotational inertia (I_c) stays on starting from the middle of the first stage and the very beginning of the second stage. It remains off for the rest of the time. The activity metric based plot is compared with a plot of U values according to [9] which is shown in Figure 5.6. This figure illustrates a significant difference between the 'U' values that can be generated according to [9] and what is found from activity calculating sensors. No other value except for the front unsprung inertia matches. Considering the

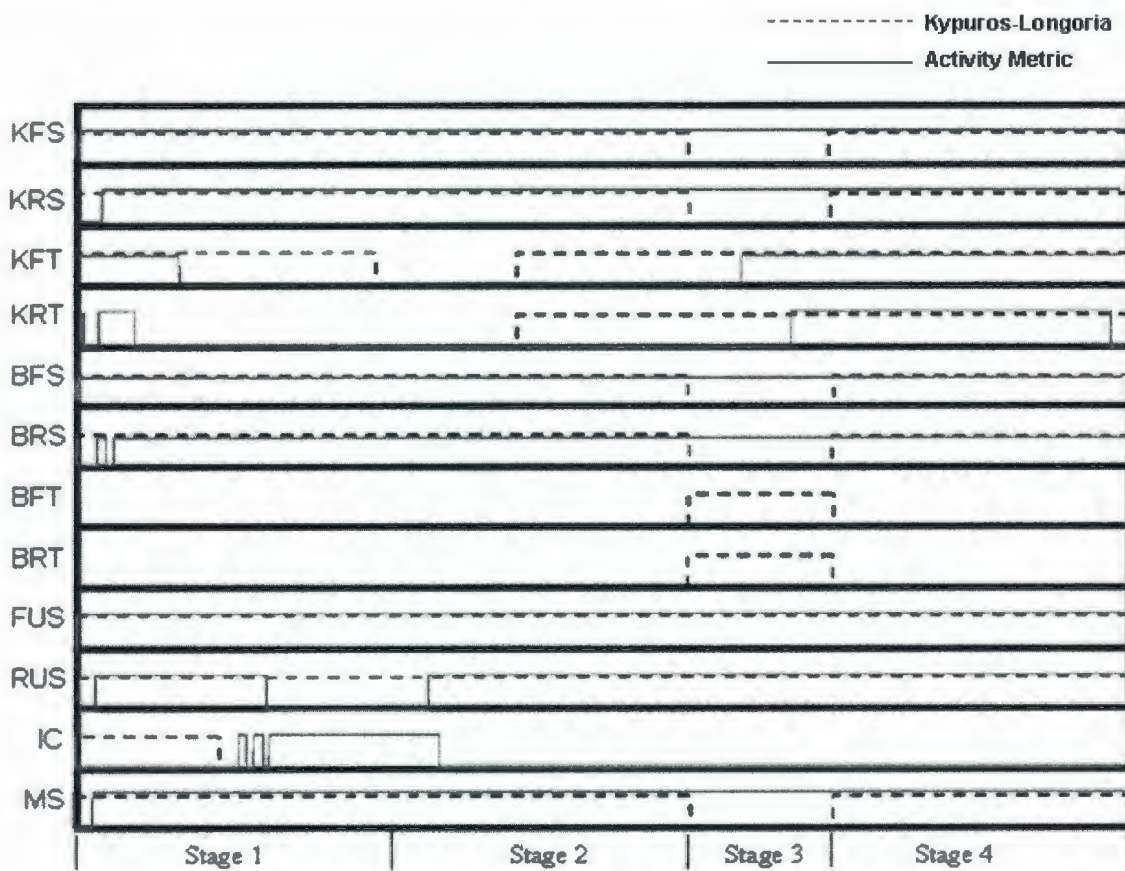


Figure5.6: Comparing 'U's from Kypuros and Longoria [9] and continuous activity based metric

case of sprung mass, Kypuros and Longoria [9] found that the sprung mass goes off at high frequency stage and stays on at low frequency stages whereas activity sensor 'U'

suggests that it should never go off. The probable reason for such discrepancy is that this activity sensor integrates the activity for entire time span and though a highly active element becomes inactive for a certain period, its present activity calculation includes all prior activity values. This shows the element activity still 'high' though it is low over a shorter time span. A more responsive metric is required, that tracks the instantaneous contribution of individual elements as opposed to the cumulative contribution of elements.

5.2.2 Global MAP based metric

To resolve the problem described in the preceding section, the moving average of absolute power (MAP) [Section 3.3] is introduced as an activity calculating metric for the half car model. Unlike the activity metric, it uses a shorter time interval to calculate the 'activity' of a element by using moving average of absolute power flow. It uses the same steps described in the previous section to find the 'U' value. Now the activity measuring sensors as shown in Figure 5.2 has a code to calculate moving average of absolute power for a certain time span. They are termed as "MAP" sensors instead of 'activity sensor'. Following the same method for calculating the activity index in the previous section, it calculates 'MAP index' for each element, i.e., sums the entire MAPs and divides the individual MAP by the total MAP. This total MAP is termed as 'global MAP' as it includes the MAP's of all the elements model-wide. Sample code inside a MAP sensor is given below

```

.....

// Absolute power
    A = abs(p1.e .* p1.f);
    interval_input = A - tdelay (A, T0);

// Calculating moving average of absolute power
    MAP = int(interval_input,0)/T0;

// MAP index calculation
if ( maxMAP > 0) then
    AI = MAP / maxMAP;
else
    AI=1;
end;

// U determination
    if (AI<port1) then
        u=0;
    else
        u=1;
    end;
.....

```

The time span to calculate MAP is taken as 0.8. A 95% threshold is used. Figure 5.7 gives the resultant plot of ‘U’ values for the model and compares them with [9]. It shows better agreement than Figure 5.6 above. For example sprung mass goes off for both the cases during the higher frequency third stage as it should. Activity based metric could not show this. On the other hand, the front and rear tire damping comes back on at the third stage according to [9] but these never stay on in the MAP based metric. These elements are very near to the Kypuros and Longoria [9] activity threshold, so slight differences in

output due to different numerical integrators could explain why they stayed off during the MAP-based analysis. ‘U’ values generated by MAP sensors take transients into account when input frequency changes. Kypuros and Longoria [9] didn’t take into account the fact that if frequency changes at time 3.14 second, then the next sub-model may not be required immediately – it may be until 3.20 seconds before transients settle, and the 2nd stage of the Kypuros and Longoria [9] sub-model would remain valid. Moreover the ‘U’s according to [9] are plotted only taking the end point activity value of each stage. Activity index is not monitored at any other point of a stage whereas the MAP based metric monitors and gives the ‘U’ for every instance of all the stages. Thus it gives a better insight of what is important or not for the system dynamics.

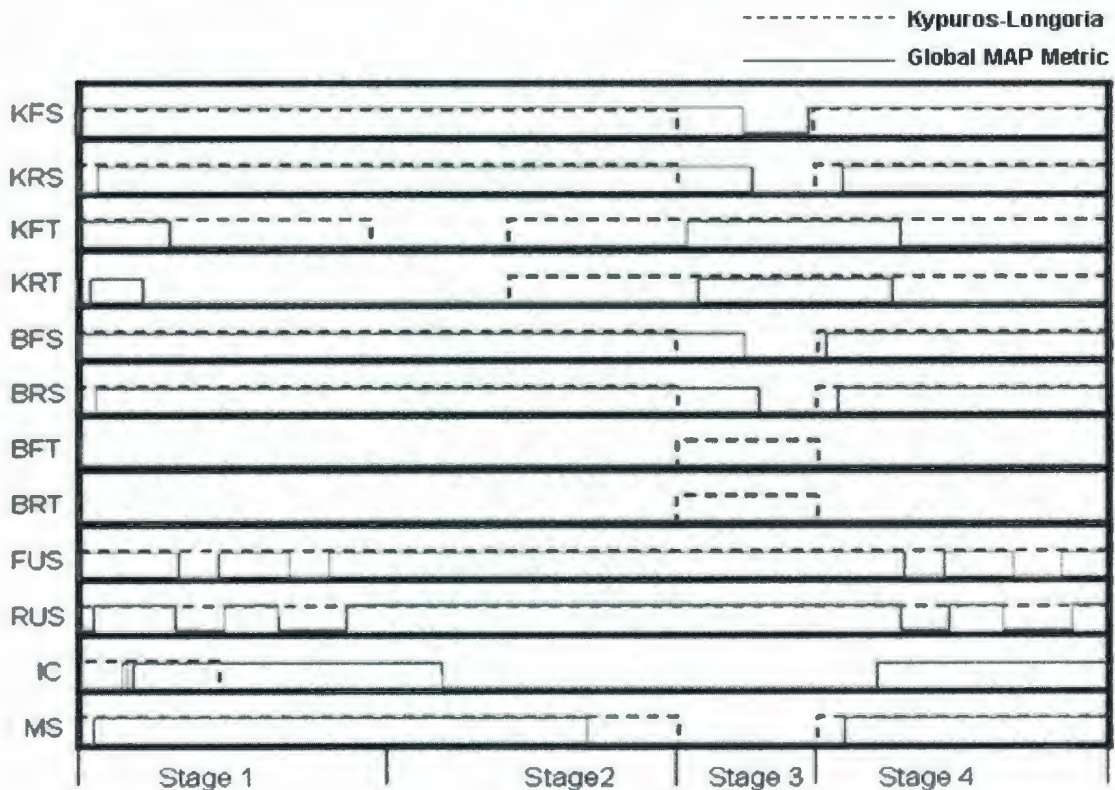


Figure 5.7: Comparing ‘U’s from Kypuros and Longoria [9] and MAP based metric

5.2.3 Local MAP based metric

Another method of searching importance of an element is finding relative importance of a bond with respect to other bonds attached to a 1-junction or 0-junction. Monitoring importance of an element 'globally' was described in the previous section whereas this section studies how well it can be monitored 'locally'. It is termed as 'local MAP' since this compares the importance of an element locally at the junction.

MAP sensors are put on each adjacent bond attached to a junction as in Figure 5.8, and the 'local MAP' is defined as the ratio of the bond MAP to the maximum bond MAP at that junction. Therefore, each bond at a junction will have a different local MAP, with the highest-MAP bond having a local MAP value of one. There are two types of sensors used. The 'solid' sensor in Figure 5.8 is used for bonds that lead to energy storage and dissipative elements (external junction structure bonds) and 'dotted' sensors are used for 'internal bonds' i.e. bond between two junctions. The solid sensor has code that calculates both MAP and relative MAP whereas dotted sensor contains code that only calculates MAP of the internal bond. The sensors of the adjacent bonds attached to a 1- or 0- junction send MAP to the 'Max_MAP' block as shown in Figure 5.8 which finds the maximum MAP among the adjacent bonds. Then the 'Max_MAP' block sends back the maximum 'local MAP' to each bond's MAP sensor which calculates the 'relative MAP' of the bond by dividing its MAP by 'maximum MAP'. U values are generated as described in the previous section, i.e., if relative MAP goes below the threshold limit then

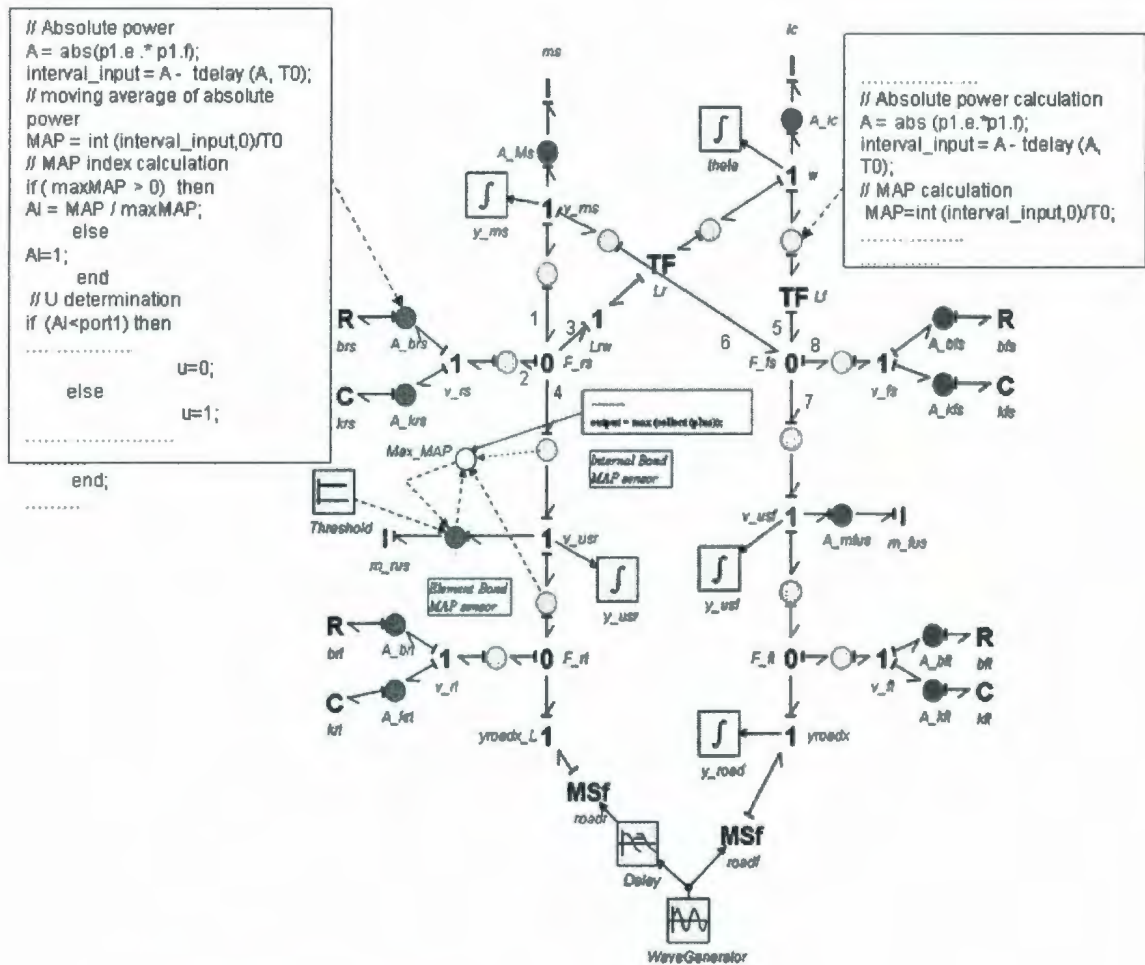


Figure 5.8: Local MAP metric for half car model

it goes to 0, and if it stays above the threshold then the U value remains at 1. But instead of U making a step change from 1 or 0 value as described in the previous section, code is used to change the U value from 1 to 0 (or vice-versa) linearly over a finite time span. This lessens the severity of the discontinuity when the transformer moduli change. Discontinuities can cause numerical instability when using implicit integrators such as Backward Differentiation Formula (BDF). The details were discussed in Section 3.2.

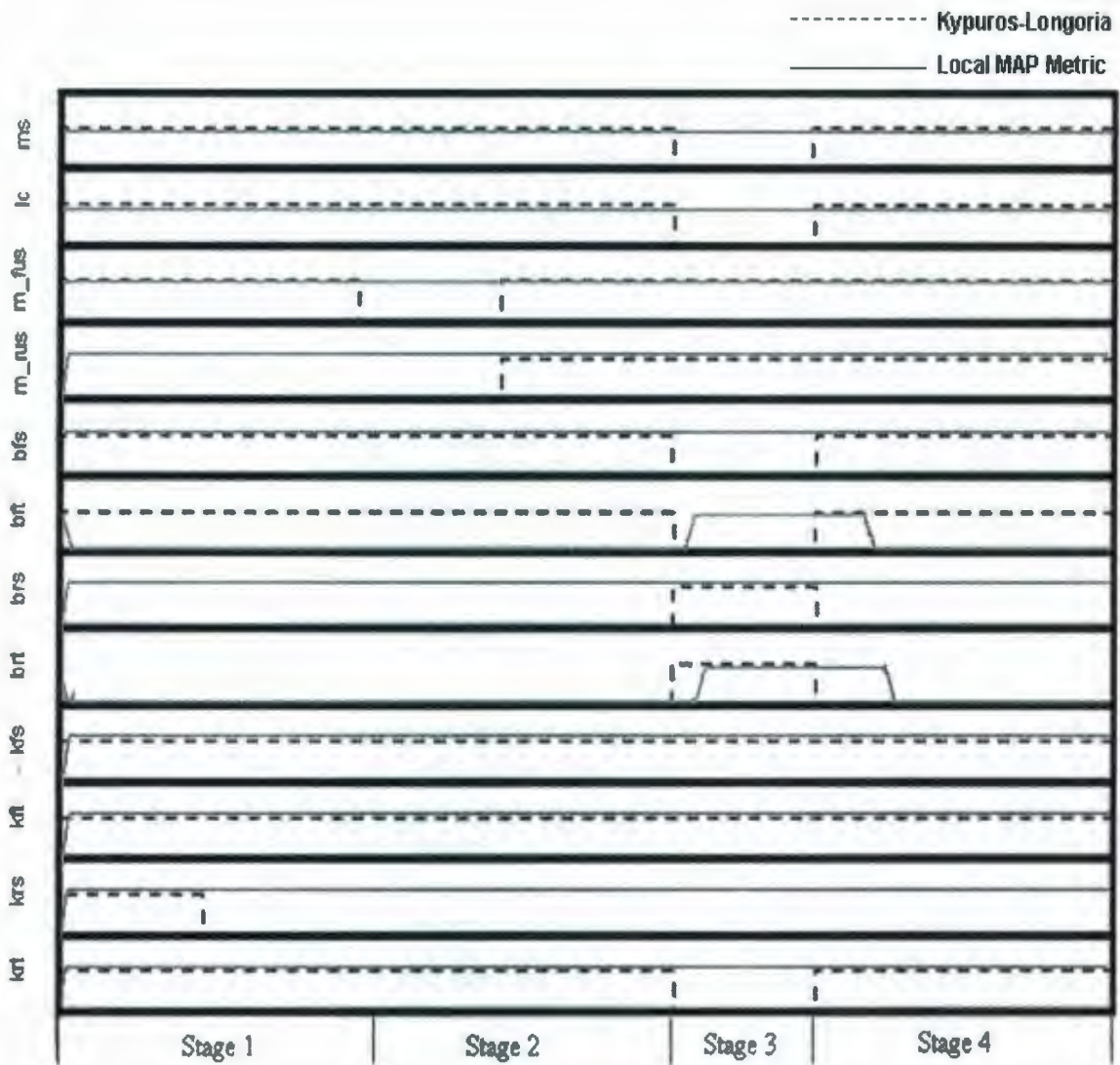


Figure 5.9: Comparing 'U's from Kypuros and Longoria [9] and local MAP based metric

A 95% threshold limit is taken. The resultant plot is drawn for each element's U value and compared with the plot of U values according to [9] which is shown in Figure 5.9. The solid curves are from local MAP sensors and the dotted curves are according to Kypuros and Longoria [9]. The plots show considerable mismatch. No spring element or

sprung inertia goes off whereas they all go off in different stages according to [9] as they should. This depicts the fact that an element might contribute considerably at a junction locally but could be insignificant when compared to all the other system elements. Thus for switching to be applied, a global MAP metric is preferred. Such switching with global MAP metric will be discussed in the next section.

5.3 Global MAP based strong and weak causality bond switch

This section describes global MAP based switches applied for the half-car model for all its strong and weak bond elements. As shown in the Figure 5.2, there are 8 weakly causal bonds for all the spring and resistive elements. Therefore the switch for weakly causal bond as described in Section 4.2 is used for these elements. The four inertial elements are connected by causally strong bonds attached to 1- junctions. Therefore switches described in Section 4.3 for causally strong bonds are used. The parasitic inertial element I_{par} with a value of 0.01kg is employed as a causality generator for causally strong inertial element switches, e.g. switch for sprung mass at $1_{v_{ms}}$ -junction, rotational inertia at 1_w -junction, rear unsprung mass at $1_{v_{rus}}$ -junction and front unsprung mass at $1_{v_{fus}}$ -junction as shown in Figure 5.2. The switched bond graph is shown in Figure 5.10. A resistive parasitic element $para_R$ having a value of $1e^6$ N-s/m is used with a 0-junction attached to each inertial element. This arrangement results in effort causality to the 1-junction which is causally weak, allowing it to be switched off. The MAP sensor sends a U signal

to the modulus of the *MTF* to switch it 'on' or 'off' as *U* transitions between 1 and 0, hence making the effort out to the rest of the system equal to zero when it is off.

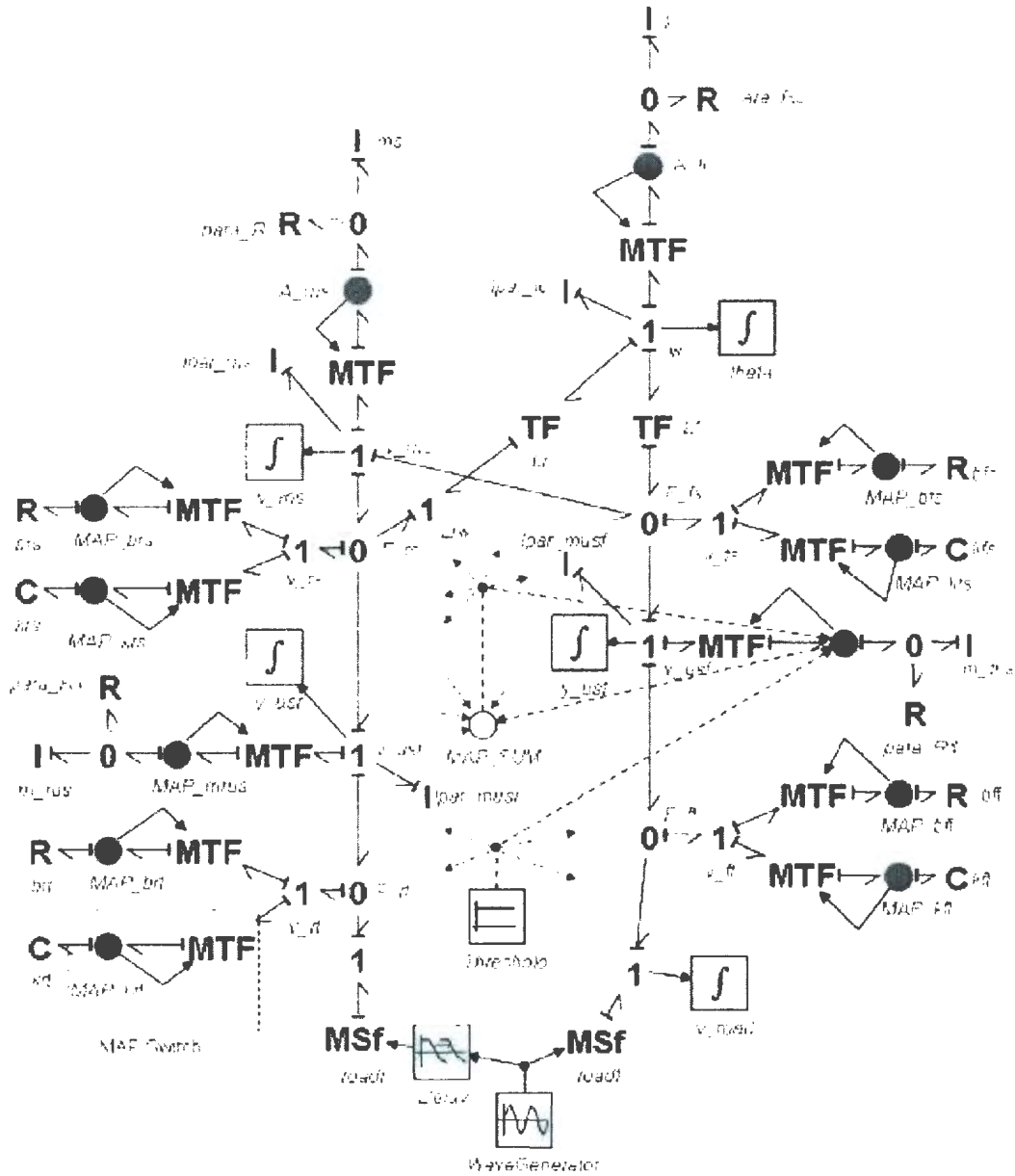


Figure 5.10: Global MAP based switches for half car model

Figure 5.11 shows plots of switched and full model system responses. Front and rear unsprung mass movement demonstrate a good similarity between the switched and full

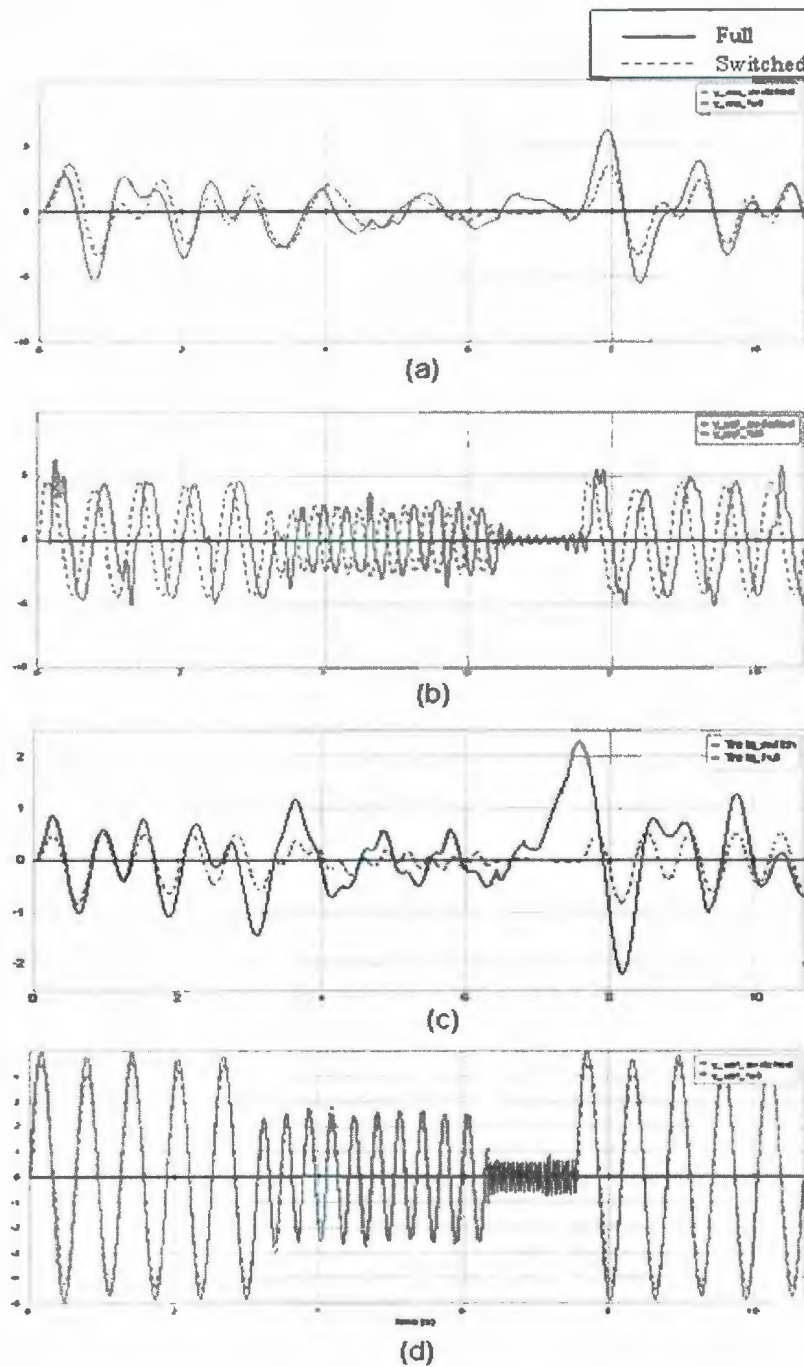


Figure 5.11: (a) Sprung mass displacement (b) rear unsprung mass displacement (c) theta (angular displacement) (d) front unsprung mass displacement

model responses whereas sprung mass movement and angular displacement shows significant dissimilarity especially at the third stage for both cases. Moreover, in Figure 5.12, 'noise' is observed in the U values for sprung mass and rotational inertia. The reason can be explained from Figure 5.13 which shows MAPs of the adjacent bonds attached to $0_{F_{fs}}$ -junction and $0_{F_{rs}}$ -junction in Figure 5.8. It shows that bond 6 has the lowest MAP among the other bonds attached to $0_{F_{fs}}$ -junction during all the four stages and especially it becomes very low during the 3rd stage. Again, at $0_{F_{rs}}$ -junction bonds 1 and 3 have the lowest MAP and these activities get very low during the 3rd stage.

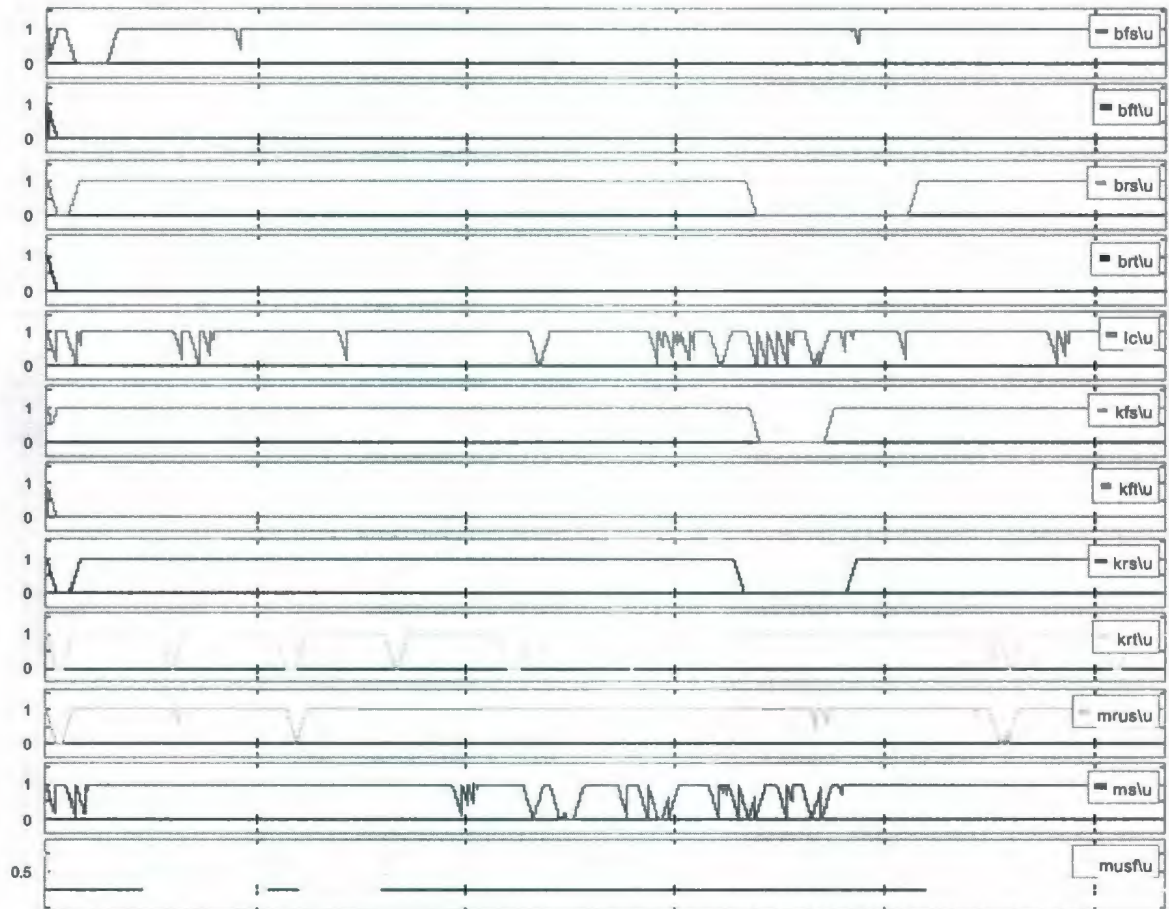


Figure 5.12: U values from global MAP switch for the half car model

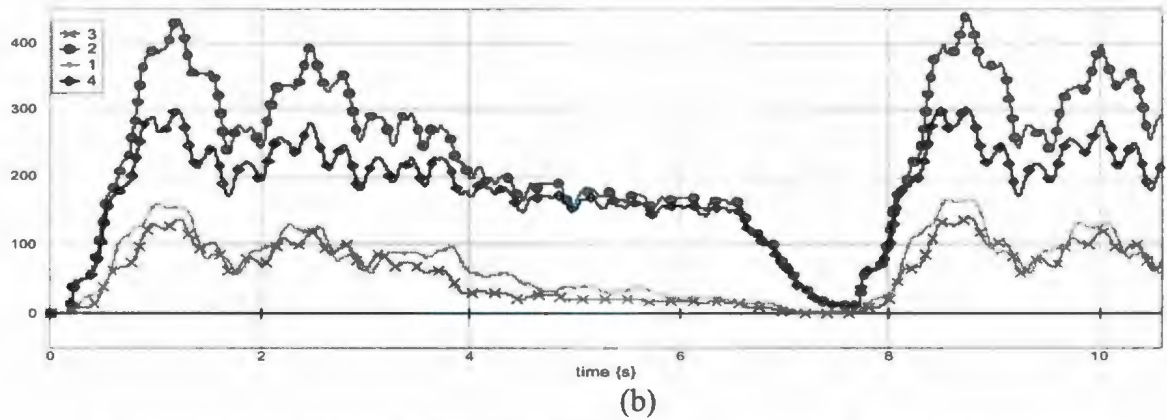
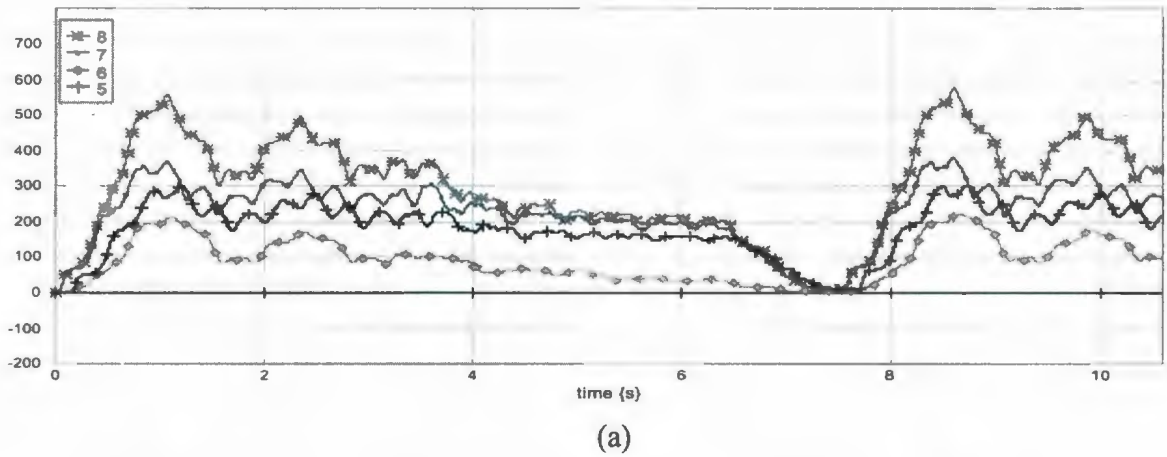


Figure 5.13: (a) MAPs of adjacent bonds at $0_{F_{fs}}$ -junction (b) MAPs of adjacent bonds at $0_{F_{rs}}$

According to Louca and Stein [8] effort to a 0-junction is assumed to be not low when considering the physical interpretation of a low activity bond. Therefore, low flow is assumed to be the cause of low activity at bonds 1 and 5 is low. Bond 1 is attached to $1_{v_{ms}}$ -junction and bond 5 is attached to 1_w -junction. Hence, flow of $1_{v_{ms}}$ -junction and 1_w -junction is globally low, especially at stage 3. This is a case where the assumptions in Louca and Stein [8] not valid, which states that low flow is not the cause of low 1-junction activity. Using a strong bond switch as shown in Figure 5.10 results in a zero

effort to the rest of the system once sprung mass and inertia go inactive. That would be correct if the flow was non-negligible and mass was considered 'zero'. As a result the transients in Figure 5.11 with sprung mass and inertia appeared. Instead, since these are low flow 1-junctions, the 'zero' flow should go to the rest of the system and the masses should be considered "infinity" and attached to the ground. The next section describes how this is done.

5.4 Half car model with weak, strong and internal bond switch

Switching sprung mass and rotational inertia by setting effort output to zero causes significant change in system response as found in the previous section. To resolve the problem, in this section we attempt to switch off sprung and rotational inertia by setting their flows equal to zero when the flow is locally low at the zero junctions to which the m_s and I_c elements are attached. As shown in Figure 5.14, junction $1_{v_{ms}}$ and junction 1_w flows are switched at $0_{F_{rs}}$ and $0_{F_{fs}}$. The inertial flows have strong causality at the 1-junction but become weakly causal soon after they pass the 1-junction and go to next 0-junctions. As shown in the Figure 5.14, the sprung mass flow passes the $1_{v_{ms}}$ -junction and then this flow goes to the $0_{F_{fs}}$ and $0_{F_{rs}}$ -junction. The rotational inertia flow leaves the 1_w -junction and then goes to the $0_{F_{fs}}$ and $0_{F_{rs}}$ -junction. Switching off the two internal bonds [Section 4.4] between the 1- and 0- junctions switches off the inertial elements from the rest of the system by setting their output flow to zero. A local MAP calculation is done to find the relative

importance of the bonds. The $0_{F_{rs}}$ -junction has four bonds including the bonds connected to the $1_{v_{ms}}$ -junction (sprung mass element) and 1_w -junction (rotational inertia element). Four

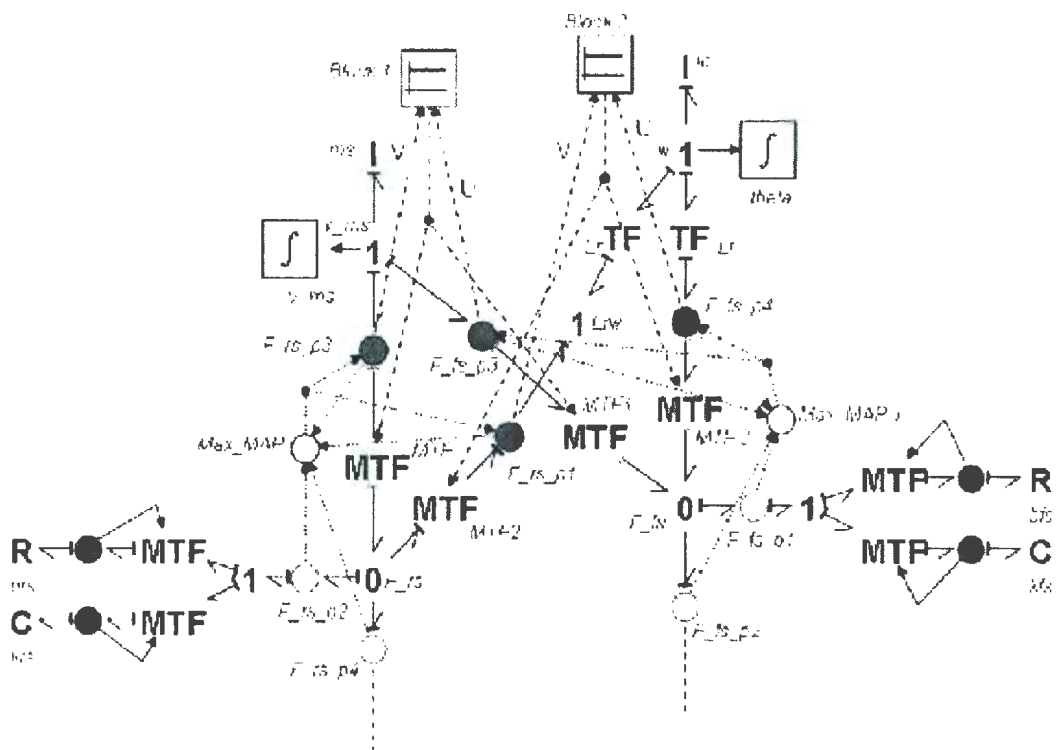


Figure 5.14: Half car model with internal bond switch

MAP sensors, F_{rs_1} , F_{rs_2} , F_{rs_3} and F_{rs_4} are used to calculate the MAP of the corresponding four bonds. The 'MAX_MAP' block finds the maximum MAP among the four bonds and sends the value back to sensors F_{rs_1} and F_{rs_3} to calculate the relative MAP of those bonds. The sensors send a 'V' signal to the 'Block 1' and 'Block 2'. 'V' gets a value of 0 or 1 once the relative MAP of F_{rs_1} and F_{rs_3} goes lower or stays above the threshold limit. Relative activity of bonds between junctions $1_{v_{ms}}$ and 1_w and the other two junctions, $0_{F_{fs}}$ and $0_{F_{rs}}$,

are determined and 'U' signals generated by the F_{fs_p3} and F_{fs_p4} sensors go to 'Block-1' and 'Block-2' respectively. The 'Block-1' and 'Block-2' have a code that tells switching to occur if both the 'U' and 'V' values are 0 values, i.e., switching 'off' the flow from the junction I_{v_ms} or I_w to the rest of the system once both the bond's MAP gets low. A 'u' signal from 'Block-1' goes to *MTF* and *MTF1* to direct the flow from I_{v_ms} junction to the rest of the system to be 'on' or 'off'. Similarly, 'Block-2' switches the I_w junction flow by sending signals to *MTF2* and *MTF3*. Sample code inside 'Block1' and 'Block 2' is given below:

```

.....
.....

if U==0 then
if V==0 then
tevent = time - t01;
if tevent < tspan then
u = 1 - (tevent/tspan)*1;
else
.....
.....
else
if u < 1 then
tevent = time - t00;
if tevent < tspan then
.....
end;
.....

```

The threshold limit for both the internal bond and for the rest of the elements is taken as 95%. Time span for sloping U_s is 0.1 and the time window for MAP calculation is 0.8. The

Vode-Adams integrator with an absolute tolerance of $1e^{-007}$ is used. The parameter values of I_{par} and R_{par} remain the same as in the previous section, 0.01 and $1e^6$ respectively.

Figure 5.15 (a) shows U values from bonds that connect the I_w -junction (1-junction connected to rotational inertia) to the rest of the system. It can be found that at stage 3 for a brief period both m_s and I_c are switched off. Figure 5.15 (b) shows U values from the bonds

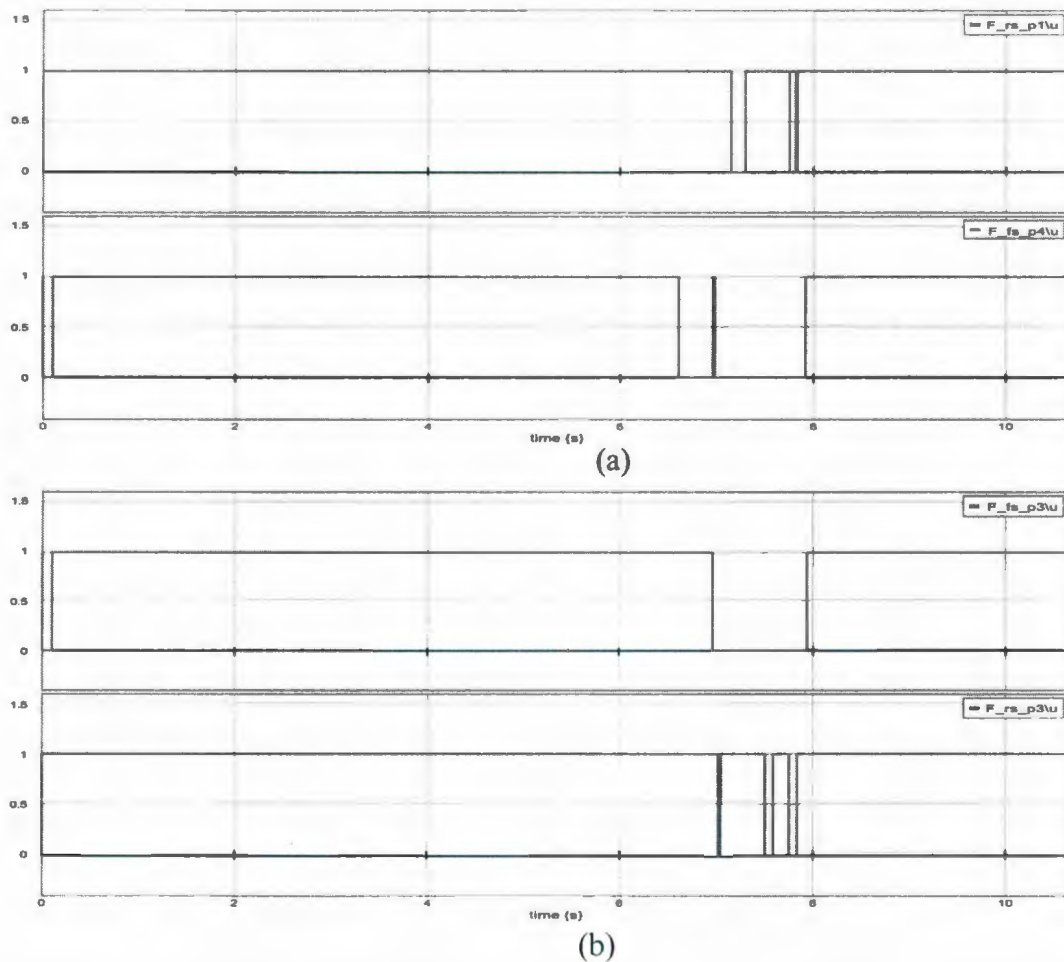


Figure 5.15: (a) U values from the bonds attached to the I_w (1 junction at rotational

inertia) (b) U values from the bonds attached to the 1_{v_ms} (1 junction at sprung mass)

that connect the 1_{v_ms} junction (1-junction that is connected to spring mass) to the rest of the system. This figure also exhibits some switching at stage 3 when both the bond U values go to 0. Figure 5.16 plots the flow from MTF 2 of Figure 5.14 which illustrates that switching at stage 3 forces to flow to briefly become 0. Figure 5.17 shows U values for all the switched elements except the sprung mass inertias since those two elements are switched with a different measure. Most of the elements show similarity with a full model. Rear and front tire damping never come on as they were at the 3rd stage in [9] and the rear tire spring comes back on during all the stages. Though in [9], rear and front tire damping came back on at the 3rd stage but still with a very low contribution. Moreover [9] only shows the ranking of the element at the end of each stage and doesn't tell anything about the interval time between the start and end of the stage. That explains this kind of

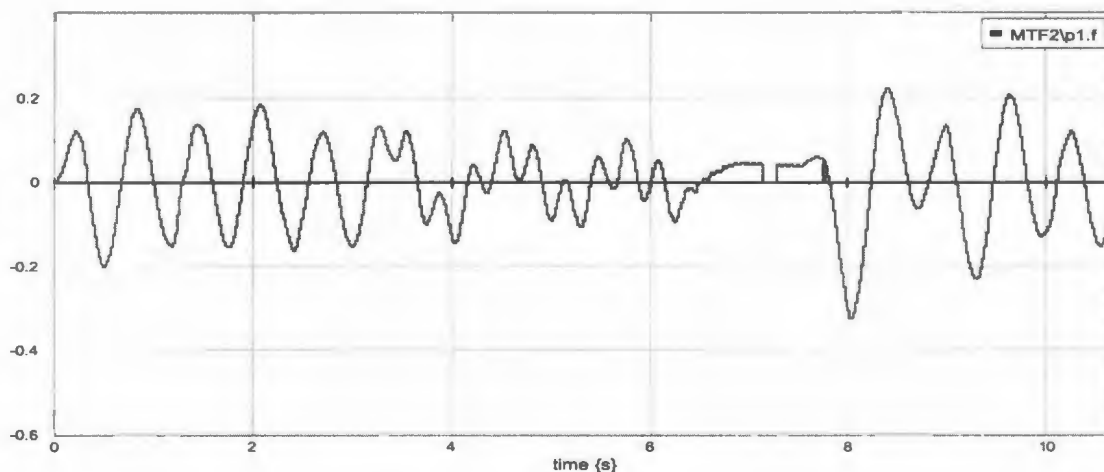


Figure 5.16: Flow from MTF2 of Figure 5.1

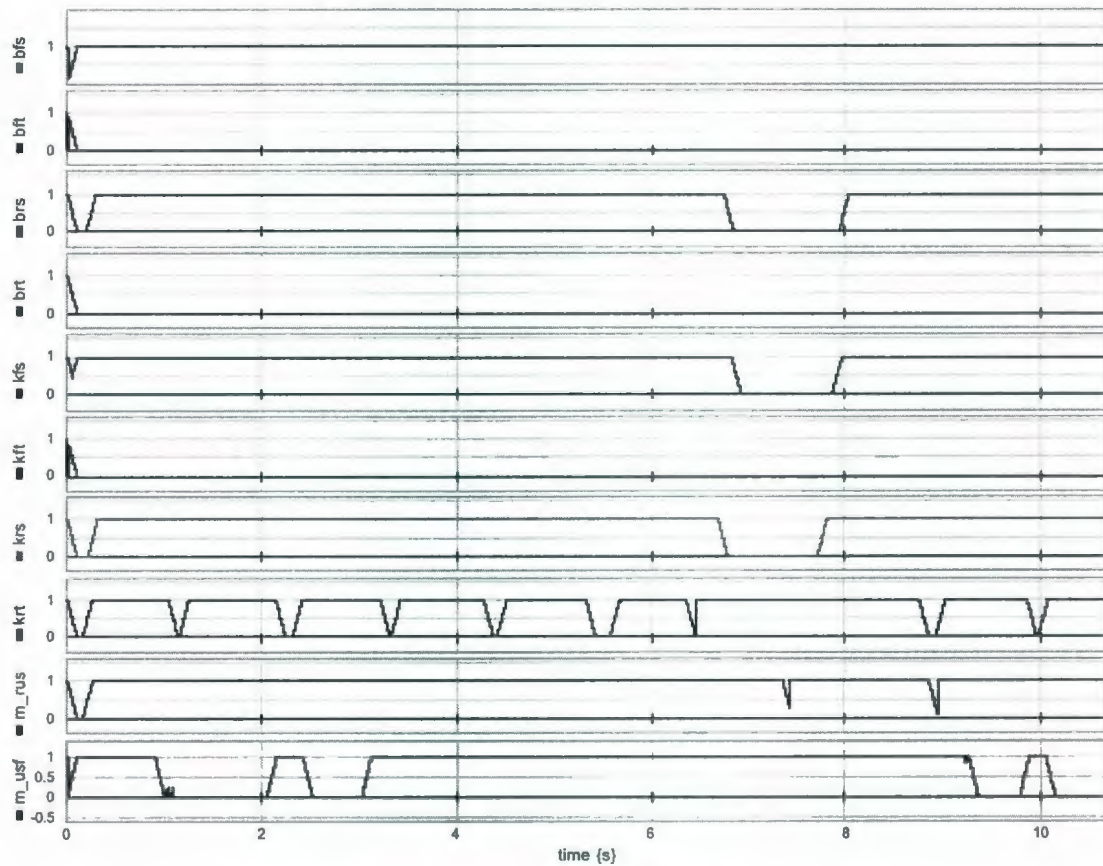


Figure 5.17: U values from different elements from the internal bond switched half car Model

discrepancy between the switched model and full model 'U' values. Figure 5.18 compares curves from the switched and full model. Front and rear unsprung mass displacement show about a perfect match. Both sprung mass and rotational inertia displacement shows discrepancy at the end of 3rd stage and rest of the 4th stage. As both were switched off for a while at the 3rd stage, a transition occurs when they come back on at the 4th stage and a discrepancy occurs due to the transients. Computation time and steps are recorded from a switched model and a model which has the elements of a switched model but sends a constant U=1 signal to the *MTF* elements.

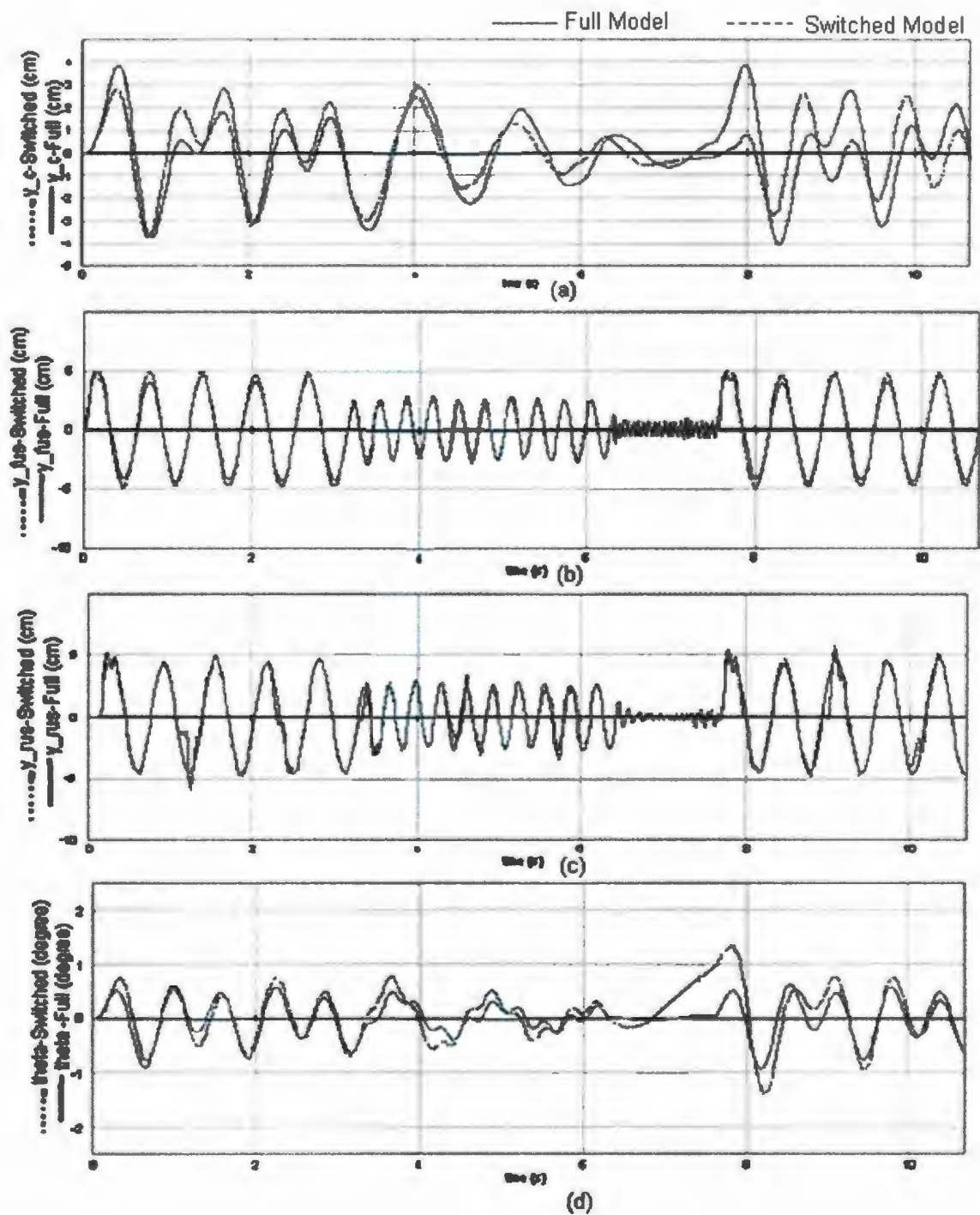


Figure 5.18: Comparing system response of switched and full model :(a) sprung mass movement (b) front unsprung mass movement (c) rear unsprung mass movement (d) angular displacement (theta)

Table 5.4: Simulation time and steps for a switched and full half car model

Model	Time (Seconds)	Steps
Switched	48.219	708545
Full	15.052	220743

The latter model works like a full non switched model .Table 5.4 summarizes the simulation time and steps. Again, no time or step saving is observed. This is due to the fact that switching usually creates transients that cause numerical difficulties which makes the simulation slower. Though computational savings is not achieved, still such switching gives a reasonably good prediction of the system response if MORA is applied and shows that importance of an element in the model can be monitored continuously and the effect of removing it from the model can be seen immediately.

The next section describes a quarter car case study model where element importance metrics and switching methods are applied to see how the methods work.

5.5 Quarter car model case study

5.5.1 Simple quarter car model

This section describes a model of a quarter car. Such a model is used in automotive engineering to simplify analysis while still returning reasonably accurate results in the early stages of design. The model has six components as shown in the free body diagram of Figure 5.19. The sprung mass m_s is the mass of the body of the car which is supported

by a suspension spring k_s and damper b_s in parallel. This suspension spring and damper connects the sprung mass with the unsprung mass m_u which is the mass of the wheel and axle. This unsprung mass is supported by the tire which is modeled by tire stiffness k_t and damping b_t . The input of the system is described by the road profile $u(t)$ which is a function of time and gives the velocity of the contact point of road and tire Louca and Stein [8]. The gravitational force effect is neglected in the model.

Figure 5.20 shows a bond graph model of the quarter car. In the bond graph model the sprung mass m_s and unsprung mass m_u are represented by the two inertial I elements, two compliant C elements are for the suspension stiffness k_s and tire stiffness k_t , and the resistive element R characterizes the suspension and tire damping i.e. b_s and b_t . As the same

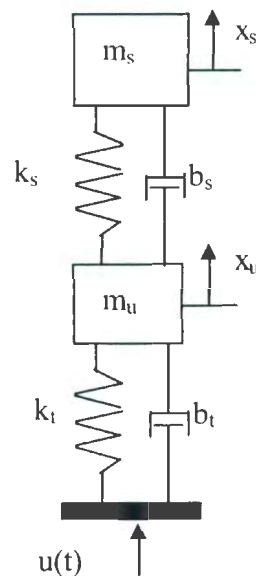


Figure 5.19: Free body diagram of a quarter car

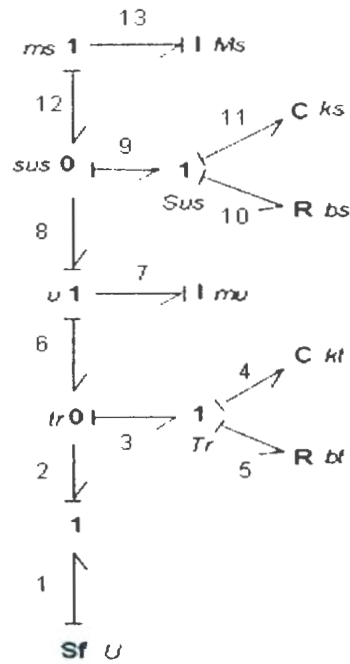


Figure 5.20: Bond graph model of the quarter car

velocity is shared by the suspension spring and damper they are connected by the I_{sus} -junction. Similarly for the tire, the spring and damping elements are connected by the I_{tr} -junction to have the same velocity. The combined effort (force) from the tire spring and damper is represented by the O_{tr} -junction

The velocity input to the tire spring and damper is the difference between the road input and the velocity of the unsprung mass, represented by the I_u -junction. Again this velocity flows to the O_{sus} -junction where it is subtracted from the flow results from I_{ms} -junction of the sprung mass to generate a velocity described by I_{sus} -junction. Table 5.5 shows the parameter values of the element used in the bond graph model taken from [8].

Table 5.5: Parameter values of different elements used in bond graph model of the Quarter car

Parameter	Values
Sprung mass m_s	267 kg
Suspension stiffness k_s	18742 N/m
Suspension damping b_s	700 N s/m
Unsprung mass m_u	36.6 kg
Tire stiffness k_t	193915 N/m
Tire stiffness damping b_t	200 N s/m

The tire and suspension elements are assumed to be linear since the road input has a small value which keeps the suspension and tire element responses within their linear range. All the models are tested for input frequencies ω of 100 rad/sec, 10 rad/sec and 100 rad/sec for the first, second and third stages respectively. Simulation is done for a total of 40 seconds, in which the 1st stage is 2 seconds long, the 2nd stage is 2 seconds long and the 3rd stage is the rest of the time. The amplitude is taken as 1.5 m, giving a road input $u(t) = 1.5\cos(\omega t)$ m/s¹.

5.5.2 Continuous monitoring of importance of the quarter car model elements

Activity Index, Relative Activity and MAP Index, the three continuous element importance monitoring metrics described in Chapter 3 are used with the quarter car model. The following sections will find which metric is most responsive.

5.5.2.1 Activity Index

Activity indexes are calculated according to the method described in Section 3.1, where the activity is calculated by integrating absolute power that flows into an element over a time span and the activity index (AI) of an element is calculated by dividing activity of the particular element by the sum of all element activities. In Figure 5.21,

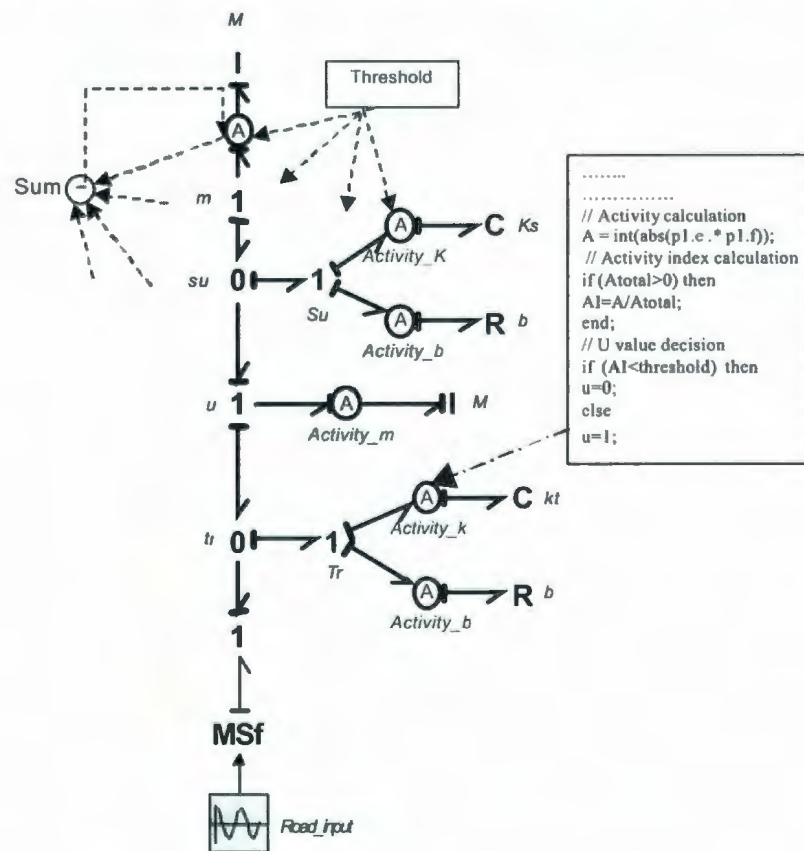


Figure 5.21: Calculating activity indices for the quarter car

activity sensors are used on each bond containing energy storage and dissipative elements. The 'sum' block sums all the activity signals. It then sends the total back to the

individual activity sensors to calculate the activity index. A 'threshold' block sends a threshold signal to the activity sensors. For this case a 95% threshold limit is taken. The U [Section 3.2] generated by the sensors goes to 0 if an activity index goes below the threshold limit and goes to 1 if activity goes above the threshold limit.

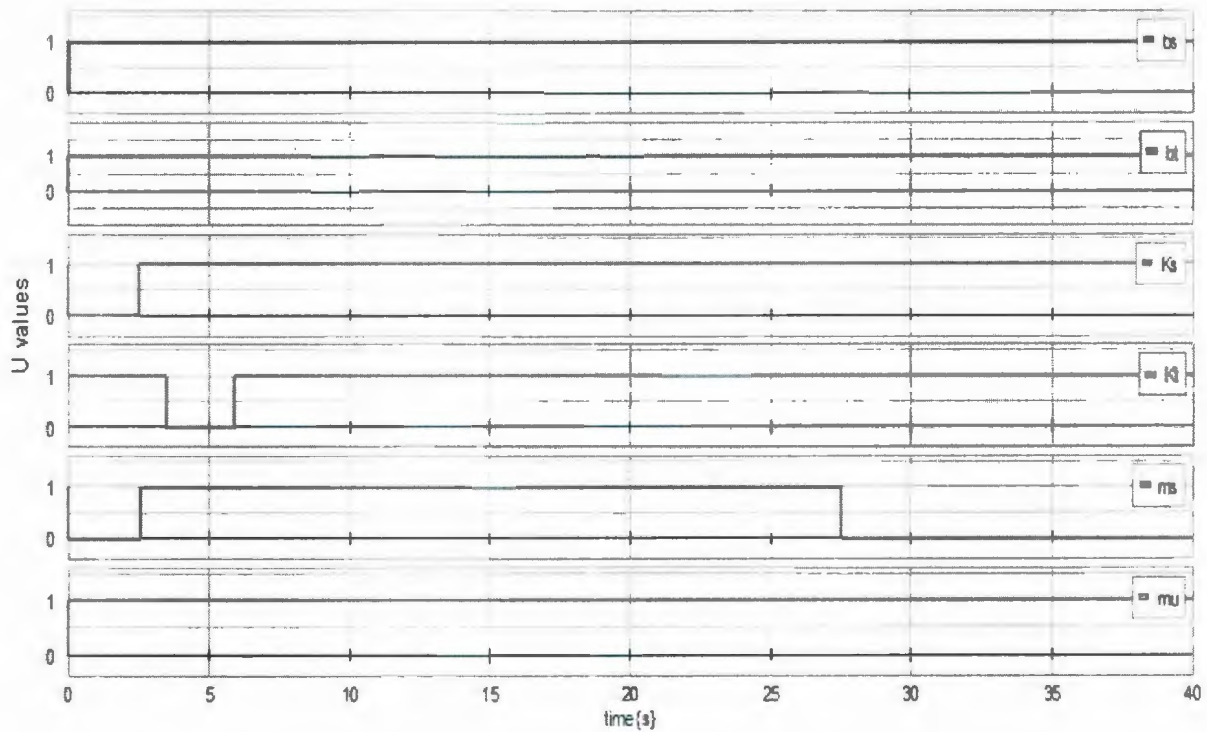


Figure 5.22: U values of the elements of the quarter car model

To monitor which elements are important and which are not, Figure 5.22 shows a plot of the U values for all the elements for 40 seconds. The plot shows that tire damping, suspension damping and unsprung mass never go off. Suspension stiffness goes off for the first 2 seconds at high frequency and comes back on during the low-frequency stage.

After that it never goes off again. Tire stiffness stays through the first stage and goes off at the second stage and continues to stay off at the beginning of the third stage. Then it comes back and stays on at the high frequency third stage and never goes off again. Sprung mass goes off at the first stage and continues to stay off at the beginning of the second stage and then comes back on. It then goes off at 27 seconds in the high frequency third stage and never comes back again. The system acts as a low-pass filter, filtering out high-frequency road inputs to the sprung mass, causing its velocity to be negligible. Therefore activity becomes lower. The next section discusses another continuous activity monitoring method and finds whether a better prediction can be achieved.

5.5.2.2 Relative activity

The relative activity metric [Section 3.1.2] compares activity of the adjacent bonds connected to a junction, as opposed to globally ranking and comparing only activities of *I*, *C*, and *R* elements. Activity of each bond at a 1- or 0-junction is calculated and divided by the activity of the most active bond at the junction to find the relative activity. The plot for the *U* values is shown in Figure 5.23. The tire damping stays off for all the stages. Sprung mass and suspension stiffness stay off during the first stage i.e. at the higher frequency stage and come back on early in the lower frequency second stage. These elements stay on for the rest of the simulation. Suspension damping, tire stiffness and unsprung mass never go off. It appears that relative activity is less responsive than activity index to predict element's activeness. Sprung mass doesn't go off during the high frequency 3rd stage but as discussed in the previous section sprung mass should go off.

Therefore activity index metric is preferred over relative activity metric. Moreover the relative activity never can eliminate both the R and C element for the tire or suspension. Because they are bonded to three-port 1-junctions, only one of the two elements will have low relative activity. The relative activity of the other element will be very close to the maximum junction activity. A three-port 1- or 0-junction can have one relatively low activity, but then the other two will be near 100%. The junction becomes similar to a flow-through junction if one bond is inactive.

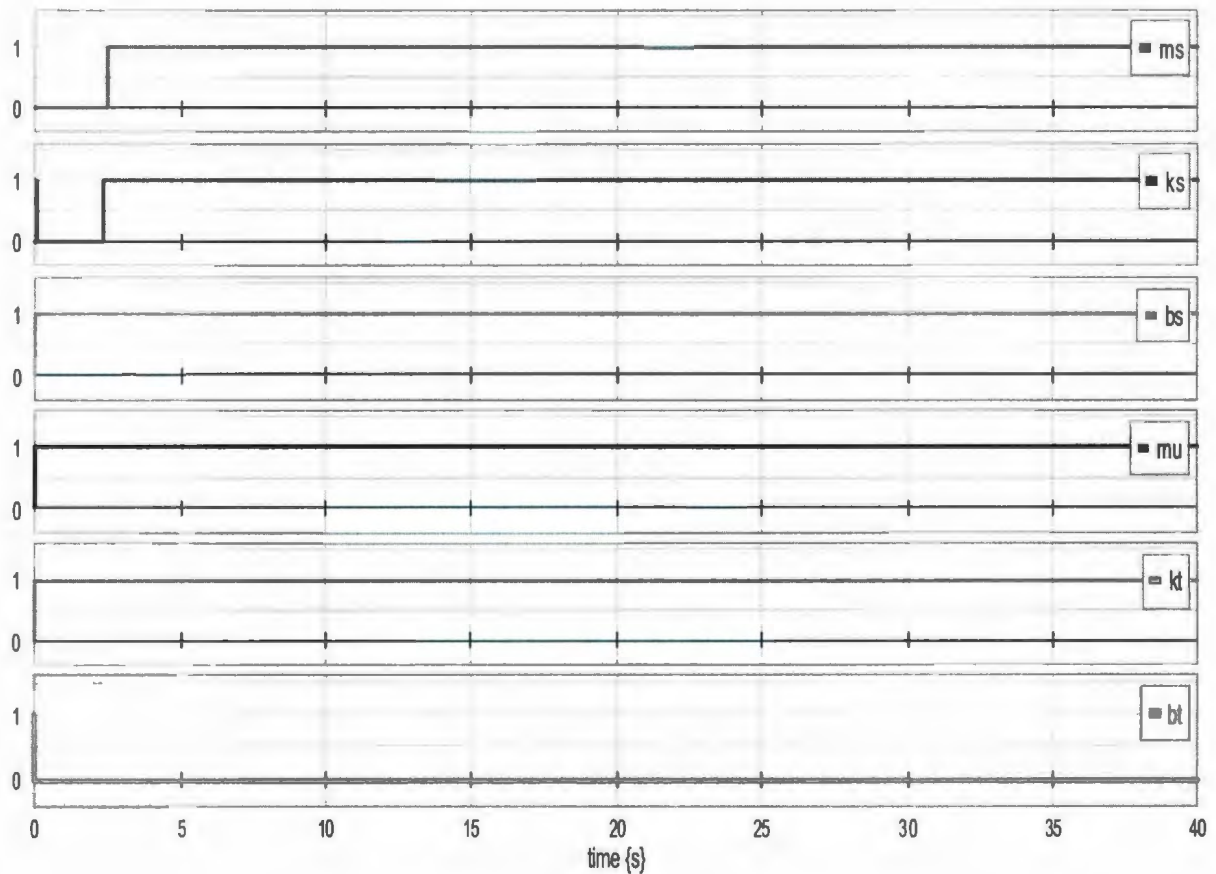


Figure 5.23: Plot of the U values using relative activity

5.5.2.3 MAP Index

MAP based metric described in Section 3.1.3 is used in this quarter car model. The generated U value uses the 'smoothing scheme' described in Section 3.2. The model is similar as shown in Figure 5.21 except, instead of activity sensors, MAP sensors are used. The road input remains the same. The simulated plot of the U values is shown in Figure 5.24. The time span is taken as 0.8 to calculate the moving average. It shows that tire damping, tire stiffness and unsprung mass go off during the low frequency stage and stay on at high frequency stages. The sprung mass and suspension stiffness stays off at high

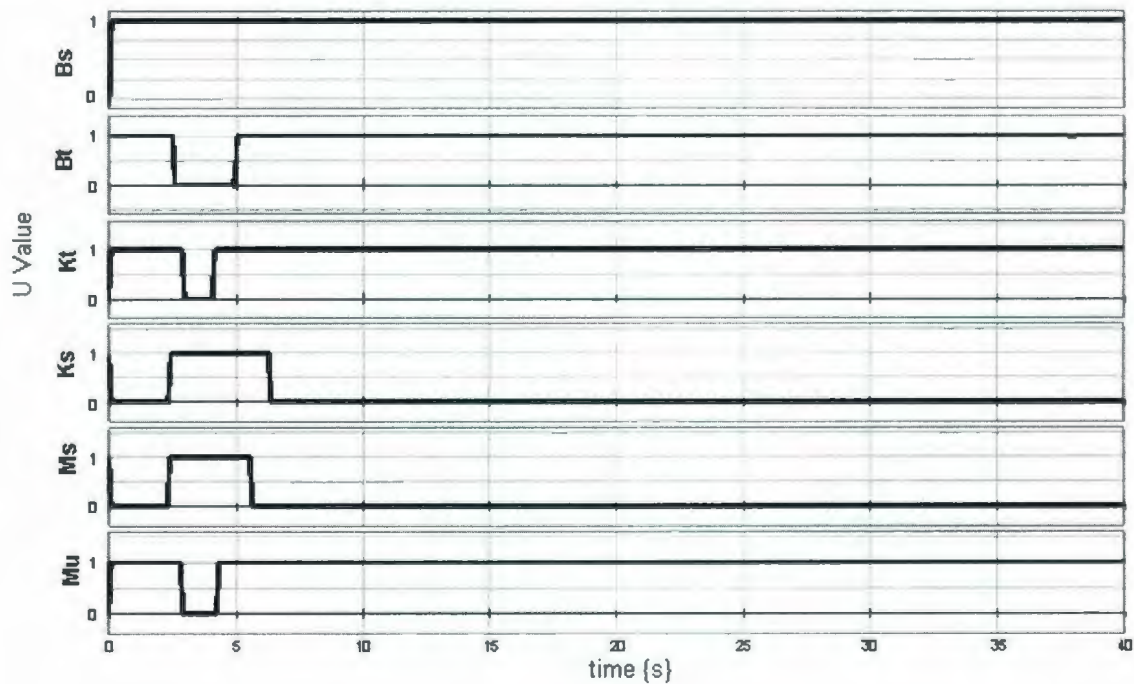


Figure 5.24: U values of the quarter car model using MAP sensors

frequency stages and come back during the low frequency stage. MAP shows a better response than activity index or relative activity as it captures more elements' inactivity

than the other two methods .It responds quicker to system input changes. For example, the sprung mass goes off sooner in the 3rd stage than in case of activity index. Use of this MAP activity sensor with a switching arrangement will be discussed in Section 5.6.3.

5.5.3 Switching for quarter car model

An element can be switched off by setting a zero flow to a 0-junction or zero effort to a 1-junction which is causally weak. *MTFs* are used for such switching. A *U* signal from the activity sensor dictates the modulus to be 0 for the ‘off’ mode and 1 for the ‘on’ mode. For details see Chapter 4. The following section discusses how the switching is done for the strong and weak bonds of the quarter car model.

5.5.3.1 Quarter car model with switch for casually weak bonds

Section 5.5.2 finds *U* values to show which elements can be eliminated, and when This section attempts to switch the model as the simulation progresses, to check for simulation accuracy and numerical issues such as stability, time and number of steps required. The switches are implemented for each causally weak bond to *I*, *C*, and *R* elements in the quarter car model. Effort to a 1-junction and flows to a 0-junction are casually weak. Thus those casually weak bonds can be switched ‘off’ by using the switches described Section 4.2. Note that the sprung mass and unsprung mass *I* elements are causally strong, and not switched. The *U* signal from each activity sensor is sent to the modulus of the appropriate (*MTF*) as shown in Figure 5.25. A 95% threshold is used.

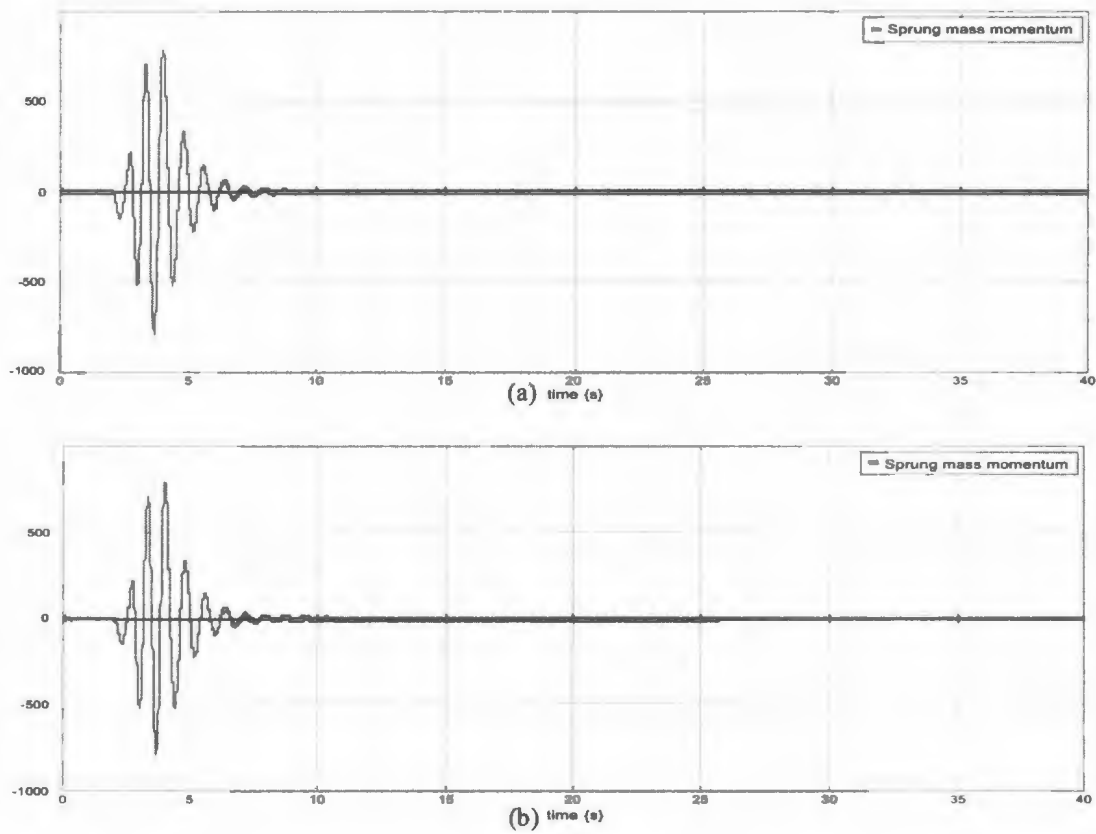


Figure 5.27: (a) Sprung mass momentum of full model (b) Sprung mass momentum for switched model

signal of 1 is sent to the modulus of the *MTFs*. Thus the model works as a full model, i.e., no switching is done. The model is simulated for 40 seconds with the Vode-Adams method using the same tolerance as before. The plot for sprung mass momentum is shown in Figure 5.27 (b). Simulation time and steps are given in Table 5.6.

The plots from switched and full model illustrates that the system response remains the same for a switched and full model. The simulation time and steps show that there is a computational time saving for the switched model compared to a full model having all

the sensors and *MTFs* as in the switched model but without a switching signal. Figure 5.28 shows the *U* values from the switched model compared with *U* values predicted in Figure 5.22, where the model is not actually switched. Suspension damping goes off during 1st and 4th stage in a switched model whereas it never goes off in the full model. Again, the tire stiffness never goes off in the switched model but in a full model it stays off during the 2nd stage.

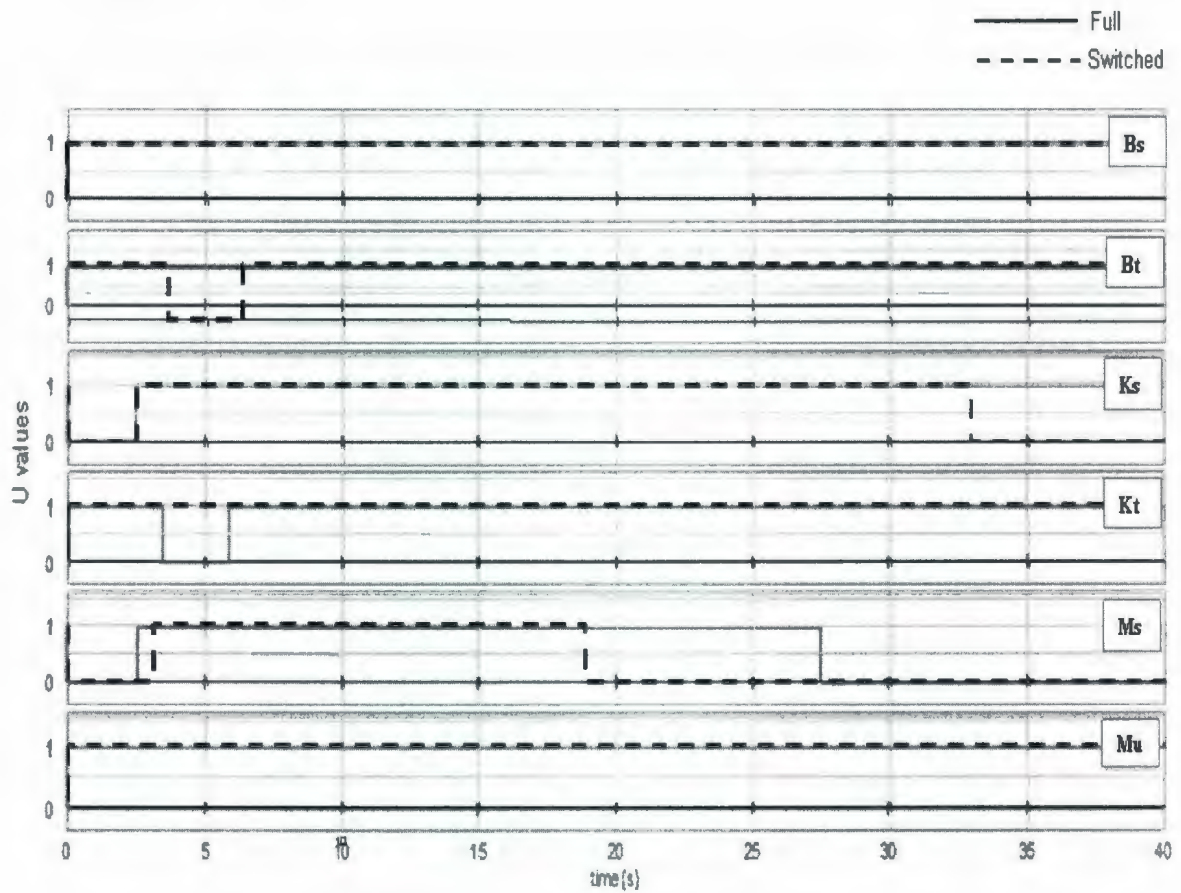


Figure 5.28: Plot of *U* values from a switched model compared with full model

In a model where actual switching occurs, the transient caused by an effort (or flow) changing from a 0 value to 1 or vice-versa will cause some finite change in the system response. The instants at which U values switch between 0 and 1 in a switched model will therefore differ from the instants predicted when the model runs in fully continuous mode.

Switching bonds for the causally weak bonds show some computational savings though not compared to a full quarter car model that doesn't have any activity sensors or *MTFs*. Since computation of activity takes significant steps to calculate, excluding these sensors would not show the actual step reduction due to the switching effect.

5.5.3.2 Switching causally strong bond for unsprung mass and weakly causal sprung mass

Louca and Stein [8] assumes that a flow to a 1-junction or an effort to a 0-junction is not low when bonds at that junction have low activity index. Switching off a causally strong bond requires changing the causality of the switched bond into a weak causality and using a causality generator to create the same causality the junction had before the switching. Details of such a switch were discussed in Section 4.2. A very low value inertial element is used as a causality generator to switch an inertial element connected to a 1-junction. A 0- junction attached with the inertial element and with a high resistive element is used to keep the causality the same for the inertial element. MAP based metric

is used with smoothing in U values since this metric is more responsive than the activity index metric. Moreover ‘smoothing’ of U values facilitates the switching of causally strong bonds since better numerical stability can be obtained by ‘smoothing’ of U.

In Figure 5.20 the unsprung mass is attached with a causally strong bond to the l_{u-} junction. It must therefore be switched with a switch for a causally strong bond [Section 4.2]. If the power flow direction for bonds 2, 6 8 and 12 in Figure 5.20 were reversed, then the l_{ms-} junction attached to the sprung mass could be removed. Such a half-arrow direction change simply represents a change in sign convention, and changes nothing more than some algebraic signs in the system equations. For this reversal of power flow the sprung mass attachment bond would become causally weak at the 0_{sus-} junction. Thus a switch for causally weak bond would be used. The model bond graph is shown in Figure 5.29 and a plot for sprung mass momentum is given in Figure 5.30. The plot shows significant similarity with the full model plot for the same input. The Runge-Kutta-Fehlberg integrator with an absolute tolerance of $1e^{-006}$ was used. A time window of 1 sec was used for averaging absolute power to calculate MAP. The threshold limit was taken as 97%. Though no time saving was recorded, this result is still significant as it allows the analyst to see how the system would respond if model complexity was changed throughout the simulation.

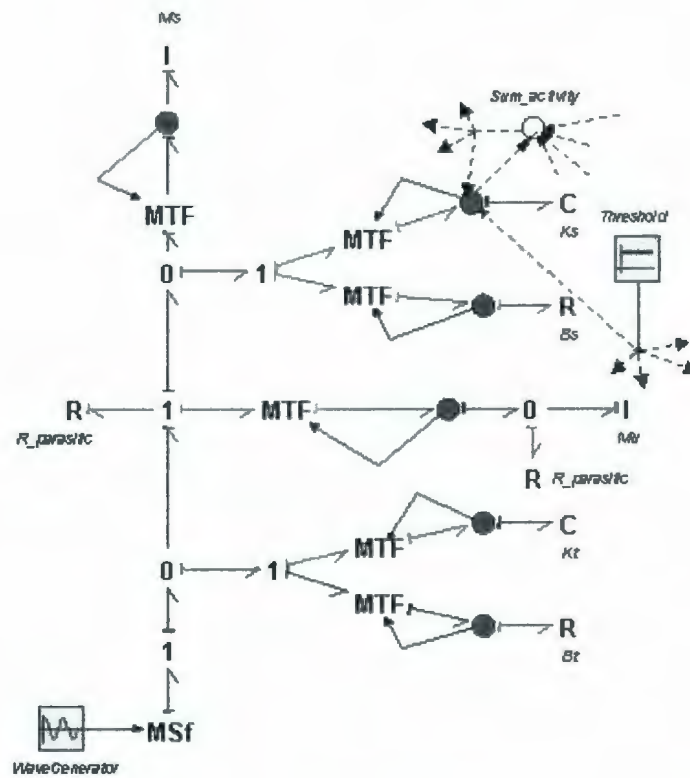


Figure 5.29: A casually weak sprung mass switched model for quarter car

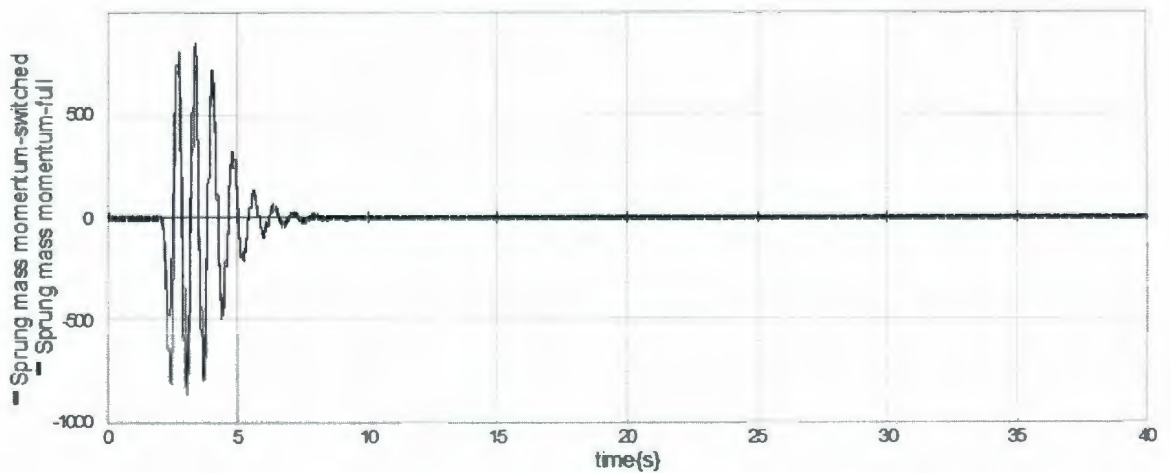


Figure 5.30: Plot of mass momentum for casually weak sprung mass switched model of the quarter car

5.5.3.3 Switching causally strong bond for sprung and unsprung mass

In the original model of the quarter car, as shown in Figure 5.20, the sprung mass is attached to the 1_{ms} -junction by a strong causal bond. Therefore it needs to use a strong causal bond switch as described in Section 4.2. Again bond 12 in Figure 5.20 is causally weak at 0_{sus} -junction and this can be switched with an internal bond switch [Section 4.3]. Figure 5.31 shows the bond graph model of the quarter car with the two switches (external and internal) for the sprung mass. If the effort is negligible then the modulus of $MTF_{External}$ gets a zero value and a zero effort results. Again, $MTF_{internal}$ goes to zero to

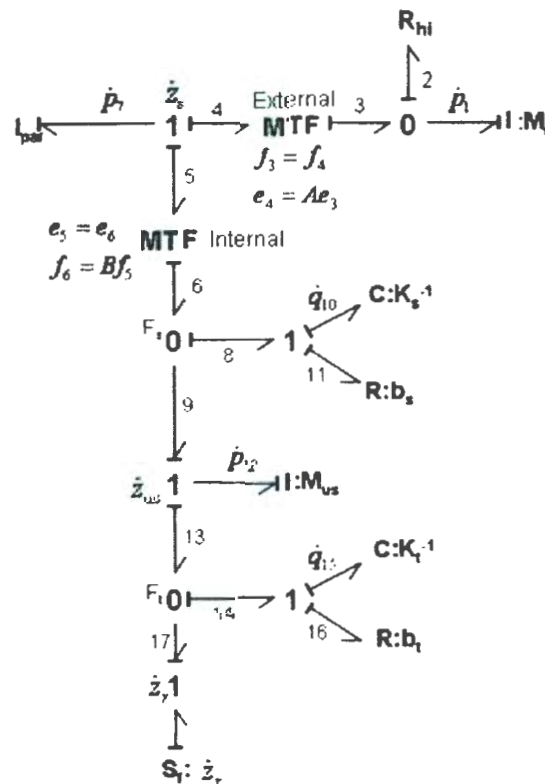


Figure 5.31: Quarter car model with switched sprung mass for eigenvalue analysis

generate a zero flow once the flow of the sprung mass becomes negligible. The suitability of these switched model modes is tested by an eigenvalue analysis. Equations from the bond graph model of Figure 5.31 are given below in a matrix form.

$$\begin{Bmatrix} \dot{p}_1 \\ \dot{p}_7 \\ \dot{p}_{12} \\ \dot{q}_{10} \\ \dot{q}_{15} \end{Bmatrix} = \begin{bmatrix} -\frac{R_{ni}}{M_s} & \frac{R_{ni}}{I_{par}} & 0 & 0 & 0 \\ \frac{AR_{ni}}{M_s} & -\frac{AR_{ni}}{I_{par}} - \frac{Bb_s}{I_{par}} & \frac{b_s}{M_{us}} & -k_s & 0 \\ 0 & \frac{Bb_s}{I_{par}} & -\frac{b_s}{M_{us}} - \frac{b_t}{M_{us}} & k_s & -k_t \\ 0 & \frac{B}{I_{par}} & -\frac{1}{M_{us}} & 0 & 0 \\ 0 & 0 & \frac{1}{M_{us}} & 0 & 0 \end{bmatrix} \begin{Bmatrix} p_1 \\ p_7 \\ p_{12} \\ q_{10} \\ q_{15} \end{Bmatrix} + \begin{Bmatrix} 0 \\ 0 \\ \frac{b_t}{M_{us}} \\ 0 \\ -1 \end{Bmatrix}$$

where

p_1 =Sprung mass momentum

p_7 =Parasitic mass momentum

p_{12} =Unsprung mass momentum

q_{10} =Suspension spring displacement

q_{15} =Tire spring displacement

A= Modulus of sprung mass MTF

B= Modulus of internal bond MTF

This equation is coded in MATLAB [2006] and the following eigenvalues are obtained for all the combinations of “on” and “off” modes for both the internal and external switches.

Table 5.7: Eigenvalues for switched sprung mass

Sprung Mass- "On" Internal Bond- "On"	Sprung Mass- "Off" Internal Bond- "On"	Sprung Mass- "Off" Internal Bond- "Off"	Sprung Mass- "On" Internal Bond- "Off"
$-1e^9$	-3475	-3475	0
$-1+7.95i$	-6999	0	$-1e^9$
$-1-7.95i$	-26.8	$-12+75.2i$	0
$-12.5+74.9i$	$-2.73+72.7i$	$-12-75.2i$	$-12+75.2i$
$-12.5-74.9i$	$-2.73-72.7i$	0	$-12-75.2i$

In the first scenario when the switches are "on", there are low- and high frequency damped oscillations corresponding to ride and wheel hop frequency, along with a stiff overdamped parasitic eigenvalue. The sprung mass is set to zero in Scenario 2, leaving the unsprung mass to oscillate atop only the tire spring and damper. The removal of the effect of suspension damping on M_{us} can be seen in the smaller real part of the eigenvalues. In Scenario 3 the sprung mass again is set to zero and the velocity node is fixed to ground. Parasitic and rigid body modes are created by the separation of I_{par} , R_{hi} and M_s . The unsprung mass oscillates between tire and suspension springs and dampers and therefore eigenvalues get very close to those of the original wheel hop mode. In Scenario 4, the sprung mass is a ground node and therefore is quite similar to the previous scenario. In conclusion, the combined effect of both the switches preserves eigenvalues of the remaining model elements regardless of whether the causally strong mass becomes inactive due to low inertial force or low velocity.

Though the eigenvalue analysis shows that using two sprung mass switches is feasible, numerical problems are created when using both of them. Using only the ‘external’ switch gives a similar numerical problem. Using only the ‘internal’ bond gives a reasonable output. MAP sensors are attached to bond 6, 8 and 9 of Figure 5.31; those are adjacent bonds of 0_s -junction. MAP index is calculated locally at this junction following the same procedure stated in Section 3.13. A threshold limit of 95% is set for the internal

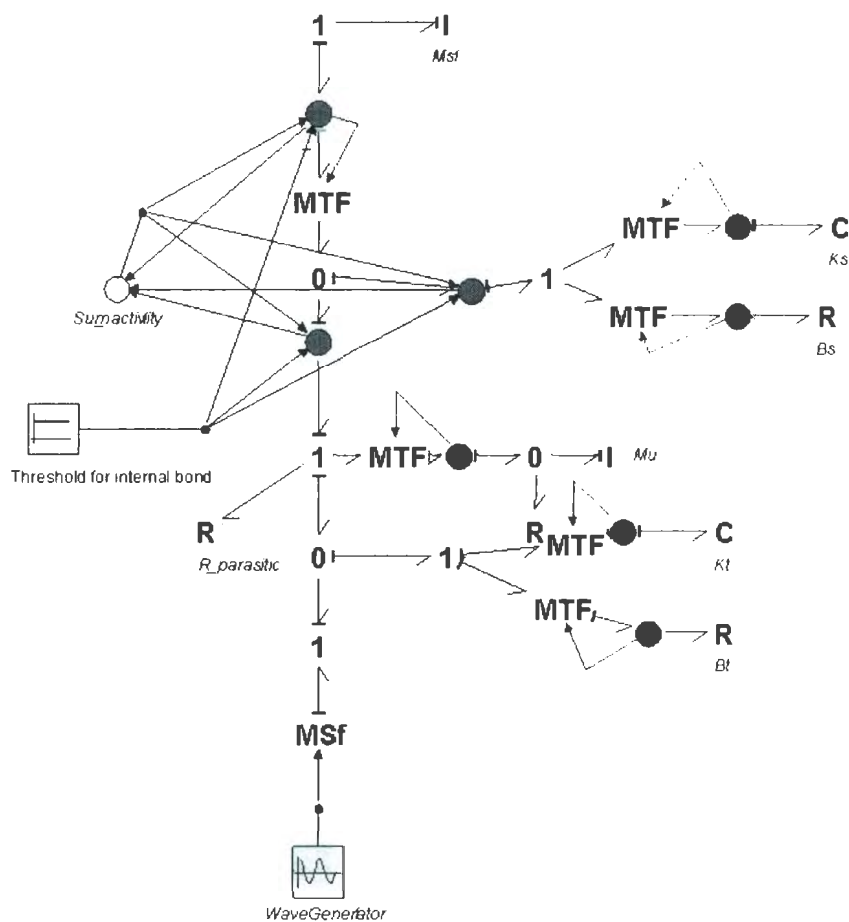


Figure 5.32: Quarter car model with strongly causal sprung mass switch

bond MAPs. Figure 5.32 shows the bond graph of the quarter car model using an internal bond switch for the strongly causal sprung mass. The other elements use the switches described in the previous section. A 95% threshold is taken for all the other element MAPs from external bonds. The Runge-Kutta-Fehlberg integrator was used with an absolute and relative tolerance of $1e^{-6}$. Figure 5.33 shows the system response from the switched model compared with the full model. A good agreement between the model responses is found.

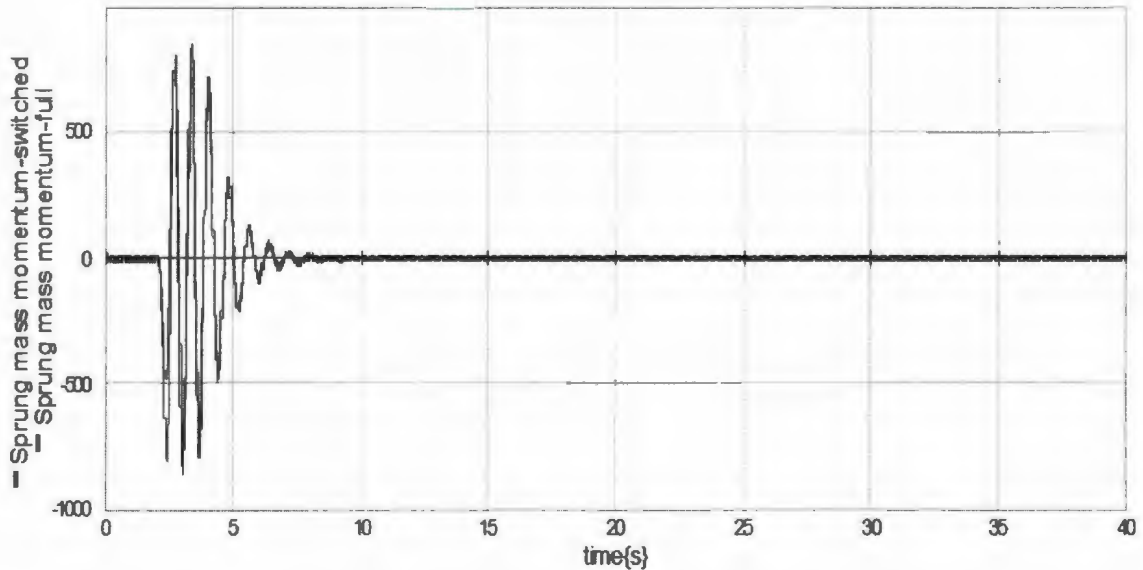


Figure 5.33: Comparison of switched and full model output

Figure 5.34 gives the plot of U values from the switched model. The presence of noise can still be observed from the plots but they are close to U values found from a full model.

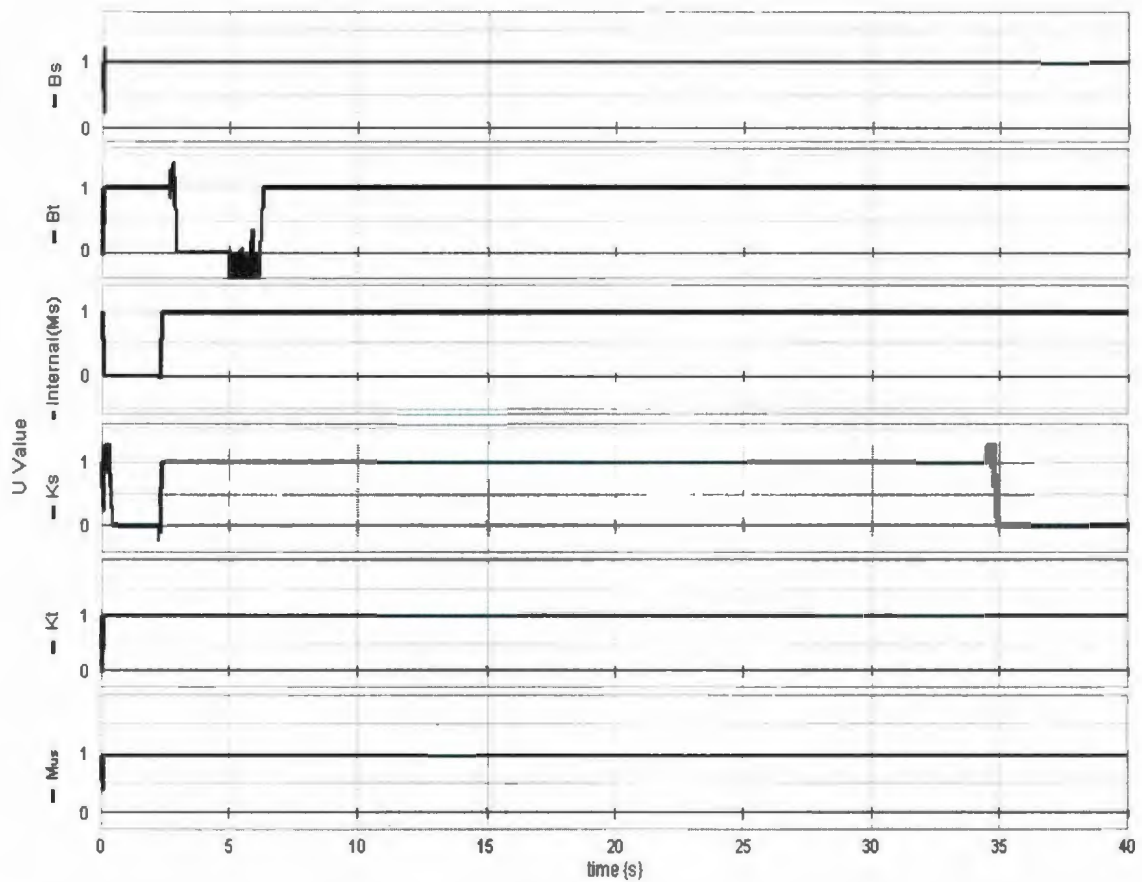


Figure 5.34: U values generated from a switched model

A copy of the model in Figure 5.32 was built, having all the arrangements of a switched model except a constant $U=1$ signal goes to the MTFs instead of a varying U . Therefore it works like a full model even though it has the components of a switched one. Simulation time and steps for both the switched and non-switched model are summarized in Table 5.8. Computational savings are not recorded. Despite the fact that computational savings are not achieved, the case study shows how a mass that is causally strong can be inactive for both low flow or effort and can be switched off in either case.

Table 5.8: Simulation time and steps of switched and non-switched model

Model Type	Time (sec)	Steps
Non-switched model	9.84	361956
Switched model	14.49	527549

This case study demonstrates the ability to see which elements are unnecessary at different times, allowing one to look for distinct stages in the simulation where different model complexities could be employed. The user could then generate proper models for each stage separately, and run them in sequence. As long as system design changes (in other words, changes to the model) were minor, one could be reasonably assured that the reduced models for each stage would remain valid. The reduced model sequence could then be run without activity calculation, and would possibly show significant computational savings. Kypuros and Longoria [9] showed this for a half car. If the model parameters or inputs were changed significantly, the MAP switched-model could be re-run to ensure that the time intervals for each stage, and the required model elements, had not changed. If changes were required to the stages or models, then the MAP-based switch analysis would automatically suggest these changes.

Chapter 6

Vehicle Frame Model Case Study

This chapter discusses how to use switches for a vehicle frame model that can be partitioned into a driven and driving sub-system as described in Section 2.1. Section 6.1 gives a brief description and some useful equations for a Bernoulli-Euler beam [23] that could be used for modeling the vehicle frame. Section 6.2 explains the vehicle frame model. Section 6.3 describes how the vehicle frame model can be partitioned using the algorithm described in Section 2.1. Section 6.4 describes how switches [see Chapter 4] can be used to partition a model only when it is appropriate to do so. The flexible modes of the vehicle frame model form driven partitions when they do not contribute significantly to overall system response. These modes are essentially eliminated when the model is partitioned. This case study thus predicts when a rigid model is acceptable, switches between a rigid and flexible model automatically, and shows how the model would respond. The analyst can then compare the variable-complexity model results with the results from a “full” flexible model over the course of the simulation, and decide if discrepancies are acceptable. Results from the variable complexity model are given in Section 6.5.

6.1 Brief description of Bernoulli-Euler beam

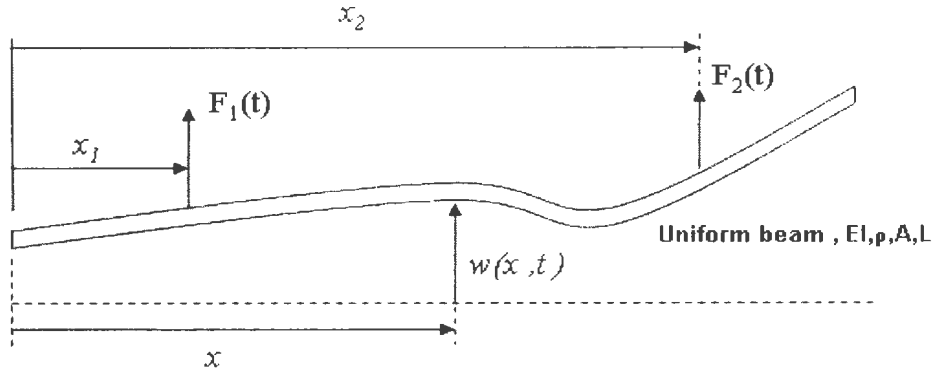


Figure 6.1: Uniform Bernoulli-Euler beam with point forces

Figures and equations used in this section are taken from Karnopp *et al.* [11]. Figure 6.1 shows a long and slender beam having a uniform cross-sectional area A , Young's modulus E , mass density ρ , area moment of inertia I and length L . Any position of the beam is defined by x . $w(x,t)$ gives the transverse displacement of the position x for any time t . Two point forces $F_1(t)$ and $F_2(t)$ are applied at points x_1 and x_2 of the beam to model suspension inputs. Neglecting the rotary inertia and shear deformation, the following Bernoulli-Euler equation for the beam can be written,

$$EI \frac{\partial^4 w}{\partial x^4} + \rho A \frac{d^2 w}{dt^2} = F_1 \delta(x - x_1) + F_2 \delta(x - x_2) \quad (6.1)$$

Mode shapes can be found from the following equation,

$$Y_n(x) = (\cos k_n L - \cosh k_n L)(\sin k_n x + \sinh k_n x) - (\sin k_n L - \sinh k_n L)(\cos k_n x + \cosh k_n x) \quad (6.2)$$

Mode frequencies are calculated using the following equation.

$$\omega_n^2 = \frac{EI (k_n L)^4}{\rho A L^4} \quad (6.3)$$

Using orthogonal property of the modes the following equation can be derived.

$$\left(\int_0^L \rho A Y_n^2 dx \right) \ddot{\eta}_n + \left(\int_0^L \rho A Y_n^2 dx \right) \omega_n^2 \eta_n = F_1 Y_n(x_1) + F_2 Y_n(x_2) \quad (6.4)$$

The quantity in the bracket of the first term is modal mass and in the second term it represents the stiffness. Figure 6.2 shows a bond graph of the force free beam. For example, considering the rigid body mode, with vertical translation,

$$Y_{00} = 1 \quad (6.5)$$

Using Eq.6.4 and Eq.6.5, the first zero frequency mode is obtained as,

$$\left[\int_0^L \rho A (1)^2 dx \right] \ddot{\eta}_{00} = F_1 + F_2$$

or

$$m \ddot{\eta}_{00} = F_1 + F_2 \quad (6.6)$$

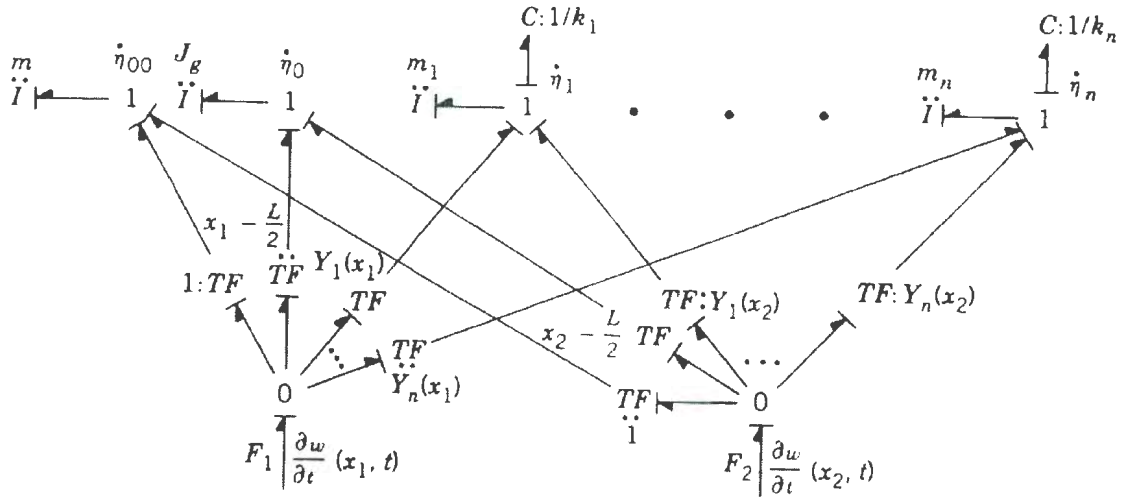


Figure 6.2: Bond graph of Bernoulli-Euler beam

The second rigid mode which is the rotational mode is given by

$$\left[\int_0^L \rho A \left(x - \frac{L}{2} \right)^2 dx \right] \ddot{\eta}_0 = F_1 \left(x_1 - \frac{L}{2} \right) + F_2 \left(x_2 - \frac{L}{2} \right)$$

or

$$J_g \ddot{\eta}_0 = F_1 \left(x_1 - \frac{L}{2} \right) + F_2 \left(x_2 - \frac{L}{2} \right) \quad (6.7)$$

This means acceleration $\ddot{\eta}_0$ is produced by the moments of external forces about the centre of mass where J_g is the centroidal moment of inertia of the beam. Eq.6.6 and Eq.6.7 is represented in the bond graph of Figure 6.3. F_1 and F_2 forces are the efforts at 0-junctions that pass through $-TF$ - elements with moduli equal to the value of the mode shape at point x_1 or x_2 . For the rigid body translation mode the modulus is given by Eq. 6.5. Then it goes to the $1\ddot{\eta}_{00}$ -junction with modal parameter, in this case the 1-junction with beam mass m . Again, in case of the second rigid mode F_1 and F_2 forces pass through

$-TF$ -s having modulus of $\left(x_1 - \frac{L}{2}\right)$ and $\left(x_2 - \frac{L}{2}\right)$ respectively. These efforts then go to the $1\ddot{\eta}_0$ -junction with modal parameter J_g . Other connections represent Equation 6.4 where modal stiffness is also added in combination with modal mass which show the flexible modes.

6.2 Vehicle frame model

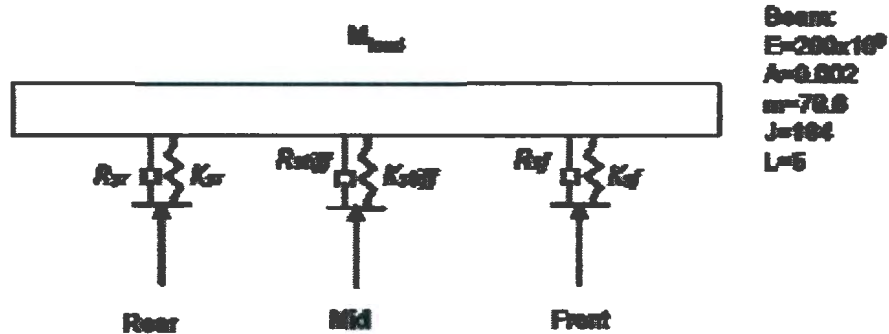


Figure 6.3: Schematic diagram of a vehicle frame

This section describes a vehicle frame model as shown in Figure 6.3. The beam is considered a Bernoulli-Euler beam as described in the previous section with a 10 kg concentrated load at the middle of the beam. Beam specifications are given in the figure. Damping and stiffness values of front, middle and rear section of the beam are given in Table 6.1. The front road input is $\sin(\omega t)$ whereas the rear road input is delayed by 1.5 seconds. The frequency ω has four stages. They are 1 rad/s, 10 rad/s, 65 rad/s and 120 rad/s for 10 seconds each.

Table 6.1: Parameter values of the vehicle frame model

Location	Damping (N-s/m)		Stiffness (kN/m)	
	Front	R_{sf}	100	k_{sf}
Middle	R_{stiff}	100	k_{stiff}	1000000
Rear	R_{sr}	100	k_{sr}	1000000

Figure 6.4 shows the bond graph presentation of the vehicle frame model. The effort source S_e produces an effort of mg at the 1_{v_load} -junction, where m is the load mass which is 10 kg and g is gravitational acceleration. This effort and the effort from damping and stiffness at the middle of the beam produce a resultant effort at the 1_{v_load} -junction that leads to I_{load} and the load mass gives a flow output to the rest of the system. The effort that goes to the 1_{v_load} -junction from K_{stiff} and R_{stiff} elements also gets to the 0_{Fmid} -junction from which the effort passes through different $-TF-$ s whose moduli are equal to the mode shape displacement at the middle of the beam. For example the effort is multiplied with $-TF_{Y00_mid}$ having a mode function of 1 and this goes to the 1_{n00_dot} -junction that represents the translational velocity of the rigid body mode. The rigid body modal mass m is also attached to 1_{n00_dot} -junction and computes the flow for the junction when it is in integral causality.

The front and rear S_f generates the four frequency stage road inputs for the system as described before. Passing the 1_{v_front} and 1_{v_rear} -junctions for the front and rear sections respectively, the flow goes to the 0 -junction that gets effort input from the spring and

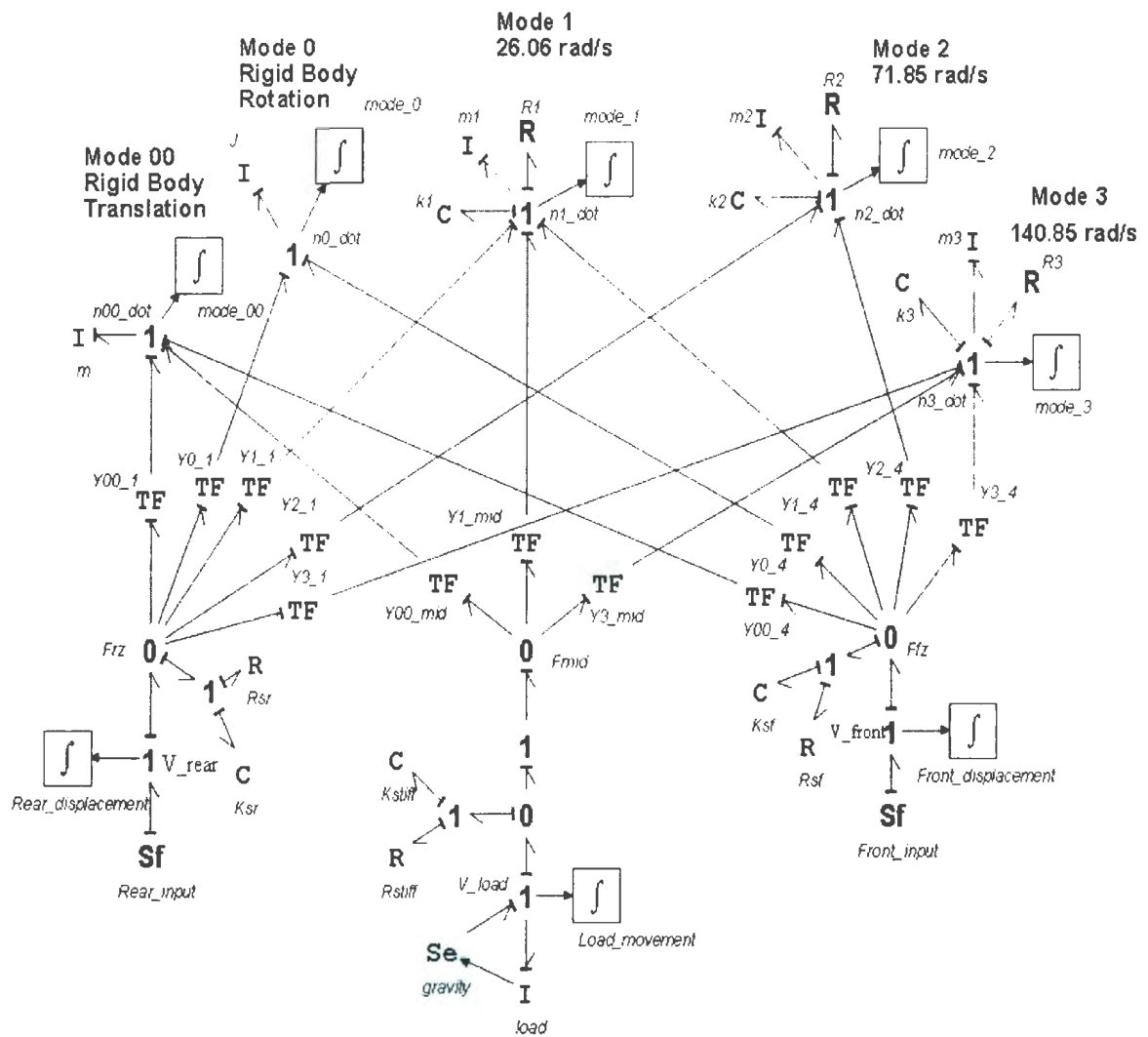


Figure 6.4: Bond graph presentation of the vehicle frame model

damper attached to the front and rear section of the beam. In the same way described for the middle section, the effort then is multiplied by the moduli of different $-TF$ -s corresponding to the mode shape displacement at the point in question. Then they go to different mode velocity 1-junctions as $1_{n_{00_dot}}$, $1_{n_{0_dot}}$ etc.

Table 6.2: Modal parameters used in the model

Mode (n)	Mode Frequency (ω_n) rad/sec	Modal stiffness (K_n) kN/m	Modal Mass (M_n) kg	Damping (R_n) N-s/m
00	0	0	78.6	0
0	0	0	163.8	0
1	26.1	55294	81.4	200
2	71.9	405126	78.5	500
3	140.9	1559400	78.6	1100

The bond graph shows five modes for the system, two rigid modes and three flexible. Mode $n00$ and mode $n0$ are the rigid modes for translation and rotation. Modes $n1$, $n2$ and $n3$ are flexible modes. The integral blocks calculate the modal displacement and the displacements can be output as time series.

Figure 6.5 shows modal amplitudes of the system for all its four stages. For the first stage, which has a lower frequency, only the rigid modes get excited and excitation in the flexible modes is insignificant. During the second stage excitation in the rigid modes becomes less and flexible modes are excited. At the third stage which is of 65 rad/s frequency, all three flexible modes are excited while rigid modes become more flat. At the fourth stage as the input frequency gets higher, mode 1 and 3 get less excited than the previous stage.

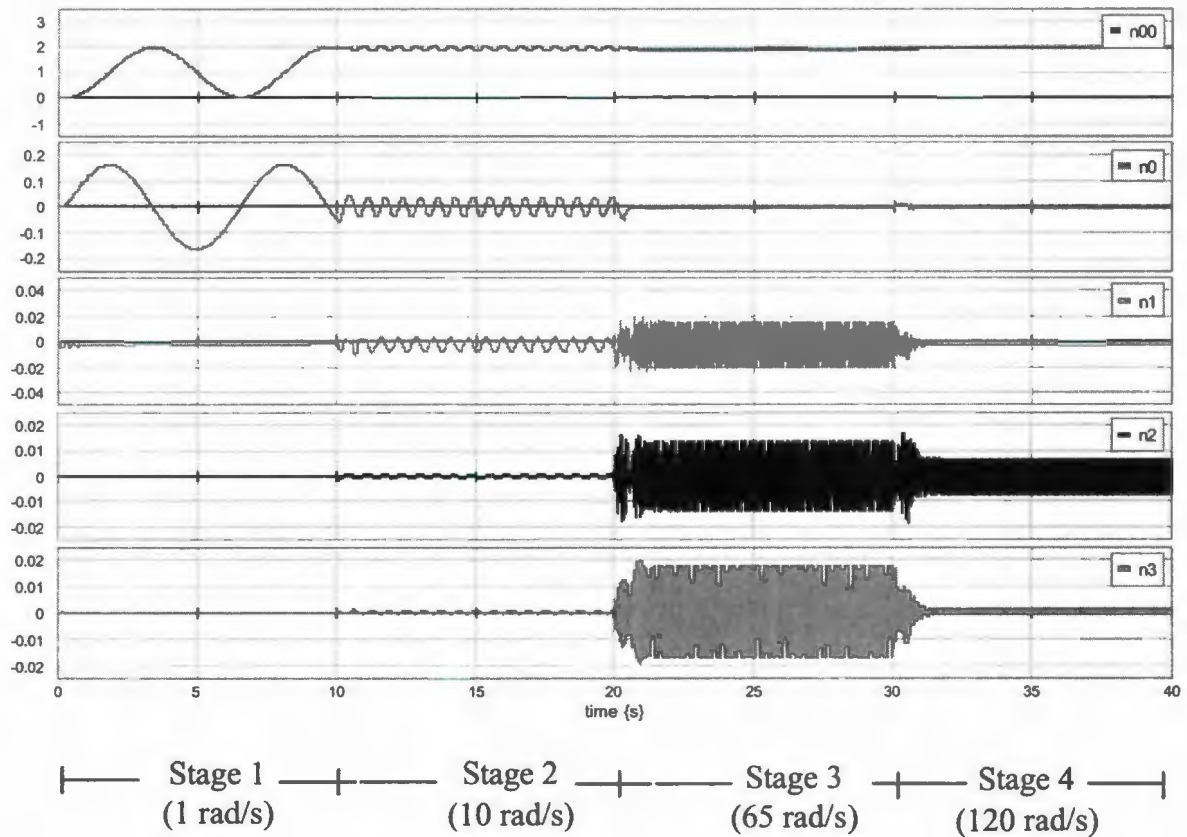


Figure 6.5: Modal amplitudes at different stages for the vehicle frame model

6.3 Partitioning of vehicle frame model

As described in Section 2.1, the partitioning method can be applied to this vehicle frame model. If a mode is found as non-contributing to the rest of the system it can be partitioned and eliminated. Partition boundaries are indicated by replacing a power bond with a modulated source and signal. This is illustrated in Figure 6.7. Two efforts to mode 2 from Q_{F1z} - and Q_{F2z} -junctions as shown in Figure 6.5 are replaced by two modulated

effort sources in Figure 6.6. Now the mode 2 sub-system is partitioned as a driven system with two modulated sources producing the efforts going through the bond B-1 and B-2 to I_{n2_dot} junction. The rest of the system is a driving partition driving mode 2. The modulated sources can be used if activity measurement shows that the modal velocity of the driven system “Mode 2”, with one compliance, one resistive and one inertial element, does not have a significant effect on the rest of the system.

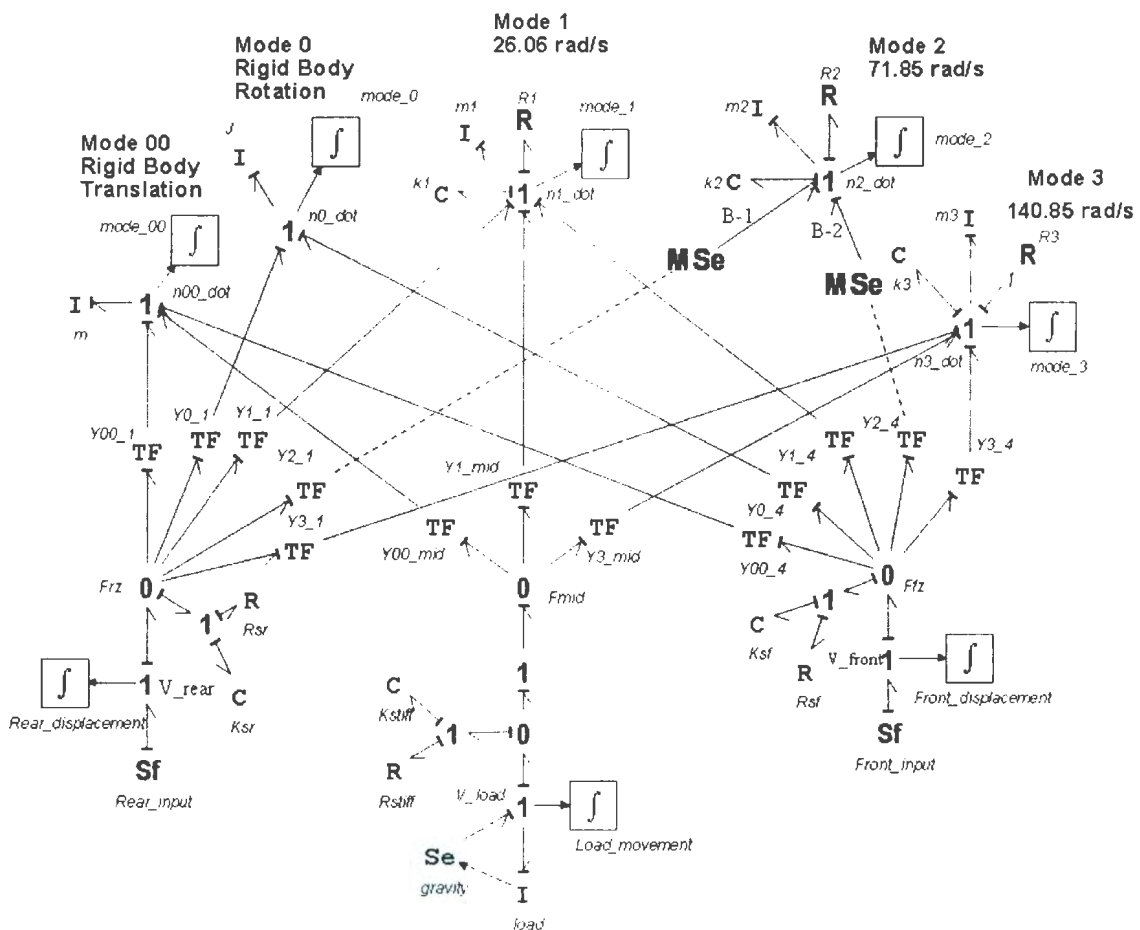


Figure 6.6: Mode 2 partitioning using modulated effort source

6.4 Partitioning by using switches

6.4.1 Assessment of partitioning possibility using MAP sensors

The times when partitioning is appropriate can be determined, and the partitioning done as necessary, by using MAP sensors between internal bonds and switches for the weakly causal bonds described in Section 4.2. The sensors calculate MAP of the bond and generate a 'U' signal that switches *MTF*'s 'on' or 'off', hence resulting in a zero flow for the rest of the system. This can be demonstrated using Figure 6.7. This figure shows a bond graph of the vehicle frame model having the MAP sensors attached. The sensors are attached with all the adjacent bonds of $0_{F_{mid}}$, $0_{F_{rz}}$ and $0_{F_{fz}}$ -junctions. Only for the $0_{F_{fz}}$ -junction, the technique for calculating relative MAP and hence, generating 'U' values is shown in the figure. Similar arrangements for $0_{F_{mid}}$, $0_{F_{rz}}$ junctions in the original model are omitted in Figure 6.7 for clarity.

A MAP sensor is attached with every bond numbered from 1 to 6 in Figure 6.8. These sensors calculate MAP for the corresponding bonds and send the value to the 'maximum' block. The 'maximum' block then finds the highest of the MAPs from the adjacent bonds attached to the junction. Each sensor's MAP is divided by the maximum MAP value to result a 'relative MAP'. The 'threshold' block sends a value to the sensors that sets A 97% threshold limit. A 'U' value without smoothing is generated as described in Section 3.4. 'U' values for the adjacent bonds of $0_{F_{rz}}$ and $0_{F_{fz}}$ -junctions are also determined in the

same way. Figure 6.8 shows the U values of the modes contributing to the force 0 junctions “F_{fz}”, “F_{rz}” and “F_{mid}” at the front, rear and middle of the beam respectively.

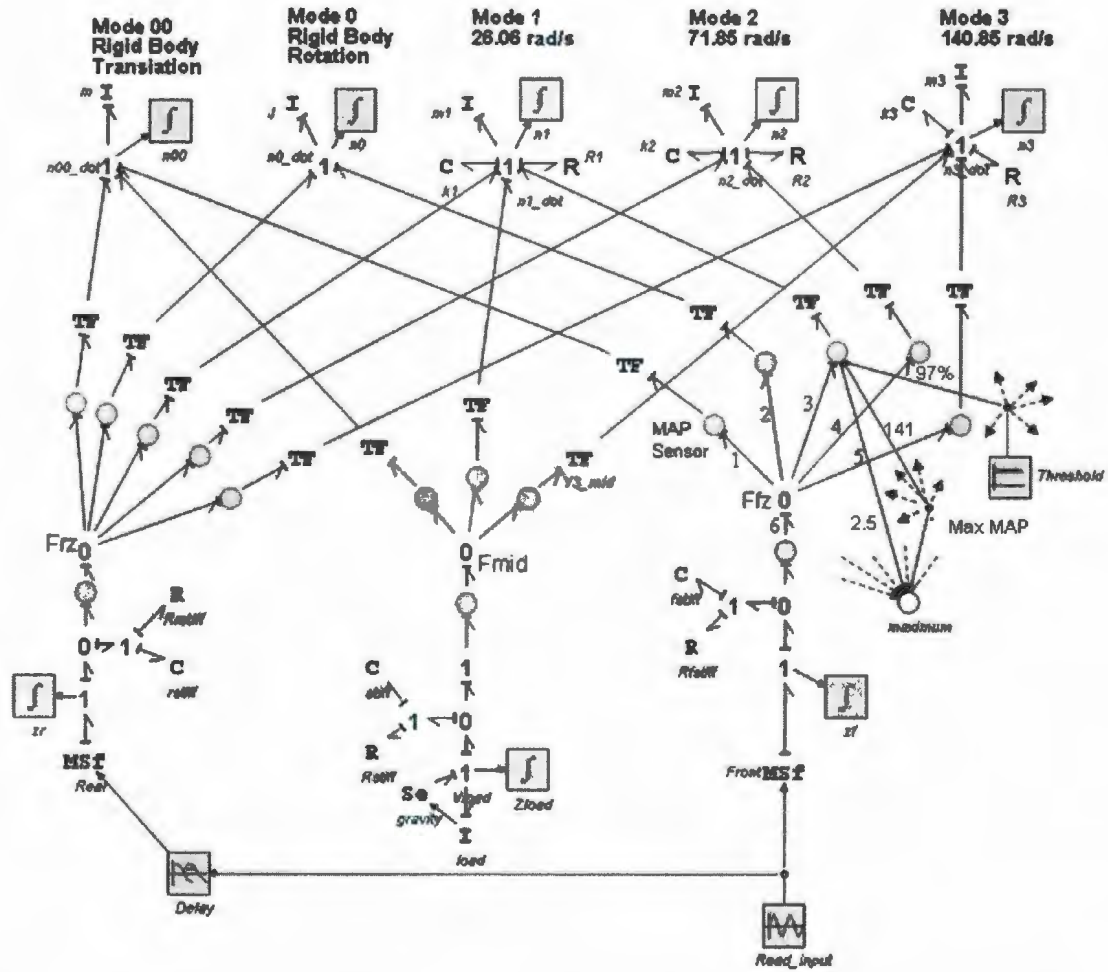


Figure 6.7: ‘U’ value determination by using MAP sensors for the vehicle frame model

During the first stage (1 rad/s), neither flexible mode is excited significantly, due to the slow input motion. At all three locations, the relative MAP of the bonds from the flexible

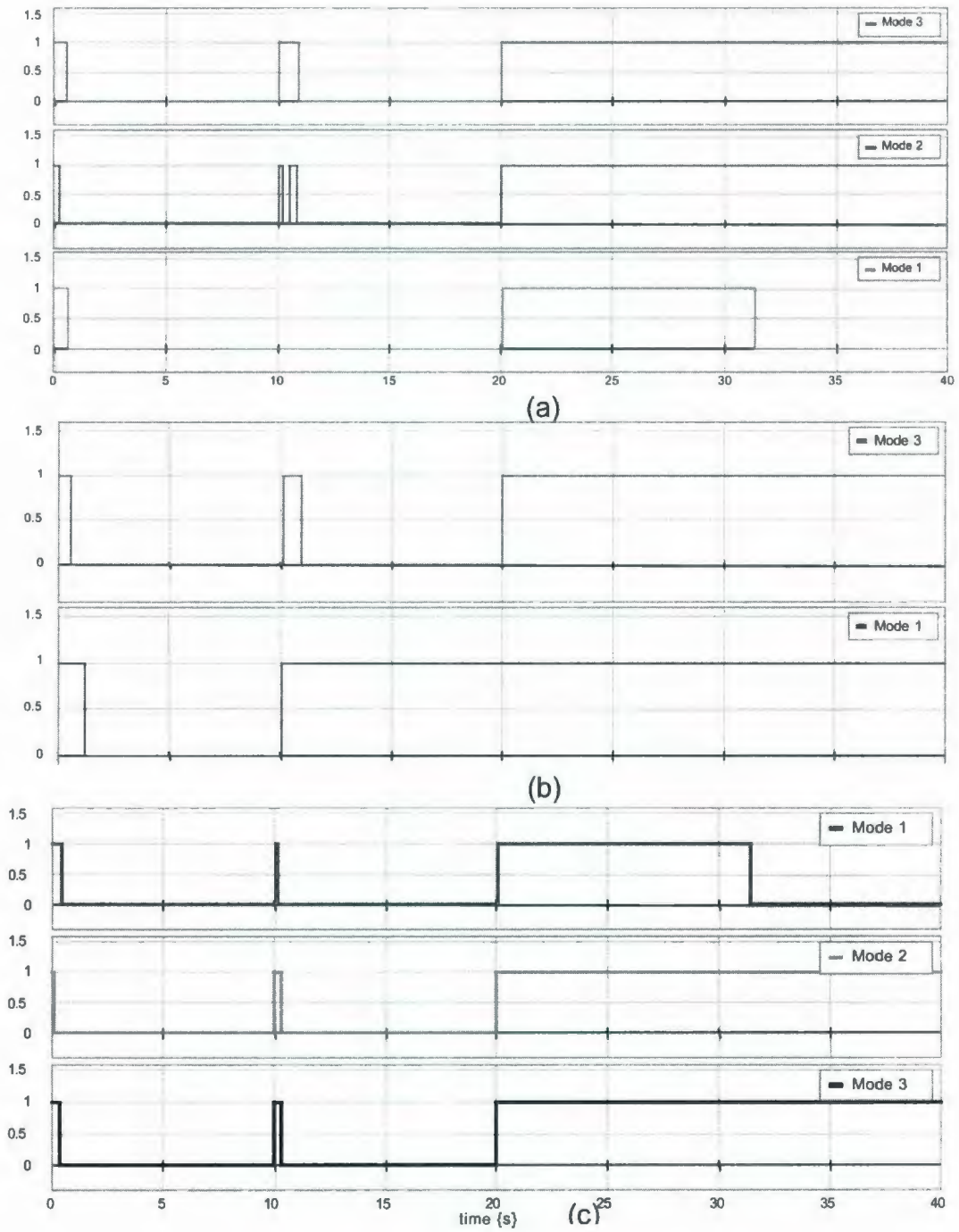


Figure 6.8: Plots of 'U' values at (a) 0_{Frz} -junction (rear) (b) 0_{Fmid} -junction (middle) (c) 0_{Ffz} -junction (front)

modes at the respective 0-junctions do not exceed the threshold of 97%. During the second (10 rad/s) and following stages, the first mode is excited significantly at the middle of the beam. Modes 2 and 3 do not affect system dynamics in the second stage, because the front and rear suspension locations are closer to nodes of these modes. The middle of the beam is exactly at a node of Mode 2, which is why Mode 2 is not shown in the middle graph of Figure 6.8. While Mode 3 also has maximum displacement at mid-span, it is still being excited far below its resonant frequency in Stage 2. In Stages 3 and 4, Modes 2 and 3 are excited closer to their natural frequencies and are active at all three locations. In Stage 4, note that Mode 1 becomes inactive again. This is due to the attenuation that occurs in vibrating systems that are excited at a frequency far above their natural frequency.

6.4.2 Switched vehicle frame model

Switches can be applied to the model described in the previous section. 'U' values show that all the three flexible modes do not contribute significantly to the system dynamics at the first stage. Thus the three modes can be partitioned. During the second stage when mode 1 has significant deflection at mid-span, mode 1 cannot be partitioned but mode 2 and 3 can still be omitted. During rest of the stages all the modes contributing to any location i.e., at rear, front and middle, never become inactive at the same time. Therefore the flexible modes cannot be completely partitioned but still a bond can be switched off once it doesn't contribute. Instead of using modulated effort source as in Section 6.3, partitioning is obtained by using 'switch of the internal bond' for weak

causality as described in Section 4.4. 'U' values go to moduli of the *MTF*s to direct the 'on' or 'off' mode as described. This can be illustrated from Figure 6.10. At 0_{Ffz} -junction, bonds numbered as 1, 2, and 3 that contribute to mode 1, 2 and 3 respectively have the switch arrangement where the 'U' signal from the MAP sensor goes to *MTF*. For 0_{Fmid} junction, bonds 4 and 5 contribute to modes 3 and 1 respectively and have switches. At 0_{Ffrz} -junction, switches are applied for bonds 6, 7 and 8 which contribute to modes 3, 2 and 1 respectively.

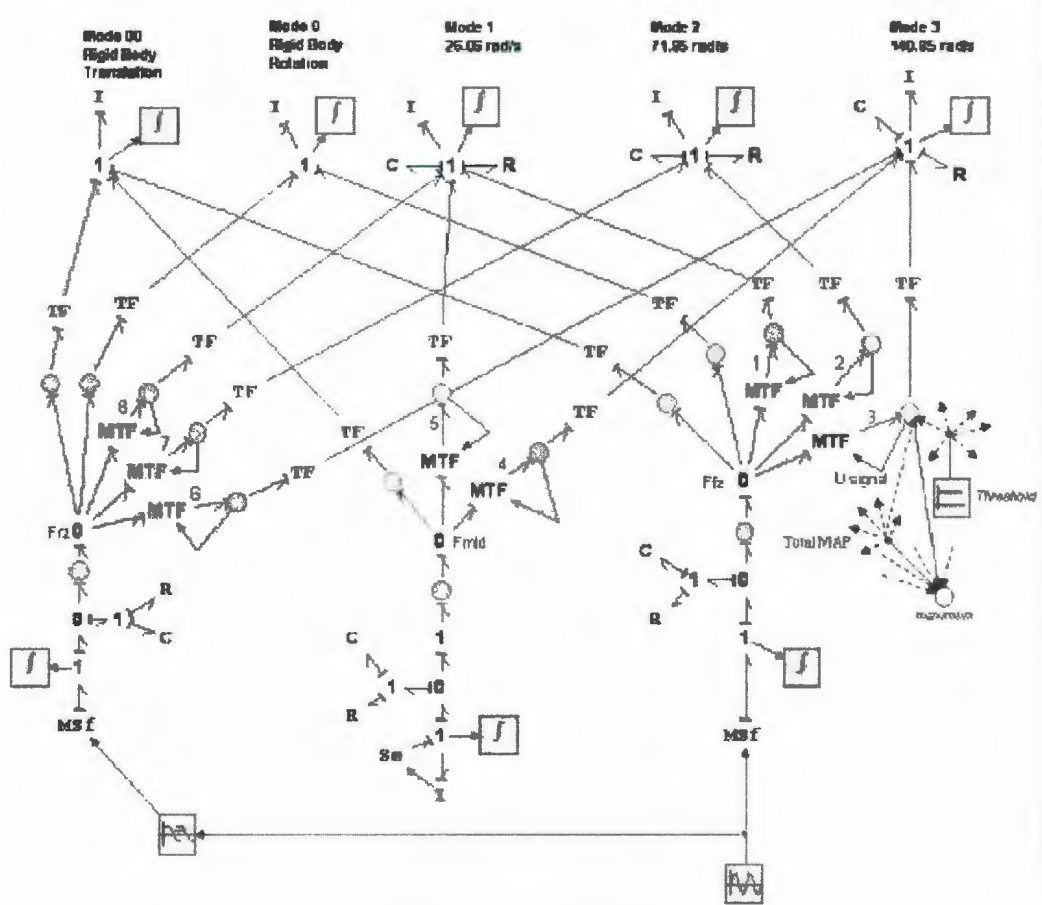


Figure 6.9: Switching arrangement applied for vehicle frame model

6.5 Result of switching the vehicle frame model

For the switched model simulation the ‘Backward Differential Formula’ integrator with a tolerance of $1e^{-006}$ is used. Figure 6.10 shows the switched model response overlaid on the full model system response. The front displacement Ffz , middle displacement $Finid$ and rear displacement Frz are plotted. Plots show that the system response for the switched and full model is the same. This proves that switching doesn’t significantly affect the system response in this case.

Table 6.3: Simulation time and step for switched and full model

Model	Time	Step
Switched	80.006	240402
Full	79.183	197866

Figure 6.11 gives ‘U’ value plots for the vehicle frame model when the switches are applied. The switched ‘U’ values confirm similar patterns when compared with the plots of full model shown in Figure 6.8, i.e., switched bonds go ‘on’ or ‘off’ for the same time span as the full model suggests. Another model is built that has all the sensors and *MTF* that a switched model has, but no switching occurs as no signal goes from the MAP sensors to the *MTFs*. Rather, a constant signal having value of 1 passes to the *MTFs* which makes the model work as a full model. Simulation time and steps taken by the switched model and the “full” model are given in Table 6.3. Use of a switched model

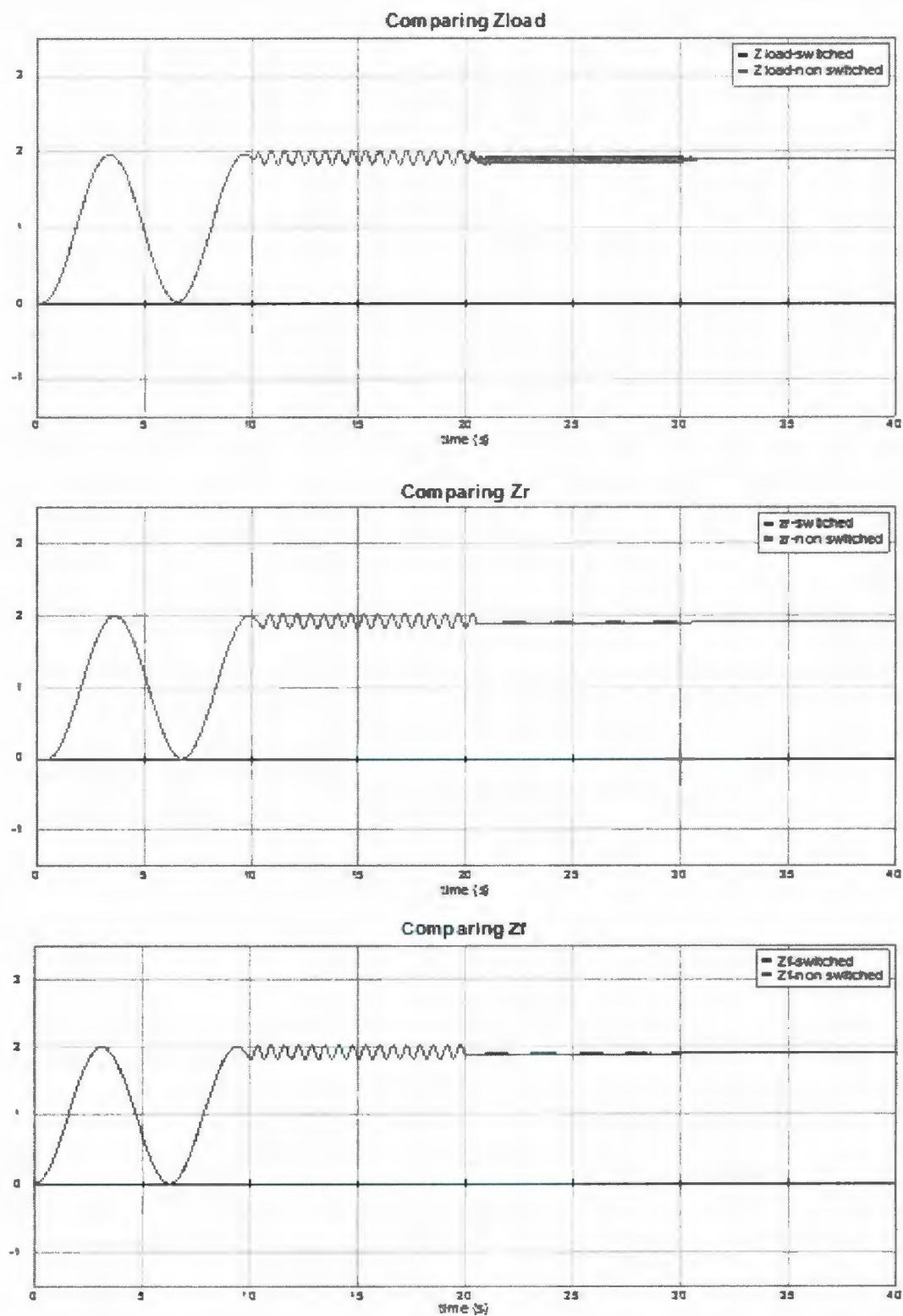


Figure 6.10: Comparing switched and full model system responses

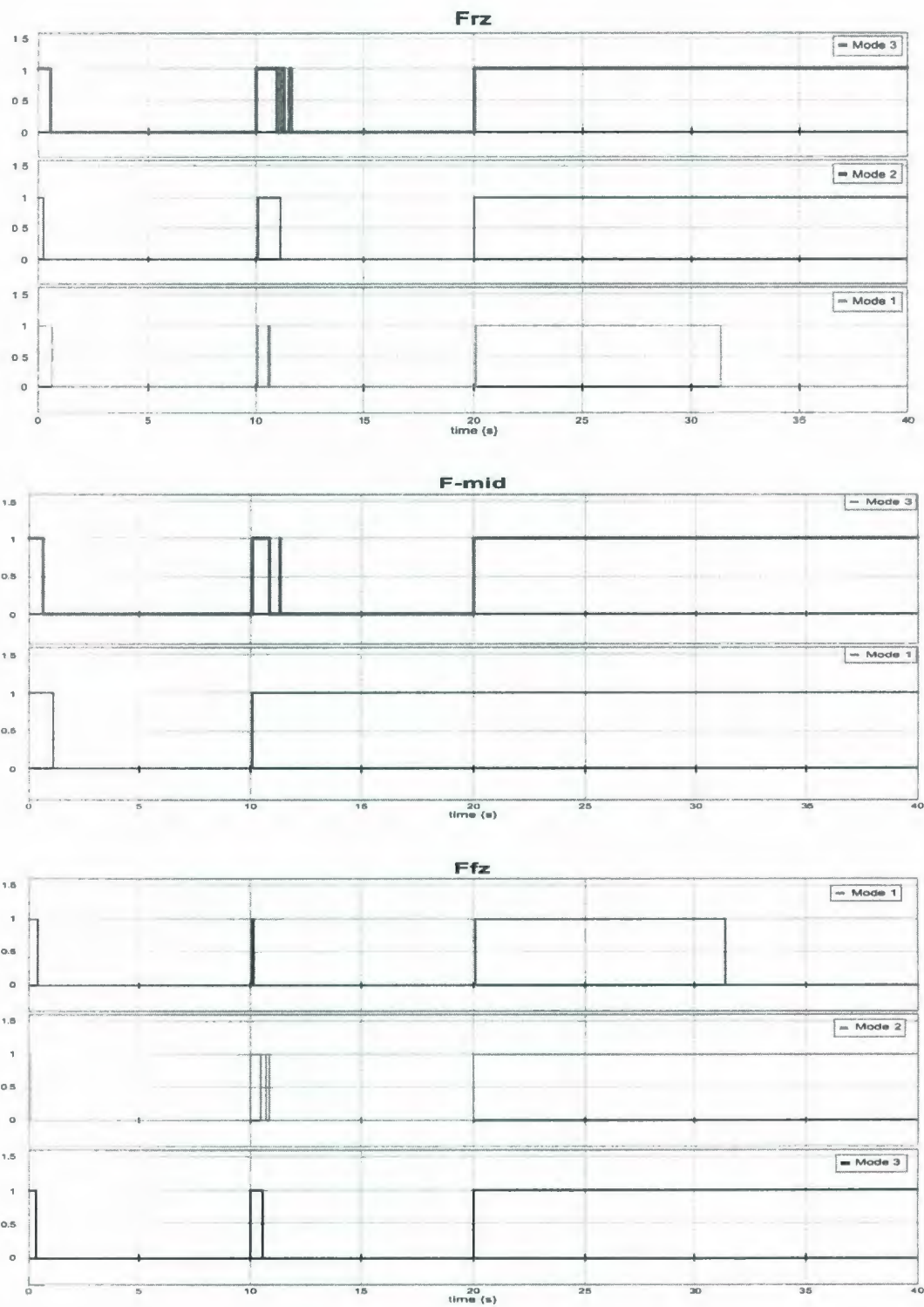


Figure 6.11: 'U' values of switched vehicle frame mode

does not give computation time or step savings, because of the numerical overhead involved with calculating activities. However, the above switched model shows that the relative MAP metric is a good predictor of when systems can be partitioned, and it shows how the system would respond if the optimal model could be used at every instant. If the modeler wanted to build a fixed-complexity model for each stage, and run them sequentially, then time savings would likely occur because there would be no need to calculate relative MAP. The switching method described here thus “designs” the fixed-complexity models for each stage, and the switched system results show how well the sequence of fixed-complexity models will work.

Chapter 7

Conclusions and Recommendations

7.1 Conclusions

This thesis work presented a method that can continuously monitor the contribution of an element to overall system dynamics and at the same time it can eliminate the effect of the element when it becomes unimportant for predicting the system response. Hence it showed how to generate proper models automatically as the system inputs or the parameters are changed. Bond graphs were used throughout the work and computer simulations were done by using 20sim [2007] software. Three element importance monitoring metrics were employed and results were compared to see which method was more responsive. It was found in several case studies that MAP (moving average of power) metric works better than activity or relative activity metrics.

Switching method was proposed and implemented to eliminate the effect of a non-contributing element as its MAP index falls below a specified threshold limit. It is important to note that such switching enables one to remove elements regardless of causality and at the same time it can calculate element importance when the element has

been removed. Modulated transformers (*MTF*) are used to switch the elements 'on' or 'off'. Sometimes *MTFs* were required to be combined with parasitic elements for performing switching of causally strong bonds.

Three different case studies were done by using the bond graph based metrics and the switches. The half car, the quarter car and the vehicle frame case studies show how the method works while using the element importance metrics along with the switches. The half and quarter car case studies used the MORA algorithm while the vehicle frame case study was done by using partitioning algorithm. In very few occasions computational saving were achieved.

The ultimate goal of such automated proper model generation was to reduce simulation time. This method takes the overhead to calculate element importance at every instant of the simulation which explains why simulations became slower while using the switches along with the metrics. Moreover parasitic elements in the switches often created numerical stiffness and slowed the simulations.

Despite of the fact that computational saving was not obtained, this thesis shows a method that can continuously monitor element importance and therefore can predict variable-complexity model structures automatically at any time instant. This also can tell how the system would respond if the proper models were generated in advance and then

simulated sequentially. Therefore it can compare the proper model response with the full model to check its validity.

7.2 Recommendations

Considering the achievements and limitations of the current thesis work the following potential research scopes can be suggested.

- A more efficient numerical method can be employed to address the numerical difficulty once switches are used.
- An arbitrary threshold limit was set for the elements to be removed. A method can be developed to find the appropriate threshold limit which would eliminate arbitrary choice.
- The current method monitors model complexity for every instant which adds more computational overhead during the simulation. Methods can be developed to minimize the amount of model complexity checking. Instead of checking of every instant, some time period can be set at which to check the model complexity. Challenge will be to select the time periods for model checking prior to the simulation.
- The MAP metric used a shorter time window than activity but the choice of the window was arbitrary. The choice of this window could be crucial to the selection of the appropriate complexity model. Selecting the right time window requires further research .

- For automating model complexity some pre-set proper models can be generated for various stage of the full maneuver. These models could be generated automatically using the method of this thesis. Switching between these pre-set models would then predict the system dynamics for the entire maneuver efficiently.

References

1. Chwif, L. and Paul, R.J (2000) "On Simulation Model Complexity." *Proc. of the 2000 Winter Simulation Conference*, pp.449-445.
2. Louca, L.S., Stein, J.L., Hulbert, G.M., and Sprague, J. (1997) "Proper Model Generation: An Energy-Based Methodology." *Proc. International Conference on Bond Graph Modeling ICGBM'97*, Phoenix, AZ. Society for Computer Simulation, San Diego, CA, pp.44-49.
3. Ferris, B.F., and Stein, J.L., (1994) "Development of Proper Models of Hybrid Systems: A Bond Graph Formulation." *Proc. of the Symposium on Automated Modeling 1994 ASME Winter Annual Meeting*, Chicago.
4. Ersal, T., Fathy, H.K., Louca, L.S., Rideout, D.G., and Stein, J.L. (2007) "A Review of Proper Modeling Techniques." *Proc. 2007 ASME International Mechanical Engineering Congress and Exhibition*, Paper No. MECE2007-42031, pp.1-17.
5. Rideout, D.G., Stein, J.L., and Louca, L.S. (2007) "A Systematic Identification of Decoupling in Dynamic System Models." *Journal of Dynamic Systems, Measurement and Control*, ASME, New York, NY, vol.129 pp. 503-513.
6. Kypuros, J.A., and Longoria, R.G. (2003) "Model synthesis for design of switched systems using a variable structure system formulation." *Journal of Dynamic System Measurement and Control*, vol.125, pp. 618-629.

7. Fortuna, L., Nunnari, G., and Gallo, A. (1992) "Model order reduction techniques with applications in electrical engineering." *Springer-Verlag*, New York .
8. Louca, L.S., and Stein, J.L. (2002) "Ideal physical element representation from reduced bond graphs." *Proc. MechE Part I: J. Systems and Control Engineering Special Issue*, vol. 216, pp. 73-83.
9. Kypuros, J.A., and Longoria, R.G. (2002) "Variable fidelity modeling of vehicle ride dynamics using an element activity metric." *Proc. ASME IMECE 2002*, New Orleans, LA, pp. 525-534.
10. Rideout, D.G., Stein, J.L. and Louca, L.S. (2007) "Extension and application of an algorithm for systematic identification of weak coupling and partitions in dynamic system models." *Simulation Modelling Practice and Theory*, Elsevier, Volume 17, Issue 1, Pages 271-292.
11. Karnopp, D., Margolis, D.L. and Rosenberg, R. C. (2006) "System Dynamics Modeling And Simulation of Mechatronic Systems." *John Wiley & Sons Inc.*, New York, 4th Edition .
12. Strömberg, J-E. , Top, J. and Soderman, U. (1993) "Variable causality in bond graphs caused by discrete effects." *Proc. ICBGM'93*, San Diego, CA, pp. 115-119.
13. Junco, S. et al. (2007) "On Commutation Modeling in Bond Graphs." *Proc. ICBGM'07*, San Diego, CA, pp. 12-19.
14. Asher, G.M. (1993) "The Robust Modelling of Variable Topology Circuits Using Bond Graphs." *Proc. ICBGM'93*, San Diego, CA, pp. 126-131.

15. Ducreux, J.P. et al. (1993) "Bond Graph Modelling of Commutation Phenomena in Power Electronics Circuits." *Proc. ICBGM'93*, San Diego, CA, pp. 132-136.
16. Karnopp, D. and Margolis, D. (1979) "Analysis and Simulation of Planar Mechanism Systems Using Bond Graphs." *Journal of Dynamics, System Measurement and Control*, pp.187-191.
17. Mosterman, P.J. and Biswas, G. (1998) "A theory of discontinuities in dynamic physical systems." *Journal of the Franklin Institute*, vol-335B, no.3, pp.401-438.
18. Ye, Y., and Youcef-Toumi, K.(1999) "Model Reduction in the Physical Domain." *Proc.1999 American Control Conference*, pp.4486-90.
19. Demir, Y., et al. (1997) "Derivation of state and output equations for systems containing switches and a novel definition of a switch using the bond graph method." *Journal of the Franklin Institute*, 334B(2), pp.191-197.
20. Umarikar, A.C., and Umanand, L. (2004) "Modelling of switching systems in bond graphs using the concept of switched power junctions." *Journal of the Franklin Institute*, 342, pp.131-147.
21. Rideout, D.G., Stein, J.L., and Louca, L.S. (2005) "System Partitioning and Improved Bond Graph Model Reduction Using Junction Structure Power Flow." *Proc. ICBGM'05, International Conference on Bond Graph Modeling*, New Orleans, LA. Society for Computer Simulation, San Diego, CA, pp.43-45.

22. Rosenberg, R._C. and Moultrie,_B.(1979) "Basis Order For Bond Graph Junction Structure.", *EEE Transactions on Circuits and Systems*, vol CAS-26, no-2, pp. 130-137.
23. Margolis, D (1994) "Applications of Bond Graphs to Hydraulic Motion Control Systems.", *Simulation Councils Proceedings Series*, vol. 27, no. 1, pp. 249-258.
24. Breedveld, P. C. (1985) "Multibond Graph Elements In Physical Systems Theory." *Journal of the Franklin Institute*, vol. 319, no. 1-2, , pp.1-36.
25. 20SIM (2007) Version 4.0, Controllab Products b.v., Enschede, Netherlands.



